Formulation of a consistent crack width calculation method for reinforced concrete members

Otto Terjesen

UiA University of Agder

Doctoral Dissertations at the University of Agder 473

Formulation of a consistent crack width calculation method for reinforced concrete members

Otto Terjesen

Formulation of a consistent crack width calculation method for reinforced concrete members

A new design code formulation, an alternative to Eurocode 2 and Model Code, based on experimental, numerical and analytical considerations.

Dissertation for the degree philosophiae doctor (PhD)

University of Agder
Faculty of Engineering and Science
2024

Doctoral dissertations at the University of Agder 473

ISSN: 1504-9272
ISBN: 978-82-8427-190-3

Otto Terjesen, 2024

Print: Make!Graphics
Kristiansand

Foreword

This doctoral thesis is submitted in partial fulfilment of the requirements for the degree Philosopiae Doctor (PhD) at the University of Agder (UiA).

The research has been carried out at the Department of Structural Engineering at UiA in Grimstad and the Norwegian University of Science and Technology (NTNU) in Trondheim, Norway. The main supervisor was Professor Terje Kanstad (NTNU, UiA), and the co-supervisor was Associate Professor Reignard Tan (NTNU and Multiconsult).

The PhD project is part of the ongoing research project "More Efficient and Environmentally Friendly Road Construction" (MEERC), partly funded by the Research Council of Norway (NFR) and Sørlandets Kompetansefond.

This thesis is written as a collection of papers with two parts. The first part highlights the research's significance, main objectives and limitations, and summarises the appended papers and presents the main conclusions. The Second part consists of four appended papers, of which three have been published, one is under review at the peer-reviewed journal *fib* Structural Concrete, while one has been published in a conference proceeding.

The author, Otto Terjesen, declares that this thesis, with its presented work, is his own and that the contributions to the jointly authored papers are as specified in detail.

March 2024, Grimstad/Trondheim
Otto Terjesen

Acknowledgements

Working on this PhD thesis has been enriching, both professionally and personally. Many people have guided and supported me through this PhD project, enabling me to complete it successfully.

First, I wish to thank my main supervisor, Professor Terje Kanstad; your unwavering dedication and passionate commitment to concrete structures were evident throughout the years. I am fortunate to have had you as my supervisor during this PhD project; your composure, patience, knowledge, and never-ending support have been indispensable for my motivation, and spending the last years at NTNU with you and our colleagues has been a privilege. Your exemplary dedication has been a great motivation for me to strive towards completing my thesis.

To my co-supervisor, Associate Professor Reignard Tan, I sincerely thank you for all our discussions over the last couple of years; your passion and scientific knowledge have helped me complete this thesis, and without your support, I do not believe I would have finished.

I would like to express my sincere gratitude to my friends and colleagues at UiA and NTNU for their invaluable contributions to my academic journey. Sharing scientific knowledge, experiences, achievements, and frustrations has enriched my research. A special thank you goes out to Ingrid Lande Larsen, whose good mood, unwavering contributions, perseverance, and constant support have been instrumental throughout this journey. Ingrid, your positive energy has been a source of inspiration. I extend my heartfelt appreciation to Gianclaudio Pinto for his essential contributions to my research. Your insights and dedication have significantly enhanced the quality and depth of my work. I am also grateful to Henrik Thorsen at Norconsult for his insightful discussions on numerical simulations. Henrik's expertise and willingness to engage in meaningful conversations have been pivotal to the development of my research.

A special mention is reserved for my girlfriend Anja, whose love, support and care have been my pillars of strength. I am grateful for the valuable discussions, her continuous belief in me, and for caring for our daughter, Olivia, While I worked long hours. Anja, you have been my unwavering source of inspiration.

Finally, I thank my daughter Olivia, who entered our lives in July 2023. It has been the best time of my life, spending moments with her, getting to know her, and witnessing the joy she brings. Olivia lights up our lives with her smile and laughter. As I look forward to the future, I eagerly anticipate a period during which we can spend more time together as a family.

To all who have played a part, big or small, in this academic endeavour, I extend my deepest thanks. Your support and collaboration have made this journey both academically fulfilling and personally enriching.

Abstract

Predicting crack widths in reinforced concrete structures is essential for Serviceability Limit State (SLS) Design. Crack widths that exceed a certain limit may impair the functionality of a structure, limit its use and reduce the service life. Cracking usually occurs with irregular distribution and different crack widths along the members. Despite a century of research, predicting them accurately and consistently is still difficult, as shown by Terjesen et al. [1]. On the other hand, the consequences of cracks related to functionality, durability, aesthetics, and economy are significant, and discussions in the research environments are ongoing [2, 3].

This thesis focuses on different calculation methods to predict crack widths in standard and large-scale concrete structures subjected to uniaxial loading conditions. Large-scale concrete structures are, in this thesis, synonymous with RC structures, which have member dimensions that can be up to several meters in height, sections with large reinforcing bar diameters, and large covers. The investigated calculation methods range from computer-based simulations using Nonlinear Finite Element Analysis (NLFEA) to design code formulations, i.e., Eurocode 2 (EC2, FprEC2, DIN) [4-6], *fib* Model Code (MC2010, MC2020) [7, 8] in addition to the Modified Tension Chord Model (MTCM) [9] and the simplified version of MTCM (SMTCM) developed in this thesis.

Evaluation of the semi-empirical formulas recommended by Eurocode 2, *fib* Model Codes, and the German National Annex (DIN) to EC2 showed that they may predict crack widths inconsistently. The assumption of a constant mean bond-stress distribution over the transfer length independent of the load level can perhaps explain the reasons for continuously calibrating the formulas, among others: i) using a lower bound for the difference in mean strains for steel and concrete to differentiate between a crack formation and a stabilized crack stage and ii) the cover addition in the crack spacing formulas.

The simplified version of the MTCM denoted SMTCM was formulated by using the basic principles in solid mechanics applying the closed form solution of a Comparatively Lightly Loaded Members (CLLM) to predict a certain mean behaviour of the Comparitively Heavily Loaded Member (CHLM) as a

simplification (SCHLM). The SMTCM was shown to predict the crack width to an excellent extent for RC beams and slabs in bending and RC ties in tension. Due to the mechanical formulation of the model, there might be significant advantages to apply in cases where there are particular risks of large cracks, e.g. i) at changes of sections, ii) near concentrated load, iii) positions where rebars are curtailed and iv) areas of high bond stress, particularly at the end of laps v) multilayered reinforcement combined with large covers.

Sammendrag

Predikering av riss i armerte betongkonstruksjoner er avgjørende for bruksgrense design. Riss som overstiger en gitt størrelse kan svekke konstruksjonens funksjonalitet, begrense bruken og redusere levetiden. Til tross for et århundre med forskning, er det fortsatt vanskelig å predikere riss nøyaktig og konsistent. I tillegg så er konsekvensene av riss knyttet til funksjonalitet, holdbarhet, estetikk og økonomi betydelige.

Forskningen presentert i avhandlingen fokuserer på ulike beregningsmetoder for å forutse rissvidder i standard- og storskala betongkonstruksjoner som utsettes for enakset lastforhold. Storskala betongkonstruksjoner er i denne avhandlingen synonymt med armeringsbetongkonstruksjoner, som har elementdimensjoner som kan være opptil flere meter i høyde, seksjoner med store armeringsstenger og store betong overdekninger. De undersøkte beregningsmetodene varierer fra numeriske simuleringer ved bruk av ikke-lineær elementanalyser til design kode formuleringer, dvs. Eurokode 2 (EC2, FprEC2, DIN), fib Model Codes (MC2010, MC2020) i tillegg til «Modified Tension Chord Model» (MTCM) og den forenklede versjonen av MTCM (SMTCM) utledet i denne avhandlingen.

Evalueringen av de semi-empiriske formlene som anbefales av Eurokode 2, fib Model Code og det tyske nasjonale tillegget (DIN) til EC2 viste at de predikerer rissvidder inkonsistent. Antagelsen om en konstant heftspenning over overføringslengden uavhengig av lastnivået kan kanskje forklare årsakene til den kontinuerlige kalibrering av formlene, blant annet: i) bruken av en nedre grense for forskjellen i gjennomsnitt tøyningene mellom stål og betong for å differensiere mellom ett rissdannelse og et stabilisert risstadium og ii) overdekningsleddet i formlene for rissavstand.

Den forenklede versjonen av MTCM kalt SMTCM ble formulert ved å bruke de grunnleggende prinsippene innen faststoffmekanikk ved å anvende den lukkede formen for løsning av «Comparatively Lightly Loaded Members» (CLLM) for å forutsi en bestemt gjennomsnittlig oppførsel av den «Comparitively Heavily Loaded Member» (CHLM) som en forenkling (SCHLM). SMTCM viste seg å forutsi rissvidder i utmerket omfang for bjelker og plater i bøyning og rene strekkstaver. På grunn av den mekaniske formuleringen av modellen, kan det være

betydelige fordeler ved anvendelser i tilfeller der det er spesielle risikoer for store riss, f.eks. i) ved seksjonsendringer, ii) nær konsentrert laster, iii) posisjoner der armeringen er skjøtet og iv) områder med høy heftspenninger, spesielt i enden av armeringskjøtene v) flerlags armering i kombinasjon med store betong overdekninger.

List of publications

This thesis is based on the work presented in the following papers:

APPENDED JOURNAL PUBLICATIONS:

Paper Ia

Larsen, I. L., Terjesen, O., Thorstensen, R. T., & Kanstad, T. (2019). Use of Concrete for Road Infrastructure: A SWOT Analysis Related to the three Catchwords Sustainability, Industrialisation and Digitalisation.
Nordic Concrete Research 60(1) 31–50. https://doi.org/10.2478/ncr-2019-0007

Paper II

Terjesen, O., Pinto, G., Kanstad, T., & R Tan, R. (2024) Performance study of crack width calculation methods according to Eurocodes, fib Model Codes and the Modified Tension Chord Model.
Structural Concrete 2024. https://doi.org/10.1002/suco.202300367

Paper III

Terjesen, O., Kanstad, T., & R Tan, R. (2024) Simplified Modified Tension Chord model: an alternative crack width calculation model to Eurocode 2 and Model Codes. *Submitted for Review to Structural Concrete 2024*

APPENDED CONFERENCE PUBLICATIONS:

Paper Ib

Terjesen. O., Kanstad. T., Tan. R. (2022) Application of NLFEA for crack width calculations in SLS. *Computational Modelling of Concrete and Concrete Structures (1st ed.)* pp. 246-254, Meschke, G., Pichler, B., & Rots, J.G. (Eds.). (2022). CRC Press. https://doi.org/10.1201/9781003316404.

AUTHOR'S CONTRIBUTIONS TO JOINTLY PUBLISHED PAPERS

The contribution of the author of this doctoral thesis to the appended papers is described here:

I. The author was responsible for the parts related to digitalisation and industrialisation, as well as a large part of the writing, with shared responsibility for the conceptualization and planning of the paper.

Ib. The author was primarily responsible for the planning, data collection, all numerical modelling, calculations and writing with the assistance of the co-authors.

II. The author of this thesis planned and wrote the majority of the paper with input from co-authors. The author was responsible for the data collection, all calculations and writing, while Gianclaudio Pinto contributed to the database collected from the literature.

III. The author of this thesis was responsible for conceptualization, the data collection, all calculations and writing with input from the co-authors. The unpublished experimental data regarding crack width profiles from the RC-ties tested by Reignard Tan was conducted by Giedrius Žirgulis at NTNU in the spring of 2017.

Contents

Foreword v
Acknowledgements vi
Abstract viii
Sammendrag x
List of publications xii
1 Introduction 1
1.1 Background and motivation 1
1.2 Objectives and limitations 3
1.3 Outline of the thesis 3
2 Cracking and tension stiffening 4
2.1 General 4
2.1.1 RC ties, beams and one-way slabs 5
3 Summary of papers 8
3.1 The papers shown in context. 8
3.2 Paper Ia 9
3.3 Paper Ib 9
3.4 Paper II 10
3.5 Paper III 11
4 Application of SMTCM to special cases in practical design 12
4.1 General formulation of SMTCM 12
4.2 RC members where the regulations may fail 12
4.2.1 Joints between members with different thickness 13
4.2.2 Large cross-sections in bending with several reinforcement layers 18
5 Conclusions 25
6 Recommendations for future research 27
List of notations 29
List of references 30
Paper I - III 32

1 Introduction

Digitalization is a popular word used by society; everyday use of the word often describes a more digital world, a more connected world with almost endless possibilities. In the past, engineers relied on manual calculations and drawings using pen and paper and hand-held calculators. Structural analysis, load calculations, and design iterations were performed manually, which could be time-consuming and labour-intensive. The emergence of computer-aided design software in the 1960s created new working methods and significantly transformed the engineering practice. In Norway, the design and construction of offshore concrete platforms in the 1970s catalyzed the development of structural analysis and design software. In 2023, computer programs are used in the everyday design of reinforced concrete (RC) structures through structural analysis and dimensioning. Despite the vast improvements in advanced commercial design programs over the last 50 years, many day-to-day operations performed by structural engineers still consist of manual calculations. One example is crack width calculations based on structural analysis with linear material models, where the procedure is usually done in two calculation steps. First, an RC member's external loading and imposed deformation are applied in the software environment, and a section analysis is performed to identify the sectional forces based on geometry and relevant mechanical properties. The second step is the crack width calculation itself, based on the sectional forces found in the first step, using typical hand calculation by a design code formulation. Both operations are performed within the software environment; therefore, the hand calculations do not necessarily need to be in the same short format with their respective mechanical simplifications that may have been determined decades ago and have become accepted approaches to a specific problem. However, it is still valuable and essential that the basic idea of hand calculations is still being used to mitigate the risk of complex structures becoming too simple to handle for the general structural engineer in the software environment.

1.1 Background and motivation

One characteristic of a reinforced concrete (RC) structure is the occurrence of cracks. These cracks usually occur in an irregularly distributed manner with different widths of the cracks along the RC member. As the literature shows, predicting these crack widths and the maximum crack spacing between two cracks

by analytical approaches has proven to be difficult [10-12]. There is a general acceptance that cracking occurs whenever the tensile strength of concrete is reached, and this might be caused by the volumetric changes in the concrete due to the hardening process, external loading, or imposed deformations at later stages, for instance, as shown by Leonhardt [13]. According to *fib* Model Code 2010 [5], the main reasons for limiting the crack widths are specified as the appearance, tightness and durability of the RC structure. However, exceeding the limit state of this crack width during design does not necessarily mean that the structure should be rejected, but instead indicates that there is a risk of reducing the functionality and or the service life and should be avoided, as stated by Basteskår et al. [2]. A structure's aesthetics is often an appearance criterion to avoid concerns from the casual observer and the users, while tightness is related to functionality and preventing or limiting structure leakage [14]. The durability of a structure is often based on limiting the surface crack width to decrease the ingress of harmful substances that could lead to corrosion of the steel reinforcement, thereby impairing the structure's lifespan and structural capacity [15, 16]. In a typical Serviceability Limit State (SLS) design, the predicted crack width (w_{cr}) determined by a chosen calculation method must be less or equal to a limiting crack width (w_{lim}) dependent on the previously mentioned criteria:

$$w_{\mathrm{lim}} \geq w_{\mathrm{cr}} \tag{1}$$

This thesis focuses on different calculation methods to predict crack widths in standard and large-scale concrete structures subjected to in-plane loading. Large-scale concrete structures are, in this thesis, synonymous with RC structures, which have member dimensions that can be several meters in height, sections with large reinforcing bar (rebar) diameters, and large covers. The investigated calculation methods range from computer-based simulations using Nonlinear Finite Element Analysis (NLFEA) to design code formulations, i.e., Eurocode 2 (EC2, FprEC2, DIN) [4-6], *fib* Model Code (MC2010, MC2020) [7, 8] in addition to the Modified Tension Chord Model (MTCM) [9] and the simplified version of MTCM (SMTCM) proposed in this thesis.

1.2 Objectives and limitations

The main objective of this PhD study is to provide suggestions and recommendations for improved crack width predictions in regular and large-scale concrete structures subjected to bending and axial loading. This will be done by:

- Investigate crack width calculation methods by numerical modelling.
- Investigate the accuracy of the crack width calculation methods in current design codes.
- Formulate a new crack width calculation model that can be used in a design code format.

The work in this PhD study is limited to predicting crack widths mainly caused by bending and axial loading. Cracking caused by volumetric changes in young hardening concrete and hardened concrete, such as plastic shrinkage, plastic settlement, the heat of hydration, internal and external temperature differences within a member and other imposed deformations in general, will not be addressed in particular. Moreover, undeformed rebars and load levels close to the ultimate load capacity will not be addressed in particular, i.e., for steel stresses after the onset of yielding.

1.3 Outline of the thesis

This thesis is written based on four papers, of which three are either published or submitted for journal publication, while one has been published in a conference proceedings. First, the basic concepts of cracking and tension stiffening are discussed. Secondly, a summary of the main findings in the papers is given. Then, the application of the proposed crack prediction model at a design code format is discussed for regular and special RC members. Finally, the main conclusions from the PhD study are drawn before proposing some topics for further research.

2 Cracking and tension stiffening

The basic concepts of cracking and tension stiffening are explained and discussed to provide background and improved understanding of crack width calculations. Over the last decades, several approaches have been developed to predict the crack widths of reinforced concrete members subjected to uniaxial stress states, such as RC beams, ties, and one-way slabs.

2.1 General

When a reinforced concrete member is subjected to tensile loads resulting from external loading or imposed deformations, the concrete member will crack when the tensile strength of concrete is reached. As these cracks develop, the reinforcement bars start to carry more of the applied load across the cracks, while between the cracks, the concrete and the reinforcement interact in a way known as tension stiffening. This effect refers to increased member stiffness due to the transmission of stresses from the reinforcing bar to the surrounding concrete, which gives tension between the cracks, as shown in Figure 1. This interaction is characterized by nonlinear behaviour mainly due to the differences in the stress-strain relationships between the two materials.

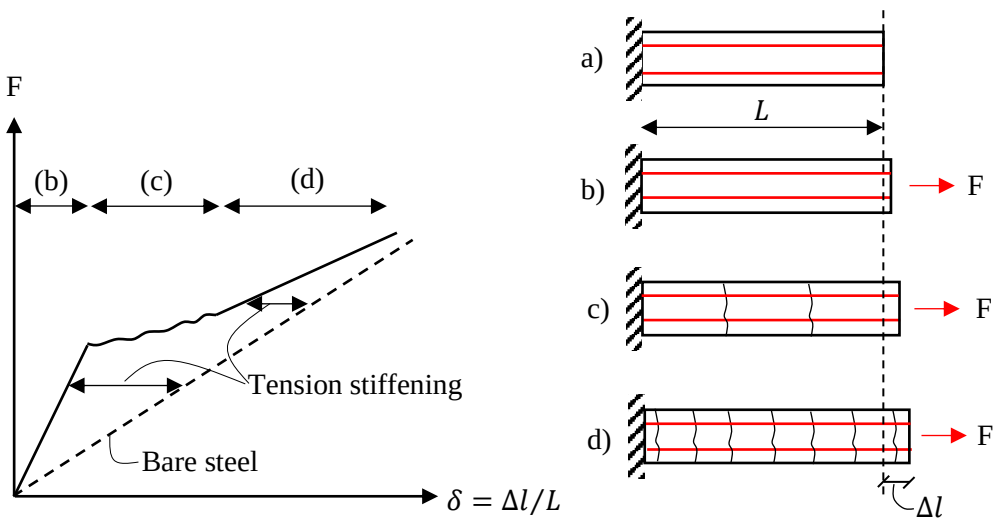

Figure 1 Load-deformation behaviour for an RC member (a) unloaded (b) uncracked (c) first cracks form (d) most cracks have formed.

2.1.1 RC ties, beams and one-way slabs

The concept of cracking and tension stiffening is elucidated by discussing the physical behaviour of RC ties subjected to a tensile force, as shown in Figure 2. It was observed by Goto [17] that the internal cracks along the ribbed reinforcement cause the crack width at the reinforcement interface (w_{int}) to be significantly smaller than that on the concrete surface (w_{surf}). Tammo et. al., [18] concluded that this is a consequence of the interlocking of the bar lugs and the confining concrete, which suggests that the internal cracking behaviour of concrete governs the bond transfer between the reinforcement and concrete.

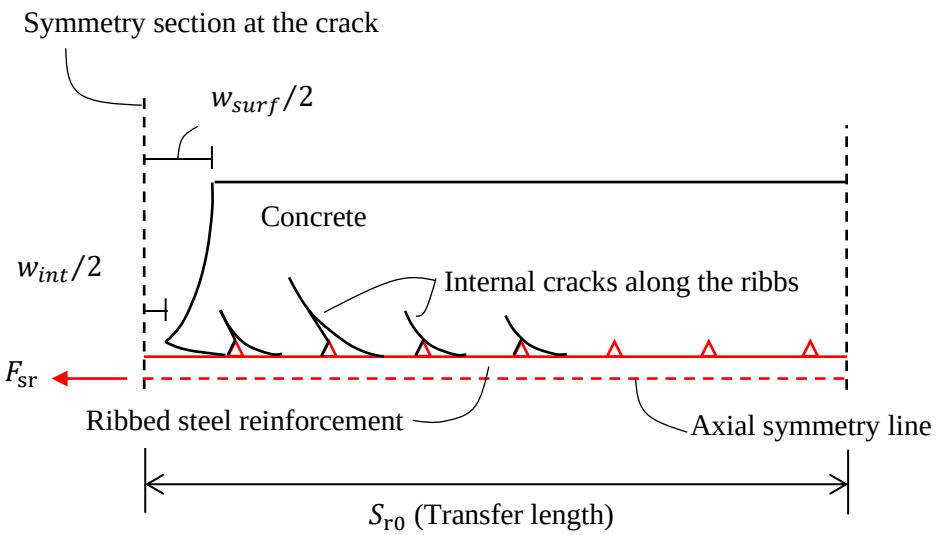

Figure 2 Physical behaviour of cracking for an RC-tie member

A simplification to describe the nonlinear behaviour of the internal cracks depicted in Figure 2 is to assume steel and concrete as elastic materials and smear this behaviour over the interface as springs [7, 19-21]. Doing this implies that the deformation caused by the internal cracks can be simplified to slip occurring between the steel and concrete at an arbitrary section. The investigated design codes in this thesis have implemented this simplification and simplified further by assuming that the bond stress is constant along the transfer length and, thus, independent of both slip and load levels, as shown in Figure 3. On the other hand, the two alternative models, the Modified Tension Chord Model (MTCM) and the Simplified Modified Tension Chord Model (SMTCM) assume that the spring behaviour is known from a bond-slip law yielding a static equivalent section of an arbitrary section in an RC tie, i.e., the bond stress and slip behaviour depend on geometry and load levels. Another important aspect of the crack width calculation

is the location of the predicted crack width, i.e., at the rebar surface or on the surface of the structural member, as there is a significant difference between them. As shown in Figure 4, the MTCM and SMTCM account for this difference by nonlinear elastic strains over the concrete cover height (shear lag) by the factor ψ, which in return affects the mean concrete strains over the cover height, which will affect the equilibrium equations for concrete as shown by Tan et al. [22]. The models use $\psi = 0{,}7$ and results in an increased transfer lengths and consequently an increased crack width at the surface (w_{surf}). The difference in elastic deformation between the steel surface and the concrete surface is neglected and is assumed constant. This means that the value at the interface is the same as the value at the concrete surface of the effective concrete area in tension (w_{eq}).

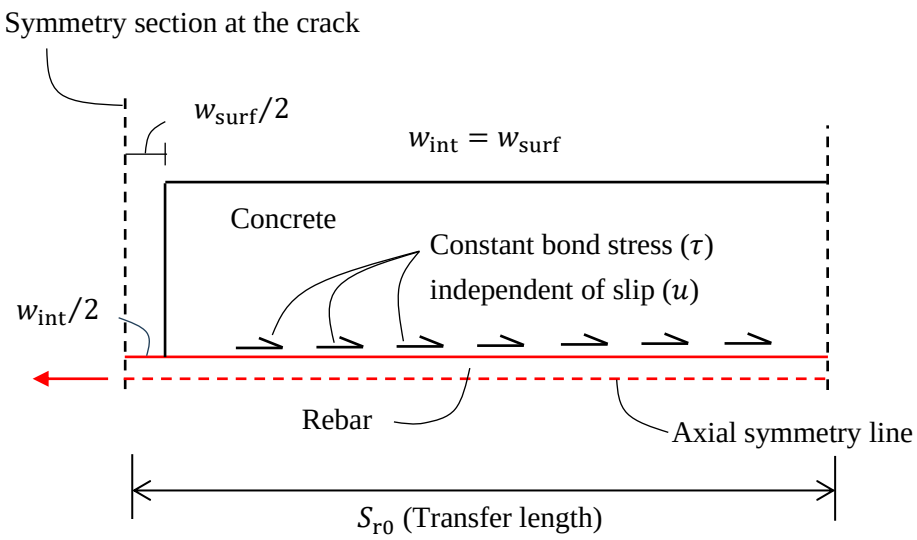

Figure 3 Design code simplifications of the nonlinear behaviour of internal cracking by bond-slip model

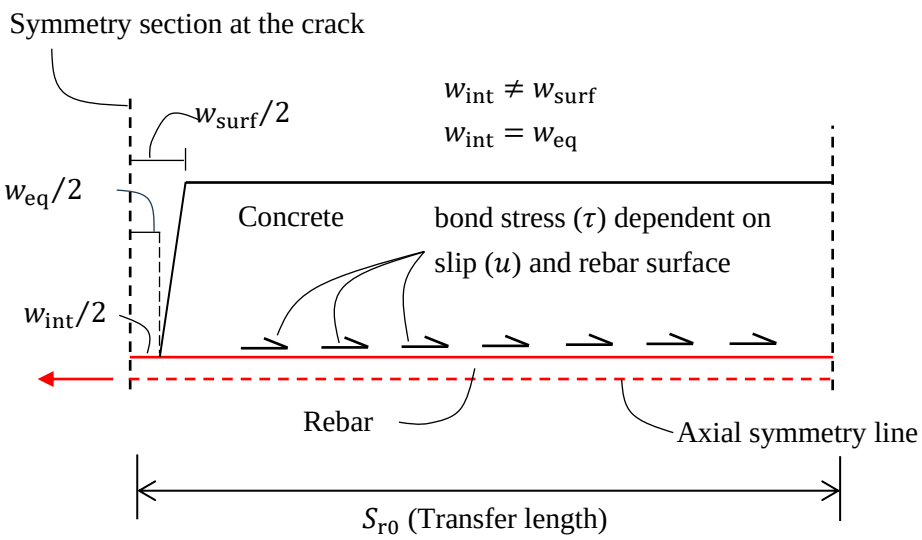

Figure 4 MTCM and SMTCM simplifications of the nonlinear behaviour of internal cracking by bond-slip model

The predicted crack width formulas applied by the design codes EC2, FprEC2, MC2010 and MC2020, except for the German annexe DIN to EC2, yield an increase in the crack width calculation model at the interface (w_{int}) to represent the surface crack width (w_{surf}) by empirical modification, i.e., the cover addition in the crack spacing formulas [1]. The concept is also extended to RC members subjected to bending by assuming that the effective concrete area surrounding the reinforcement is treated as an RC tie. For these cases, the design codes have different approaches for further increasing the surface crack (w_{surf}) due to the difference in stress distributions over the cover height and curvature effects. The crack width locations of the different prediction models are shown in Table 1.

Table 1 Predicted crack width locations

Model	**Description**	
EC2	w_{surf}	At the outermost concrete face
FprEC2	w_{surf}	At the outermost concrete face
MC2010	w_{int}, w_{surf}	At reinforcement height and outermost concrete face.
MC2020	w_{surf}	At the outermost concrete face.
MTCM SMTCM DIN	w_{surf} w_{eq}	At the outermost concrete face and a representative crack width over the surface of the effective tensile area

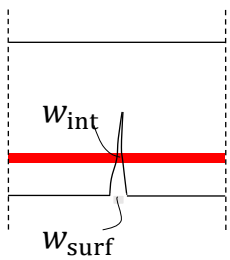

The predicted crack width for all considered models is obtained as the difference between the integrated steel and concrete strains over the crack spacing and can be expressed in its basic form as

$$w_{\mathrm{k}} = S_{\mathrm{r}}(\varepsilon_{\mathrm{sm}} - \varepsilon_{\mathrm{cm}}) \tag{2}$$

where S_{r} is the crack spacing and ($\varepsilon_{\mathrm{sm}} - \varepsilon_{\mathrm{cm}}$) is the strain difference between steel and concrete. The design codes calculate the maximum crack spacing based on equilibrium from the simplified spring behaviour mentioned earlier over a cracked member at a fully stabilized crack stage. However, this crack spacing is also used for lower load levels where the RC members are in a crack formation stage. The strain difference is also calculated by equilibrium from the assumption of constant bond stresses independent of slip, which yields a linear decrease in strains over the cracked section. In contrast, the MTCM and SMTCM use a more detailed simplification of the internal cracking by solving the Second Order Differential

Equation (SODE) for the slip with a bond-slip law acknowledging that the internal cracking is naturally more extensive close to the crack. Therefore, the MTCM and SMTCM can also describe the crack width during a crack formation stage using the concept of Comparative Lightly Loaded Member (CLLM) behaviour, which was previously impossible or at least unclear in the design codes.

3 Summary of papers

3.1 The papers shown in context.

Figure 5 shows an overview of the papers and how they form the overall research approach applied in this PhD study.

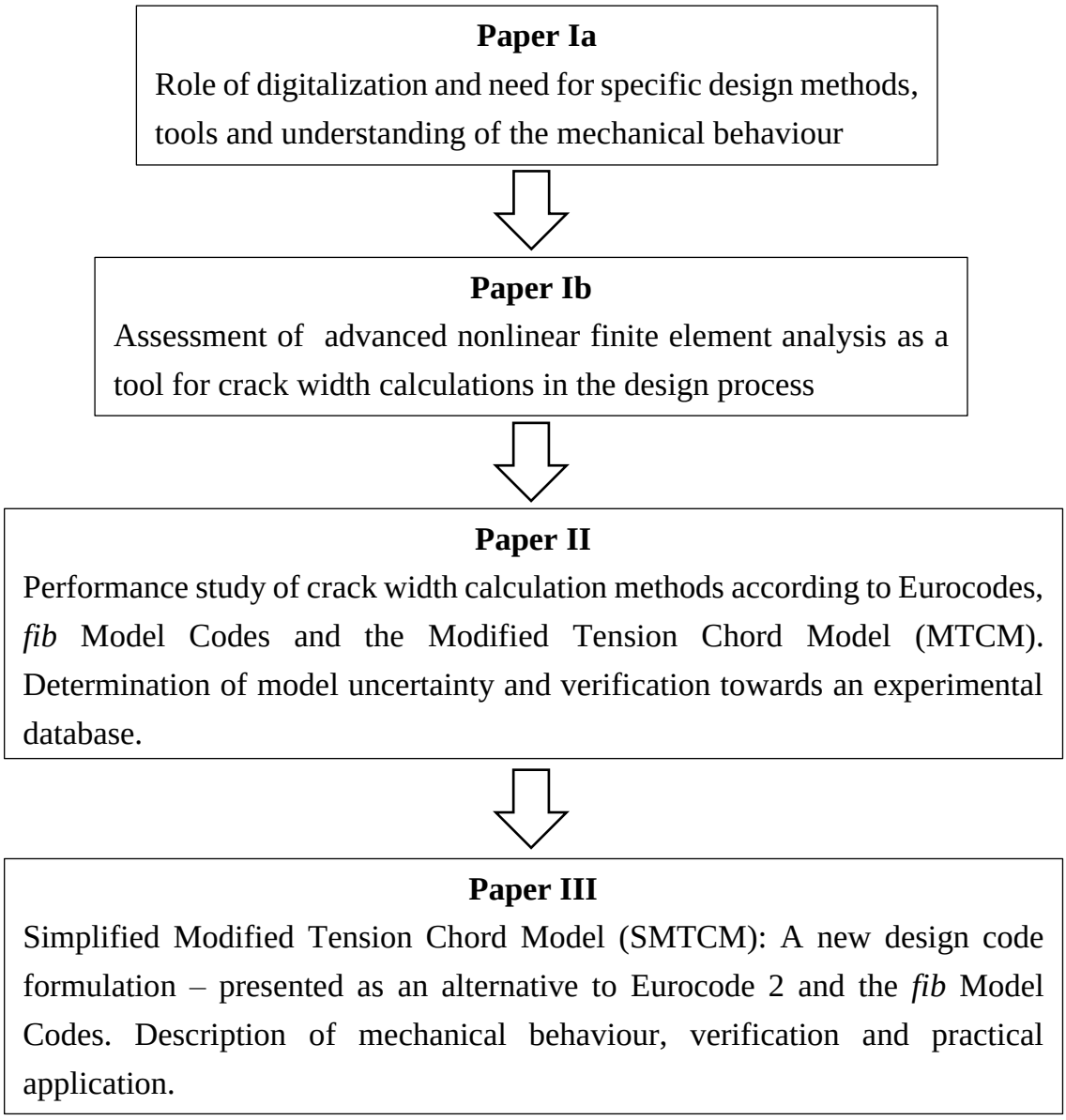

Figure 5 Overall research approach

3.2 Paper Ia

The first paper was co-authored with another PhD candidate funded by the same gross project and investigated the sustainable use of concrete for road infrastructure in a novel industrialized context. The study applied a SWOT analysis (Strengths, Weaknesses, Opportunities, and Threats) related to the frequently used terms Sustainability, Industrialization and Digitalization. The author of this thesis mainly contributed to the industrialization and digitalization part of the article.

This paper's findings related to industrialization and digitalization were that the direct application of Building Information Models (BIM), the growing sophistication of computer programs, increased computer capacity over the years, and decreasing costs give extensive possibilities for improved design and structural optimization. However, a risk when using more advanced software is that complex structures may become too simple to handle in the software's environment. In worst-case scenarios, this may lead to severe faults, reduced service life and structural failures with immense consequences due to a lack of understanding of structural behaviour among engineers. Therefore, engineers must understand and maintain competence within their field. Some advanced structural analysis programs now available for the industry were previously only available in academic environments.

3.3 Paper Ib

This paper investigated the applicability of computer-based simulation using the Finite Element Analysis (FEA) package Abaqus to predict crack widths in reinforced concrete (RC) beams. The main objective was to investigate the accuracy of computational crack widths compared to two beams from an experimental series from the literature with large concrete covers of 63 and 112mm.

The numerical modelling of the RC beams was performed with 3D solid elements and embedded 2D reinforcement rebars where no slip was possible, i.e., a perfect bond between the concrete and the reinforcement. The Concrete Damage Plasticity (CDP) model was applied as a constitutive material model for the concrete. The model describes the behaviour of concrete using scalar damage variables by defining a stress-strain softening curve and fracture energy. In addition, the accuracy of the semi-empirical formulas for predicting crack widths by Eurocode

2 (EC2) [4], the draft for the new EC2 (prEC2) [23] and *fib* Model Code 2010 (MC2010) [7] was investigated.

The results showed that the 3D Nonlinear Finite Element Analysis (NLFEA) with a CDP model correlated well with the experimentally investigated beams. However, predicting crack widths in practical cases by applying advanced NLFEA requires refined assessments of the analysis results, crack strains, crack bandwidth theories, etc., and is very time-consuming compared to a design code formulation that hand calculations can solve. On the other hand, EC2, prEC2 and MC2010 underestimated the crack widths at the outermost concrete face to different extents, while they were conservative if the crack widths at the reinforcement level on the side surface of the beam were considered.

3.4 Paper II

This paper's main objective was to investigate the accuracy of various crack width prediction models and the newly proposed Modified Tension Chord Model (MTCM). For this purpose, a large number of experimental crack widths were collected from the literature, including 203 specimens of reinforced concrete (RC) members subjected to bending and tension. The modelling uncertainty applied to evaluate the methods showed that the *fib* Model Code 2010 and MTCM provided the best crack width predictions of the collected databases. At the same time, *fib* Model Codes [7, 8] and Eurocode 2 [4] contain empirical formulas that violate the basic principles of equilibrium for calculating the maximum crack spacing. In contrast, the MTCM has the fewest mechanical simplifications of the investigated models and no empirical modifications for fitting towards experimental results. However, *fib* Model Code 2010 predicted the crack width reasonably well and is more suited for practical dimensioning than the MTCM.

The findings in this paper suggested that a simplified version of the MTCM should be developed to obtain a code-type formulation that could challenge the current code formulations. The first step for this approach was to obtain a closed-form solution in the case of Comparatively Heavily Loaded Member (CHLM) behaviour by the MTCM, which led to Paper III.

3.5 Paper III

This paper was motivated by the findings in Paper II, and the Simplified Modified Tension Chord Model (SMTCM) was formulated in a design code format to determine a design crack width. The model aims to calculate a decisive design crack with a simple approach that may be implemented in day-to-day structural design- and special-purpose softwares used by the industry. The calculation model was derived using the concept of MTCM for Comparatively Lightly Loaded Members (CLLM) to predict the behaviour in the Comparatively Heavily Loaded Members (CHLM) as a simplification (SCHLM). These concepts are analogous to the terms crack formation stage (CLLM) and the stabilized cracking stage (SCHLM) frequently used in the literature.

The design input for the SMTCM is the steel strain found from structural analysis and section analysis, assuming a cracked stage in addition to the geometry and reinforcement layout of the structural member and the mechanical properties of the material parts. The SMTCM was benchmarked against the experimental database in Paper II, which showed accurate crack width predictions by the model.

4 Application of SMTCM to special cases in practical design

4.1 General formulation of SMTCM

Input to the model is the steel strain (ε_s) found from structural analysis and section analysis assuming a cracked stage in addition to the geometry and the relevant mechanical properties.

Depending on the steel strain ε_s (σ_s/E_s) the structure is in a crack formation stage when $\varepsilon_s < \varepsilon_{s,cr}$ and in the stabilized cracking stage, when $\varepsilon_{s,cr} \leq \varepsilon_s \leq \varepsilon_{s,y}$ where:

$\varepsilon_{s,cr}$	is the steel strain at cracking determined as $\varepsilon_{ctm}(1+\xi)/\psi\xi$.
ξ	is the ratio $\alpha_e \rho_{s,ef}/\psi$.
α_e	is the modular ratio E_s/E_{cm}.
$\rho_{s,ef}$	is the effective reinforcement ratio $A_s/A_{c,ef}$.
ψ	is a constant for the relation between mean concrete strains over the concrete cover height and concrete strains at the steel bar surface at an arbitrary section over the bar length and can be set as 0.7.
ε_{ctm}	is the mean concrete tensile strain limit determined as f_{ctm}/E_{cm}
$\varepsilon_{s,y}$	is the characteristic yielding strain for the reinforcement determined as f_{yk}/E_s.

The calculated surface crack width may be determined as:

$$w_{cal} = S_r(\varepsilon_{sm} - \varepsilon_{cm}) \tag{3}$$

Expressions for S_r and the difference in mean strains ($\varepsilon_{sm} - \varepsilon_{cm}$) are calculated for the respective cracking regime and are shown in Paper III.

4.2 RC members where the regulations may fail

The methods in the regulations typically have a validity range limited to stabilized cracking and cases with a constant moment and constant cross-section over specific lengths. A more general mechanical model for crack width calculations is needed for cases where this doesn't hold. The MTCM and SMTCM might then be better solutions than the code formulations in several cases due to their more

consistent mechanical basis. To show the potential of the models and contribute to discussions and further progress in crack width prediction two examples are considered in the following. However, it should be noted that theoretical deductions and or experimental research are still needed to establish generally accepted solutions for such cases.

4.2.1 Joints between members with different thickness

Eurocode 2 section 7.3.3(4) addresses the particular risks of large cracks occurring in sections where there are sudden changes of stress, e.g. i) at changes of section, ii) near concentrated load, iii) positions where bars are curtailed and iv) areas of high bond stress, particularly at the end of laps. Due to these cases, actions should be taken in such areas to minimize the stress changes wherever possible. However, the calculated design crack width is considered adequate for these situations, provided the rules for detailing reinforcement in sections 8 & 9 are followed. To state that these particular risks are accounted for in the general crack width formula by specifying minimum reinforcement solutions, rebar spacings, rules for joint lengths, etc., is a significant simplification in the author's opinion. A joint between members with different thicknesses is shown in Figures 6 and 9 to highlight cases of i), iii) and iv).

As illustrated in Figure 6, the left side of the crack (w_{k}) will reach a stabilized cracking stage earlier than the right side of the crack. The assumed effective concrete area in tension ($A_{\mathrm{c,ef}}$) for both sides represents the spreading of the bond force from the reinforcement to the surrounding concrete. However, for the situation shown in Figure 6, there will be a difference in the effective area between the two beam members before cracking occurs for each element. The reinforcement at the right side will behave as a pullout bar before the larger beam also cracks, i.e., we may assume that a larger effective tensile zone is acting in the crack formation stage for the same reinforcement stress that brings the left side to the stabilized cracking stage.

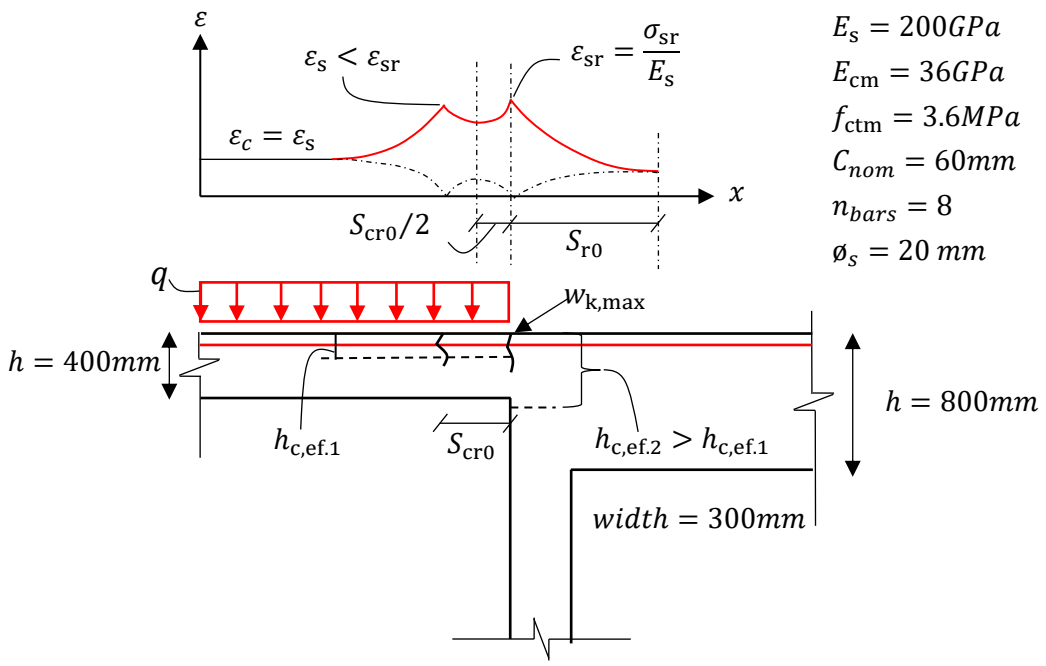

Figure 6 Connection between members with different geometry.

Left side of the crack: Right side of the crack:

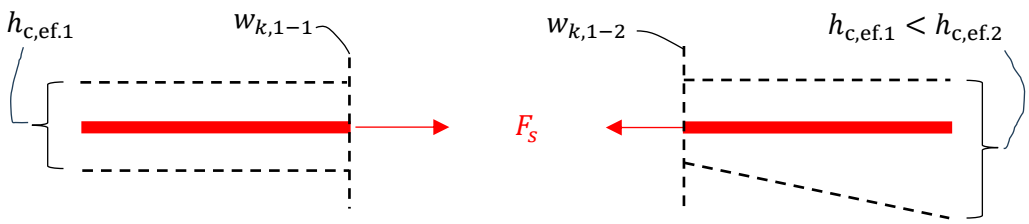

Figure 7 Illustration of the effective concrete area in tension from Figure 6

The effective height of the concrete area surrounding the rebars in tension may be determined as

$$h_{c,ef} = \min\left\{2{,}5\left(c + \frac{ø_s}{2}\right); h - x; \frac{h}{2}\right\} \tag{4}$$

However, for the case shown in Figure 6, this formulation would yield the same effective height for both sides of the joint. Therefore, due to the assumption that the right side of the crack will not crack and, therefore, behave as for a pullout failure, the effective concrete area is taken as half the beam height as a first trial.

The most extensive crack will appear at the intersection between the two members, denoted $w_{\mathrm{k,max}}$ in Figure 6. Using the SMTCM and engineering assumptions of what happens within the effective concrete area in tension when a crack is formed at the intersection between the two members, it is possible to estimate a crack width purely based on mechanical considerations, as shown in Figure 8. The Figure illustrates the effect of varying the height of the effective tensile area on the right side. To further elaborate on the results in Figure 8, the difference between the two different crack width approaches is shown in Table 2. It is seen that the increased height of the effective tensile zone gives up to 19,4% increased crack width.

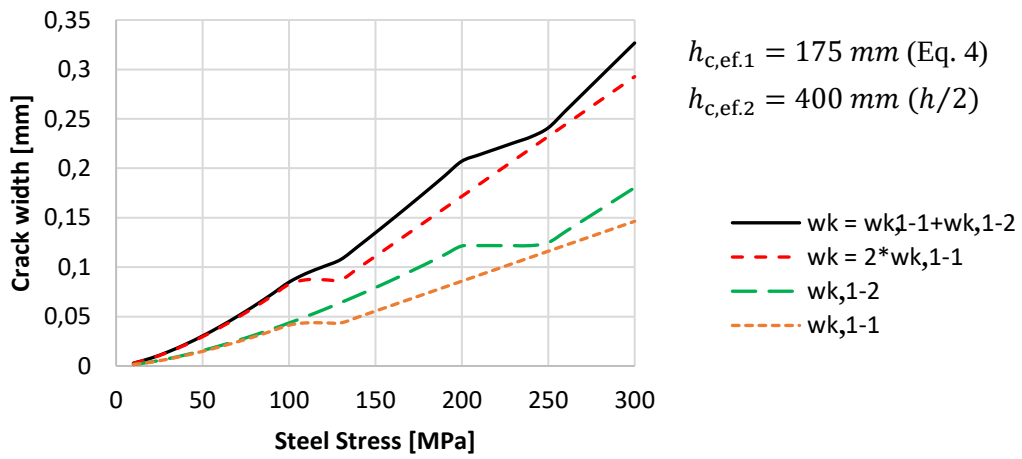

Figure 8: Crack width prediction by SMTCM at the connection between the two members in Figure 6.

Table 2 Difference in crack width between the two solutions from Figure 8

Steel stress	**Crack width $w_{\mathrm{k.max}}$ [mm]**		**Difference**
	$2w_{\mathrm{k.1-1}}$	$w_{\mathrm{k.1-1}} + w_{\mathrm{k.1-2}}$	$\frac{w_{\mathrm{k.1-1}} + w_{\mathrm{k.1-2}}}{2w_{\mathrm{k.1-1}}} - 1$
100	0,083	0,085	2,4 %
110	0,087	0,094	7,4 %
120	0,087	0,101	13,9 %
130	0,087	0,108	19,4 %
140	0,099	0,121	18,2 %
150	0,111	0,135	17,8 %
160	0,123	0,149	17,4 %
170	0,135	0,163	17,2 %
180	0,147	0,177	16,9 %
190	0,159	0,192	17,2 %
200	0,172	0,207	16,9 %

Another important point is that in real cases related to Figure 6, there is often a casting joint with two different reinforcement solutions. Due to the moment

gradient and the double reinforcement solution, as illustrated in Figure 9, the left side of the crack at the construction joint would also yield a situation close to a pullout failure of the intersection. Close to the construction joint, the rebar anchorage length at the section where two rebars are often bundled will influence the bond stress due to the difference in the concrete surrounding each rebar and, in return, influence the transfer length and, implicitly, the crack width.

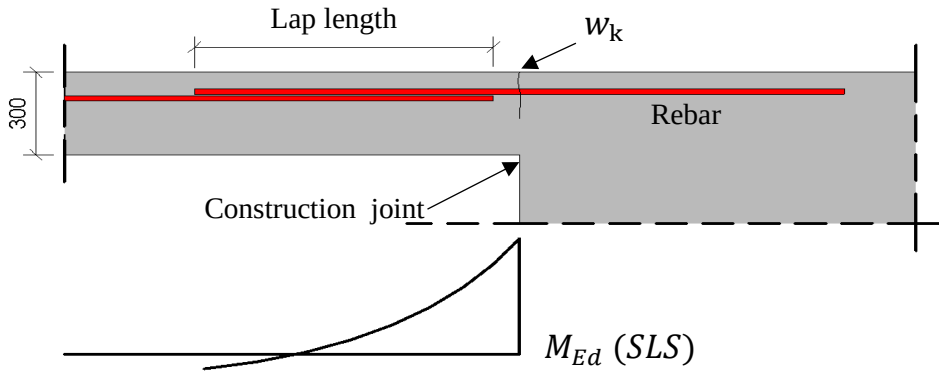

Figure 9 Double reinforced solution and moment gradient at a construction joint.

Using the properties from Figure 6 in Figure 9, assuming pullout behaviour on both sides of the crack would mean that after the initial crack (w_k) in Figure 9, there would be no more cracks along a certain length to each side of the first crack. Therefore, assuming that the effective concrete area in tension is infinite, the crack width can be estimated from and will always remain in the crack formation stage, as highlighted below in Figure 10.

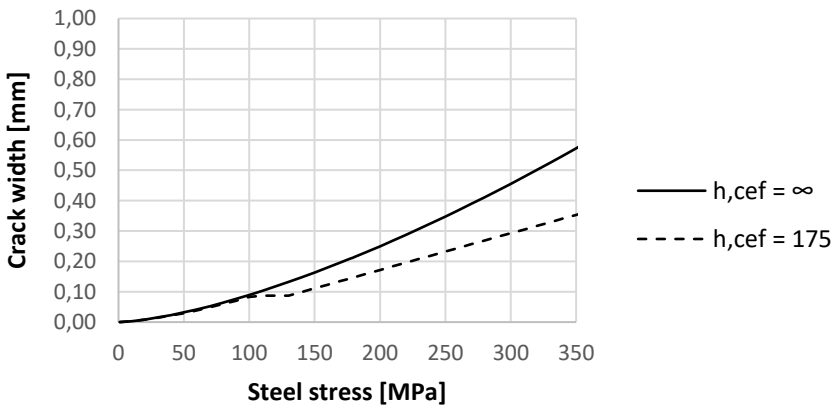

Figure 10 Crack width from the assumption of an infinite concrete area in tension, $\zeta = 1{,}0$.

In addition, there is also a possibility to adjust for the point that the bond stress might be different around the rebar's circumference at the beginning of the joint length and at the mid-section of the joint length, which would result in a longer

transfer length compared to a single rebar, by adjusting the constant χ that transforms the cross-section to an equivalent cross-section and acknowledge that the bond stress is not uniformly distributed over the concrete cover. The factor ζ in Eq. (5) considers the bond stress τ not being constant around the circumference of the steel bar in nonaxisymmetric cases as shown in [22], such as when the cover to steel surface varies in a cross-section or along the lap length of the rebars.

$$\zeta = \frac{\tau_{\mathrm{m}}(u)}{\tau(u,\theta)} \leq 1 \tag{5}$$

where $\tau_{\mathrm{m}}(u)$ is the mean bond stress around the circumference of the steel bars in an arbitrary cross-section, and $\tau(u,\theta)$ is the maximum, as shown in Figure 11.

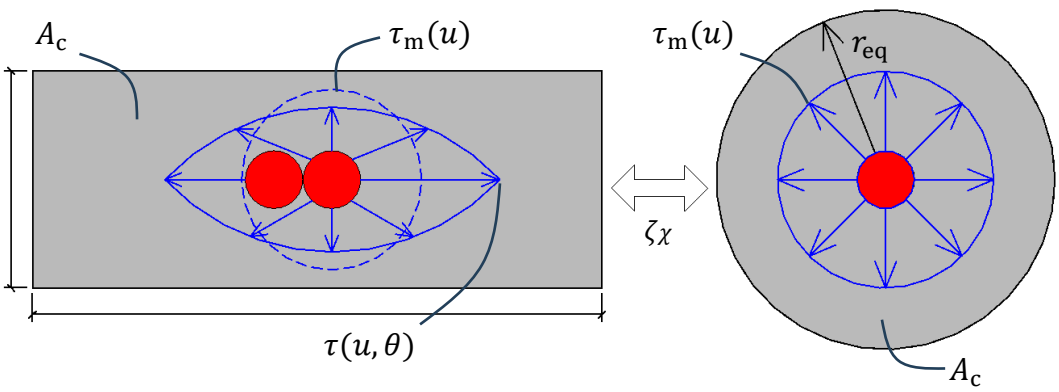

Figure 11 Equivalent cross-section when using the second order differential equation for the slip by SMTCM with a modified value of ζ for two rebars in in a lap length.

For these cases, there would be a need to further investigate the proper value for ζ; however, to highlight the effect, the parameter ζ is now reduced from 1,0 to 0,5, as shown in Eq. (6) and Figure 13.

$$\chi_{0.5} = \zeta\chi = 0{,}5\left(\frac{\sum \pi\phi_{\mathrm{s}}}{A_{\mathrm{s}}E_{\mathrm{s}}}(1+\xi)\right) \tag{6}$$

The difference in bond stress around the rebar's circumference increases the transfer length along the joint length for the assumption of an infinite concrete area in tension, as shown in Figure 12.

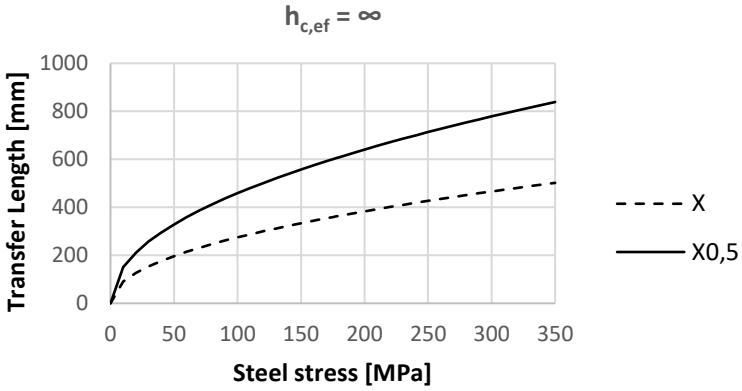

Figure 12 Increase of transfer lengths due to the difference in bond stress along the circumference of the rebars along the joint length.

Following up the increased transfer length in Figure 12, Figure 13 shows the corresponding increase in crack widths.

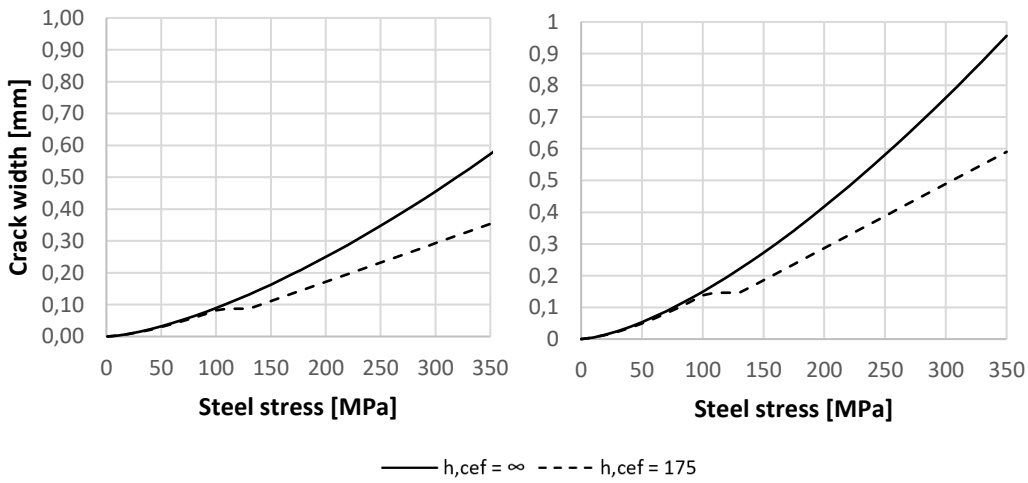

(a) (b)

Figure 13 Crack width assuming (a) $\zeta = 1{,}0$ and (b) $\zeta = 0{,}5$.

The examples presented in Figure 6 and Figure 9 show that the SMTCM can be used to calculate crack width for special RC members. However, more research is needed for actual cases and different reinforcement solutions to establish generally accepted solutions for these types of problems.

4.2.2 Large cross-sections in bending with several reinforcement layers

Solutions with large covers and large rebars placed in several layers are quite common in exposed large concrete structures. In the case of significant bending moments, the steel stresses in the rebar layers may vary extensively due to the need for large spacing between the layers. The assumed effective concrete area in

tension ($A_{c,ef}$) is influenced by the spreading of the bond force from the reinforcement to the surrounding concrete. In the calculations, the reinforcement area will vary depending on the applied effective tensile area, as shown in Figure 16.

To highlight and discuss the benefit of using SMTCM as a design code for large-cross sections with several reinforcement layers, a real case from a culvert on E18, "the west corridor, E102 Fornebukrysset" in Oslo, is shown below. For this cross-section and the given load case, a refined crack width control by EC2 and FprEC2 required a three-layer reinforcement solution.

Table 3 Geometrical and material properties of the investigated real structural member

Cross-section height	$\boldsymbol{h = 700\ mm}$	**Mean tensile strength**	$\boldsymbol{f_{\mathrm{ctm}} = 3,8\ MPa}$
Cross-section width	$b = 1000\ mm$	**Young's modulus concrete**	$E_{\mathrm{cm}} = 36,28\ GPa$
Rebar bottom	$ø = 32\ mm$	**Young's modulus steel**	$E_{\mathrm{s}} = 200\ GPa$
Rebar top	$ø = 40\ mm$	**Allowable crack width** [1)]	$w_{\mathrm{k,lim}} = 0,39\ mm$
Concrete cover	$c = 90\ mm$		

[1)] *According to NS-EN 1992-1-1*

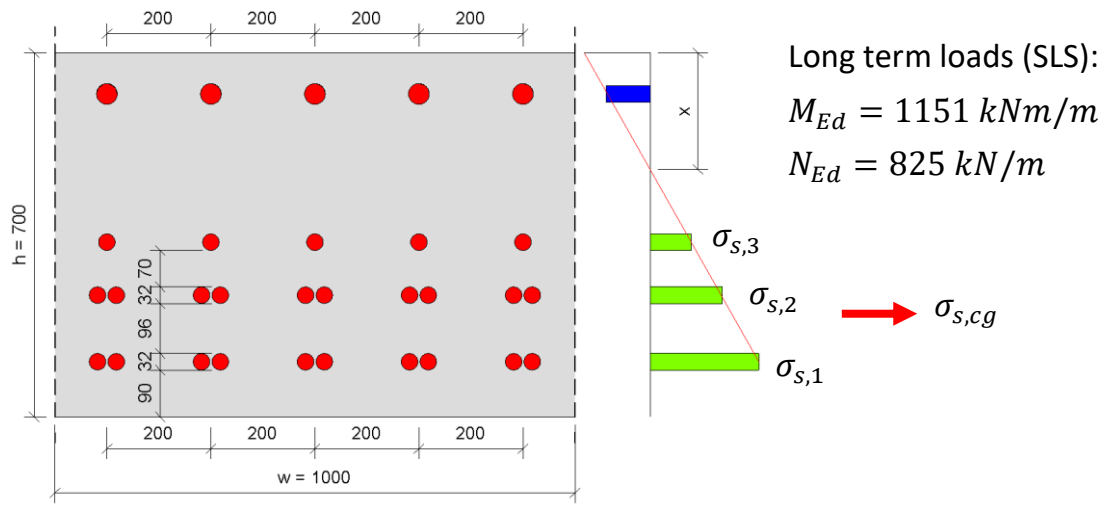

Figure 14 Reinforced cross-section of 1-meter width with three layers of tensile reinforcement (in scale drawing)

Table 4 Calculated steel stresses in the three different rebar layers

	$\boldsymbol{\sigma_{s,1}}$	$\boldsymbol{\sigma_{s,2}}$	$\boldsymbol{\sigma_{s,3}}$	$\boldsymbol{\sigma_{s,cg}}$ [1)]
		MPa		
One layer	331	-	-	-
Two layers	220	148	-	196
Three layers	209	139	79	166

[1)] *Steel stress in the tensile reinforcement centre of gravity*

EC2 determines the effective tensile zone height as:

$$h_{\mathrm{c,ef}} = min\left(2{,}5(h-d)\,; \frac{h-x}{3}\,;\, \frac{h}{2}\right) \tag{7}$$

while FprEC2 applies:

$$h_{\mathrm{c,ef}} = min\big(min\big(a_{\mathrm{y}} + 5ø; 10ø; 3{,}5a_{\mathrm{y}}\big) + (n-1)s_{\mathrm{y}}; h-x\big) \tag{8}$$

where a_{y} is the distance from the surface to the middle of the outermost reinforcement layer and s_{y} is the centre distance between the rebar layers.

For SMTCM applied to large RC members in bending with multilayered reinforcement and large vertical distances between them, two alternative proposals for the effective height are investigated:

1) $h_{\mathrm{c,ef}} = min(2{,}5(h-d)\,; h-x\,)$ (9)

2) $h_{\mathrm{c,ef}} = h_{\mathrm{c,ef}} = min(2{,}5(c + ø_{ekv}/2)\,; h-x\,)$ (10)

Where $ø_{ekv}$ is calculated as shown in paper III and EC2 [4]. The first alternative $h_{\mathrm{c,ef}} = 2{,}5(h-d)$ might be criticized because the bond stresses around each rebar layer will vary significantly due to the large vertical distances between the reinforcement layers compared to the cross-section height. The crack spacing will probably be mainly influenced by the stress situation around the rebar layer closest to the tensioned surface, as illustrated in Figure 15. On the other hand, the crack width will also vary depending on the distance from the rebar surface, as shown in Paper III. Adding additional rebar layers with a relatively large distance to the most tensioned surface might, therefore, in practice, only contribute to smaller crack widths through the stress reduction in the rebar layers.

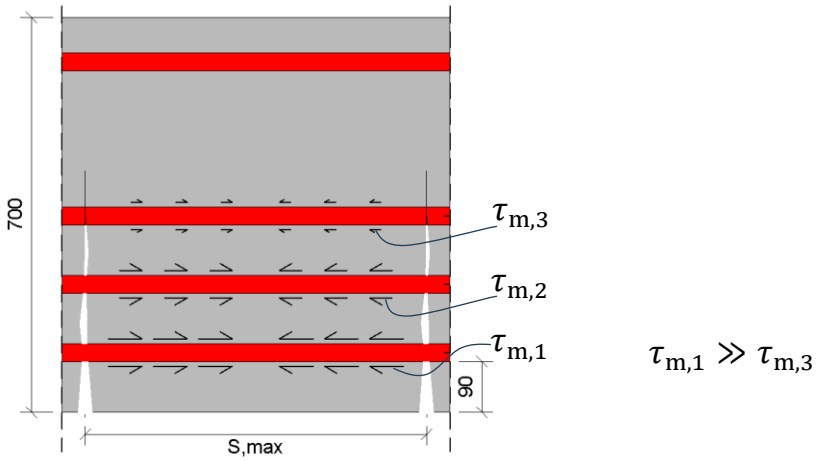

Figure 15 In scale illustration of variation of mean bond stress distribution over the crack spacing for the multilayered cross-section in Figure 14

Another possible solution that would acknowledge that the crack spacing is mainly influenced by the rebar layer closest to the most tensioned surface is to determine the effective height based on Eq. (11):

$$h_{\mathrm{c,ef}} = min\left(a_{\mathrm{y}} + \frac{ø_{ekv} + s_{\mathrm{y}}}{2}\ ; h - x\right) \tag{11}$$

This formulation will, however, not account for the fact that the bond stress distribution around each rebar layer will affect the crack width. The effective height ($h_{\mathrm{c,ef}}$) calculated by EC2, FprEC2 and the two alternatives for SMTCM are visualized in the correct scale in Figure 16. As seen in Figure 16b and Table 5, the effective height by FprEC2 [23] in the case of three-layer reinforcement increases the effective height to include all three rebar layers. The SMTCM accounts for the effect of cover in Eq. (9) & (10) by increasing the concrete area confining the rebars, which increases the crack spacing and, implicitly, the crack width. The effective height predicted by Eq. (11) is considerably smaller than predicted by alternative 1) and 2).

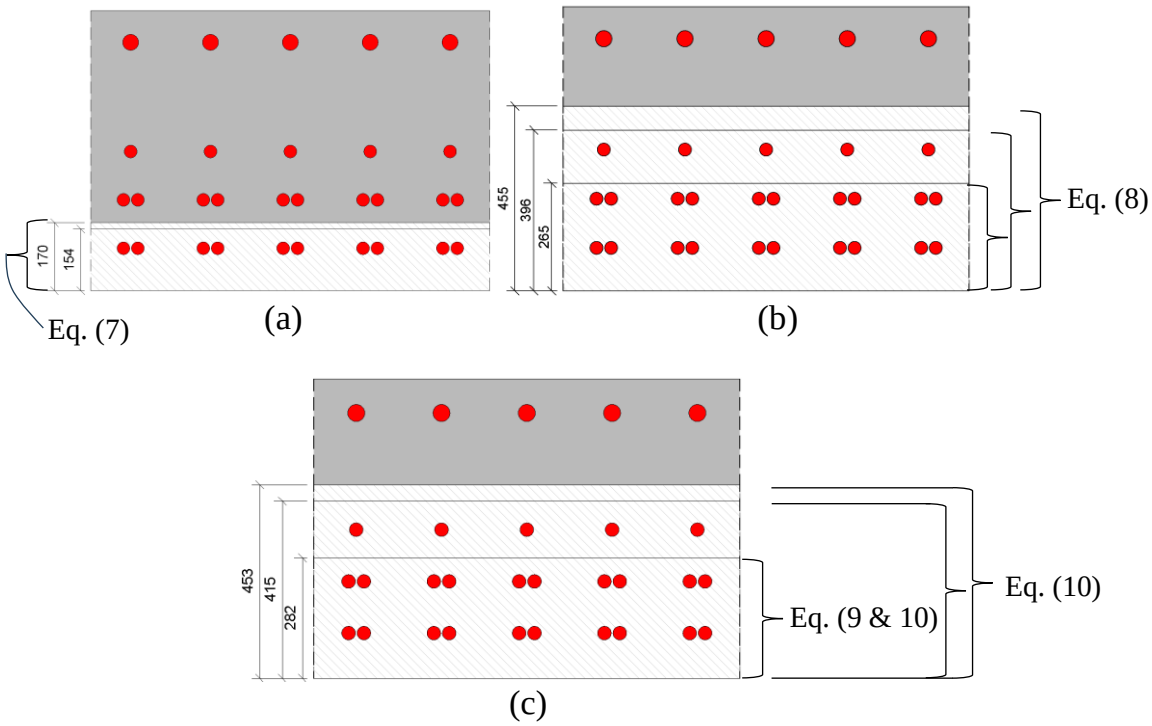

Figure 16 Effective height for three different reinforcement layers by (a) EC2, (b) FprEC2 and (c) SMTCM

As shown in Table 5, for a reinforcement solution of one layer, the crack width limit is exceeded for EC2 by 74%, FprEC2 by 79%, and SMTCM by 92%. For two rebar layers, the crack width in EC2 is exceeded by 5% and with FprEC2 by 8%. On the other hand, by applying SMTCM with Eq. (10) to calculate the effective height ($h_{\mathrm{c,ef}}$) based on the size of the cover, the crack width limit is not exceeded, while with $h_{\mathrm{c,ef}}$ based on the effective depth in Eq. (9), the limit is exceeded by 31%. However, this is reduced to 10% by using the steel stress in the centre of gravity ($\sigma_{\mathrm{s,cg}}$) instead of the stress in the rebar layer closest to the tensioned surface ($\sigma_{s,1}$). For the solution with three rebar layers, all models yield a crack width within the limit. From Table 6, it can be seen that SMTCM with $h_{\mathrm{c,ef}}$ from Eq. (11) gives crack widths comparable to the other alternatives for solutions with one or two reinforcement layers and the lowest crack widths for the solution with three reinforcement layers.

Table 5 Calculated crack width by EC2, FprEC2 and SMTCM for three alternative reinforcement solutions

	Model	σ_s [MPa]	h_{ef} [mm]	A_s [mm^2]	ρ_{ef} [%]	w_k [mm]	$w_k/w_{k.lim}$
One layer	EC2	331	170	8042	4,7	0,68	1,74
	FprEC2		266		3,0	0,70	1,79
	SMTCM		282(1)(2)		2,9	0,75	1,92
Two layers	EC2	220	154	8042	5,2	0,41	1,05
	FprEC2		396	16085	4,1	0,42	1,08
	SMTCM		415(1)		1,9	0,51	1,31
			282(2)		2,9	0,38	0,97
		196*	415(1)		1,9	0,43	1,10
Three layers	EC2	209	151	8042	5,3	0,39	1,00
	FprEC2		455	20106	4,4	0,37	0,95
	SMTCM		453(1)	20106	2,2	0,36	0,92
			282(2)	16085	2,9	0,34	0,87
		165*	453(1)	20106	2,2	0,26	0,67

(1) $h_{c,ef}$ calculated by Eq. (9)
(2) $h_{c,ef}$ calculated by Eq. (10)
* Steel stress is taken at the centre of gravity of the stress distribution

Table 6 Calculated crack width by SMTCM for three alternative reinforcement solutions and $h_{c,ef}$ by Eq. (11)

No. Layers	Model	σ_s [MPa]	h_{ef} [mm]	A_s [mm^2]	ρ_{ef} [%]	w_k [mm]	$w_k/w_{k.lim}$
One	SMTCM	331	170	8043	2,4	0,78	1,92
Two		220				0,41	1,05
Three		209				0,24	0,62

The MTCM and SMTCM have previously, in papers II & III, been proven to yield accurate crack width predictions for cross-sections with large rebars and covers, which show their potential as a mechanical crack width model with extensive application possibilities in RC structures. However, the choice of the effective concrete area in tension significantly impacts the crack width calculations, as shown in Table 5 and Table 6. The experimental database included in papers II & III does not include RC members with several rebar layers and large distances between them; therefore, the problem of determining the accuracy of the MTCM and SMTCM in these cases should be further investigated.

Perhaps the most reasonable solution is to account for the significant difference in steel stress for each layer and the bond stress distribution by calculating $h_{c,ef}$ from

Eq. (10) and using the steel stress in the centre of gravity ($\sigma_{s,cg}$) for the rebar layers instead of at the rebar layer closest to the tensioned surface. This is supported by the fact that there is a significant difference between the tensile forces for large cross-section heights calculated by linear or nonlinear analysis stress distribution, which also will affect the height of the effective concrete area in tension, as shown by Tue et al. [24] and illustrated in Figure 17.

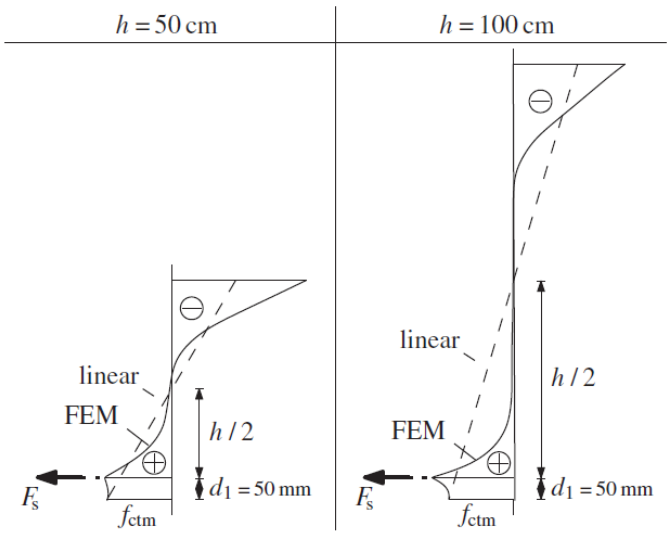

Figure 17 Stress distribution in the effective tensile area for flexural members with different member thicknesses, reprint from [24]

With this in mind, the SMTCM should be taken seriously as an alternative method to be implemented in the national annexe to EC2 to complement the current crack width calculation, which could potentially have a significant economic and environmental impact. However, there is a need to determine the calculation procedure for the effective concrete height for cases of large cross sections, covers and rebars in addition to a significant difference in steel stresses as discussed above.

5 Conclusions

The growing sophistication of computer programs, increased computer capacity and decreasing costs give extensive possibilities for improved design and structural optimization. It is now possible to predict accurate crack widths by computational modelling with programs previously only available in academic institutions, as shown in Paper Ib by Nonlinear Finite Element Analysis (NLFEA) using the Concrete Damage Plasticity (CDP) model. The model describes the behaviour of concrete using scalar damage variables by defining a stress-strain softening curve and fracture energy. However, predicting crack widths by NLFEA is time-consuming and requires a lot of implicit choices by the user and refined assessments of the analysis compared to linear analysis and standard hand calculations. As discussed in Paper I, there is also an additional risk when using more advanced software because complex structures may become too simple to handle in the software's environment. In worst-case scenarios, this may lead to severe faults, reduced service life and structural failures with immense consequences due to a lack of understanding of structural behaviour among engineers.

In the second journal paper (Paper II), a performance study of the crack width calculation methods recommended by Eurocode 2 (EC2), *fib* Model Codes (MC2010 & 2020), and the German National Annex (DIN) to EC2 showed that these models might predict crack widths inconsistently:

The models showed non-conservative crack width predictions for RC beams in bending. In contrast, the Modified Tension Chord Model (MTCM) gave the best crack width predictions regarding the mean values for the modelling uncertainty, but the results were still to the conservative side. MC2010 yielded the best crack width predictions for slabs in bending, while EC2, FprEC2, MC2020 and DIN underestimated the crack width to around the same extent as for beams in bending. For RC-ties in tension, all the investigated models predicted crack widths with reasonable accuracy except for EC2, which overestimated the crack widths to a large extent.

From paper III presenting the simplified code type model (SMTCM), the following conclusions may be drawn:

The proposed Simplified MTCM (SMTCM) gave accurate crack width predictions for beams in bending, RC ties in tension and slabs in bending. The more consistent mechanical basis of SMTCM yields crack width predictions close to reality without empirical calibration, indicating a broader range of applicability than the design codes, for instance, large covers and RC ties having various rebar configurations. In addition, depending on the rebar diameter and the concrete cover, the measured crack width on the surface of an RC member is not always representative of the crack width profile at the location of the reinforcement. The experimental observations showed that the crack width profile for an RC tie with a rebar diameter of 20mm, 90 mm concrete cover and a steel stress of 231 MPa did not reach the reinforcement but had a significant surface crack of 0,33 mm. Therefore, limiting a design crack width on a surface in a specific direction may not be the best approach for cases with large concrete covers. In contrast, the SMTCM yields a design crack width representative over the surface of the effective concrete area in tension.

6 Recommendations for future research

The work in this thesis facilitated a simplified calculation model capable of predicting crack widths in large-scale concrete structures subjected to bending and axial loading for SLS design. However, there is still a need for improvement, and my recommendations for future research are:

- Investigate experimentally and theoretically with nonlinear finite element analysis alternative approaches for the effective concrete area in tension to be used by MTCM and SMTCM for large concrete sections with multiple rebar layers. An RC member in bending will have a significant difference in the stress distribution in large cross-sections calculated by linear or nonlinear analysis.
- Evaluate the crack width prediction accuracy of the MTCM and SMTCM for structural members with special geometry, for example, retaining walls and their connection towards the foundation by experimental data and NLFEA.
- Investigate the distribution of bond stress over the rebar's joint lengths to adjust the factor ζ which accounts for the fact that the bond stress distribution around the circumference of the rebars is not uniformly distributed.
- Develop a solution procedure and investigate the accuracy of crack width calculations applying SMTCM for cases where imposed deformations are decisive. In particular, restrained deformations in combination with static loads, as the simplification by the design codes of constant bond stress and a lower bound for the difference in steel and concrete strains, might not capture the behaviour correctly for when the cracked member is expected to remain in the crack formation stage, which could potentially cause a considerable underestimation of the crack widths. The SMTCM gives a consistent formulation for when an RC member is in a crack formation stage through the concept of *Comparatively Lightly Loaded Members* (CLLM), where the transfer lengths vary as a function of the stress level, geometry and material parameters and the stabilized cracking stage by the concept of *Simplified Comparatively Heavily Loaded Members* (SCHLM).
- Investigate the durability of large rebars with large concrete covers from ingress of harmful substances for cases shown in Paper III.

- Investigate how the influence of tensile strength on generating a random crack pattern can be accounted for in the SMTCM/MTCM, as it significantly influences the cracking behaviour in real-life structures.
- Investigate how the bond-slip parameters can be modified to make the SMTCM/MTCM valid for steel fibre-reinforced concrete (SFRC) or other new materials.
- Use the content of this thesis as a basis for developing nationally determined parameters in FprEC2 for crack width predictions. In addition, the SMTCM can be implemented as a possible crack width calculation model in the relevant Norwegian Public Road Administration handbooks.

List of notations

A_{s}	Area of rebars
E_{c}	Youngs modulus concrete
E_{c}	Youngs modulus steel
E_{c}	Tensile strength of concrete
c	Concrete cover
h	Height of section
$h_{\mathrm{c,ef}}$	Effective height surrounding rebars in the tensile zone
$A_{\mathrm{c,ef}}$	The effective concrete area surrounding rebars in the tensile zone
S_{r0}	Transfer length in the crack formation stage
S_{cr0}	Crack spacing in the stabilised cracking stage
F	Force in the rebar
w_{k}	Crack width predicted at the concrete surface
w_{surf}	Crack width at the concrete surface
w_{int}	Crack width at the interface
w_{eq}	Crack width at the surface over the surface of the equivalent concrete area in tension
x	Height of the concrete compression zone
σ_{s}	Steel stress
$\sigma_{\mathrm{s,cg}}$	Steel stress in the centre of gravity
τ_{m}	Mean bond stress at the interface
ϕ_{s}	Rebar diameter
ϕ_{n}	Number of rebars
ρ_{ef}	Reinforcement ratio
ε_{s}	Steel strains
ε_{c}	Concrete strains
$\varepsilon_{\mathrm{sr}}$	Steel strains at the crack
$\varepsilon_{\mathrm{cm}}$	Mean concrete strains at the interface
$\varepsilon_{\mathrm{sm}}$	Mean steel strains at the interface

List of references

[1] O. Terjesen, G. Pinto, T. Kanstad, and R. Tan, "Performance study of crack width calculation methods according to Eurocodes, fib model codes and the modified tension chord model," *Structural Concrete*, vol. n/a, no. n/a, doi: https://doi.org/10.1002/suco.202300367.

[2] M. Basteskår, M. Engen, T. Kanstad, and K. T. Fosså, "A review of literature and code requirements for the crack width limitations for design of concrete structures in serviceability limit states," *Structural Concrete*, vol. 20, no. 2, pp. 678-688, 2019, doi: https://doi.org/10.1002/suco.201800183.

[3] M. Basteskår, M. Engen, T. Kanstad, H. Johansen, and K. T. Fosså, "Serviceability limit state design of large concrete structures: Impact on reinforcement amounts and consequences of design code ambiguity," *Engineering Structures*, vol. 201, p. 109816, 2019/12/15/ 2019, doi: https://doi.org/10.1016/j.engstruct.2019.109816.

[4] "CEN. EN 1992-1-1, Eurocode 2: Design of Concrete Structures—Part 1-1: General Rules and Rules for buildings. Brussels: European Committee for Standardization; 2004.."

[5] "CEN-TC 250-SC 2_N2049_FprEN_1992-1-1 as submitted to CEN-TC 250 for FV " 2022.

[6] "DIN: EN-1992-1-1/NA. 2011-01, National Annex – Nationally determined parameters – Eurocode 2: Design of concrete structures – Part 1-1: General rules and rules for buildings; 2011.."

[7] *fib Model Code for Concrete Structures 2010*, Berlin: International Federation for structural concrete, 2013.

[8] "2nd Draft of ModelCode 2020 - December," 2022.

[9] R. Tan, "Consistent crack width calculation methods for reinforced concrete elements subjected to 1D and 2D stress states A mixed experimental, numerical and analytical approach," Philosophiae Doctor, Department of Structural Engineering, Norwegian University of Science and Technology, 2019. [Online]. Available: http://hdl.handle.net/11250/2607051

[10] A. Caldentey, J. Bellod, L. Torres, and T. Kanstad, "Serviceability Limit States according to the new Eurocode 2 proposal: Description and justifications of the proposed changes," *Hormigón y Acero*, 01/26 2023, doi: 10.33586/hya.2023.3104.

[11] A. Caldentey, R. Garcia, V. Gribniak, and A. Rimkus, "Tension versus flexure: Reasons to modify the formulation of MC 2010 for cracking," vol. 21, pp. 2101-2123, 09/30 2020, doi: 10.1002/suco.202000279.

[12] A. Pérez Caldentey, H. Corres Peiretti, J. Peset Iribarren, and A. Giraldo Soto, "Cracking of RC members revisited: influence of cover, ϕ/ρs, ef and stirrup spacing – an experimental and theoretical study," *Structural Concrete*, vol. 14, no. 1, pp. 69-78, 2013, doi: https://doi.org/10.1002/suco.201200016.

[13] F. Leonhardt, "Cracks and Crack Control in Concrete Structures," *Pci Journal*, vol. 33, pp. 124-145, 1988.
[14] B. AW., *Corrosion of reinforcing steel in concrete and its relation to cracking*. 1978, pp. 77-81.
[15] S. Robuschi, O. L. Ivanov, M. Geiker, I. Fernandez, and K. Lundgren, "Impact of cracks on distribution of chloride-induced reinforcement corrosion," *Materials and Structures*, vol. 56, no. 1, p. 7, 2022/12/30 2022, doi: 10.1617/s11527-022-02085-6.
[16] D. Schlicke, E. M. Dorfmann, E. Fehling, and N. V. Tue, "Calculation of maximum crack width for practical design of reinforced concrete," *Civil Engineering Design*, vol. 3, no. 3, pp. 45-61, 2021, doi: https://doi.org/10.1002/cend.202100004.
[17] G. Yukimasa, "Cracks Formed in Concrete Around Deformed Tension Bars," *ACI Journal Proceedings*, vol. 68, no. 4, 4/1/1971, doi: 10.14359/11325.
[18] K. Tammo and S. Thelandersson, "Crack Behavior near Reinforcing Bars in Concrete Structures," *ACI Structural Journal*, vol. 106, pp. 259-267, 05/01 2009.
[19] G. Russo and F. Romano, "Cracking Response of RC Members Subjected to Uniaxial Tension," *Journal of Structural Engineering*, vol. 118, no. 5, pp. 1172-1190, 1992, doi: doi:10.1061/(ASCE)0733-9445(1992)118:5(1172).
[20] G. L. Balázs *et al.*, "Design for SLS according to fib Model Code 2010," *Structural Concrete*, vol. 14, no. 2, pp. 99-123, 2013, doi: https://doi.org/10.1002/suco.201200060.
[21] K. Salah, "Cracking analysis of reinforced concrete tensioned members," *Structural Concrete*, vol. 7, pp. 111-116, 01/09 2006, doi: 10.1680/stco.2006.7.3.111.
[22] R. Tan, M. A. N. Hendriks, M. Geiker, and T. Kanstad, "Analytical Calculation Model for Predicting Cracking Behavior of Reinforced Concrete Ties," *Journal of Structural Engineering*, vol. 146, no. 2, p. 04019206, 2020. [Online]. Available: https://ascelibrary.org/doi/abs/10.1061/%28ASCE%29ST.1943-541X.0002510.
[23] "CEN-TC250-SC2-WG1_N1296_FprEN_1992-1-1_e_stf_2022-07-24 FIN clean," 2022.
[24] N. V. Tue, E. Fehling, D. Schlicke, and C. Krenn, "Crack width verification and minimum reinforcement according to EC 2: Current model with specifications in Germany and Austria vs proposal for revision," *Civil Engineering Design*, vol. 3, no. 5-6, pp. 210-228, 2021, doi: https://doi.org/10.1002/cend.202100045.

Paper I - III

Paper Ia

Use of Concrete for Road Infrastructure: A SWOT Analysis Related to the three Catchwords Sustainability, Industrialisation and Digitalisation.

Larsen, I. L., Terjesen, O., Thorstensen, R. T., & Kanstad, T. (2019).

© Article authors. This is an open-access article distributed under the Creative Commons Attribution-NonCommercial-NoDerivs license. (http://creaticecommons.org/licenses/by.ncnd/3.0/).

Nordic Concrete Research – Publ. No. NCR 60 – ISSUE 1 / 2019 – Article 3, pp. 31-50, DOI: https://doi.org/10.2478/ncr-2019-0007

---

sciendo

Nordic Concrete Federation

© Article authors. This is an open access article distributed under the Creative Commons Attribution-NonCommercial-NoDerivs license. (http://creaticecommons.org/licenses/by.nc-nd/3.0/).

ISSN online 2545-2819
ISSN print 0800-6377

DOI: 10.2478/ncr-2019-0007

Received: March 31, 2019
Revision received: June 14, 2019
Accepted: June 18,2019

Use of Concrete for Road Infrastructure: A SWOT Analysis Related to the three Catchwords Sustainability, Industrialisation and Digitalisation

Ingrid Lande Larsen, M.Sc.
PhD Research Fellow, University of Agder
Jon Lilletuns vei 9,
4879 Grimstad
ingrid.larsen@uia.no

Otto Terjesen, M.Sc.
PhD Research Fellow, University of Agder
Jon Lilletuns vei 9,
4879 Grimstad
otto.terjesen@uia.no

Rein Terje Thorstensen, M.Sc.
Professor, University of Agder
Jon Lilletuns vei 9,
4879 Grimstad
rein.t.thorstensen@uia.no

Terje Kanstad, Ph.D.
Professor, Norwegian University of Science and Technology
Richard Birkelands vei 1A,
7491 Trondheim
terje.kanstand@ntnu.no

ABSTRACT
This paper aims at identifying the direction for more sustainable development of the use of concrete in road infrastructure in an industrialised context.

The increase in the global mean temperature is one of the most severe challenges today. The concrete industry is responsible for significant emissions of greenhouse gases, most attributable to cement production. However, concrete is one of the most important building materials in the world and indispensable for the societal development in countries at all development stages. Thus, the concrete industry needs to take measures for reducing emissions.

This paper investigates possible directions for the development of the concrete industry, to reduce climatic impact and accommodate positive societal growth. The investigation is carried out as a SWOT analysis, focusing on three terms dominating the present discussion on any development within the construction industry; sustainability, industrialisation and digitalisation. The result is a thorough discussion and a set of recommendations for the direction of future research and innovation on sustainable use of concrete in the construction of road infrastructure. The major opportunities and threats are summarised in the conclusions, and future research to be carried out in two of the authors' PhD-projects are described.

Keywords: Concrete infrastructure, Sustainability, Digitalisation, Industrialisation, SWOT analysis

1. INTRODUCTION

In a world striving towards sustainable development, economic, societal and environmental perspectives have to be implemented simultaneously. All these issues are challenging to the construction industry. The development of road infrastructure is fundamental to the growth of the economy and welfare.

The increase in the global mean temperature is currently one of the most severe sustainability issues [1]. According to the Intergovernmental Panel on Climate Change (IPCC), the global mean temperature has increased rapidly during the last 50 years and is projected to rise [2], clearly influenced by anthropogenic emissions of greenhouse gases. The prospects of continued emission are further global warming and long-lasting changes in climate systems, increasing the severe, negative effects for people and ecosystems [2]. In order to limit these climate change risks, substantial reductions in greenhouse gas emissions are required. Consequently, IPCC has established global reduction goals on CO_2 emissions for all nations. Norway has committed to reduce the greenhouse gas emissions of at least 40% compared to 1990 levels within 2030 [3]. Other authoritative sources define different goals and different deadlines for when these goals are to be met. Accommodating different time span requires implementation of different strategies. Some of these strategies might even be conflicting [4].

Concrete is indispensable for the development of countries at all development stages. The annual growth in consumption of concrete in highly developed countries has diminished. However, densely populated countries are still rapidly evolving, consequently experiencing rapid growth in the use of concrete. Hence, the world's demand for concrete is growing. The development of societies and climatic changes lay premises for the development and use of concrete. Three topics

are presently dominating most discussions on industrial and societal development; i) sustainability, ii) industrialisation and iii) digitalisation. These terms are widely used, and each user tends to define the contents slightly differently.

In this article, a functional definition of the three catchwords is stated, and SWOT analysis is executed for each of them to help identify the direction of sustainable development for the use of concrete in road infrastructure in an industrialised context. The main opportunities and threats are summarised and used as a basis for future research in the first and second authors' PhD-projects.

3. RESEARCH METHODOLOGY

A SWOT analysis is executed to investigate premises for sustainable growth in the use of concrete in road infrastructure, and to identify research needs. SWOT is an abbreviation for the four terms Strength, Weaknesses, Opportunities and Threats, and is a well-known tool in economic and strategic management. The usage is not equally widespread in the construction industry. However, successful implementation is emerging. Jiang et al. [5] applied a SWOT analysis to study off-site construction in China. Yuan [6] correspondingly investigated successful construction waste management. Both gathered data for the SWOT analysis through interviews or meetings with experts, combined with literature reviews including research, regulations, and government reports [5, 6]. Inspired by these researchers, we applied a model for research methods, as illustrated in Figure 1. In this study, SWOT analysis is executed on the three topics; i) sustainability, ii) industrialisation and iii) digitalisation.

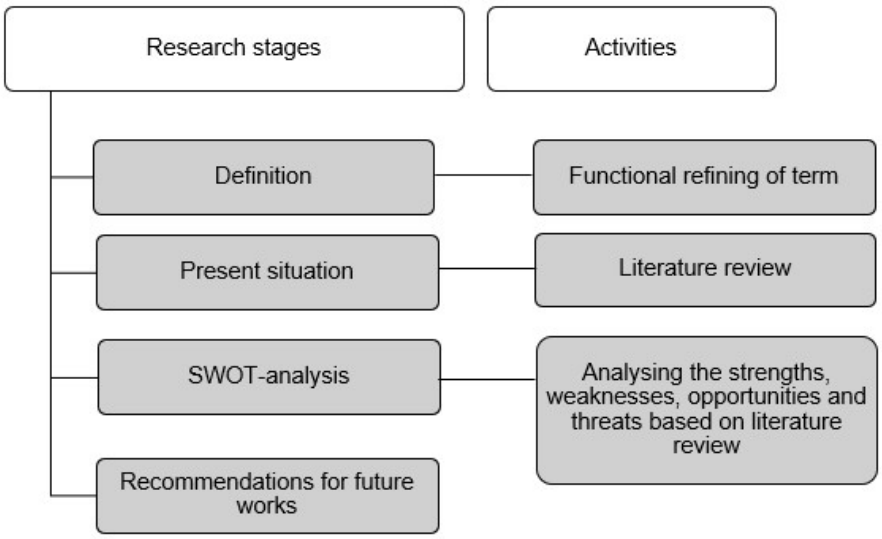

Figure 1 – Applied research methodology, similar to Yuan [6].

4. RESULTS AND DISCUSSION

4.1 Sustainable use of concrete

Functional refinement of the term
Sustainability is a broad term, often defined as "development that meets the needs of the present without compromising the ability of future generations to meet their own needs". This definition origins from *Report of the World Commission on Environment and Development: Our Common Future* from 1987 [7]. Different professions tend to define sustainability in either economic, societal or environmental terms. All of these are necessary preconditions to support the needs of future generations. In the book *Concrete and Sustainability*, Jahren and Sui [4] define sustainability as the overlapping field between economy, social development and environment. This definition is applied in the following discussion. However, "environment" is in this paper limited to climate issues only.

Figure 2 – Sustainable development, according to [4].

Present situation
According to the European Cement Association CEMBUREAU, the total cement production in the world was 4.65 billion tonnes in 2016 [8]. Anticipating an average world consumption of 300 kg cement per cubic meter concrete, the present cement production corresponds to almost 2 cubic meters of concrete per capita in the world is built into new structures every year. Scrivener et al. [9] illustrate the consumption of concrete relative to other conventional building materials (Figure 3, left part), according to a report based on the efforts from the UN Environmental Program Sustainable Building and Climate Initiative. Without even arguing on the mechanical and durability properties, price or geographic availability of various materials, it is evident from a pure volume perspective that no other material can fully substitute concrete.

According to Jahren and Sui [4], Asia is responsible for approximately 80% of the world's cement production. The major part of the growth is due to countries outside China, India and Japan [4], mostly in low-income countries with strong growth in population and economy. In 2017 the world population was 7.6 billion, expected to grow to nearly 10 billion within 2050 [10]. Assuming cement consumption per capita remaining at today's level, the production of cement will have to grow to 6 billion tonnes in 2050, only considering the population growth. This result corresponds to an estimate made by the International Energy Agency [9].

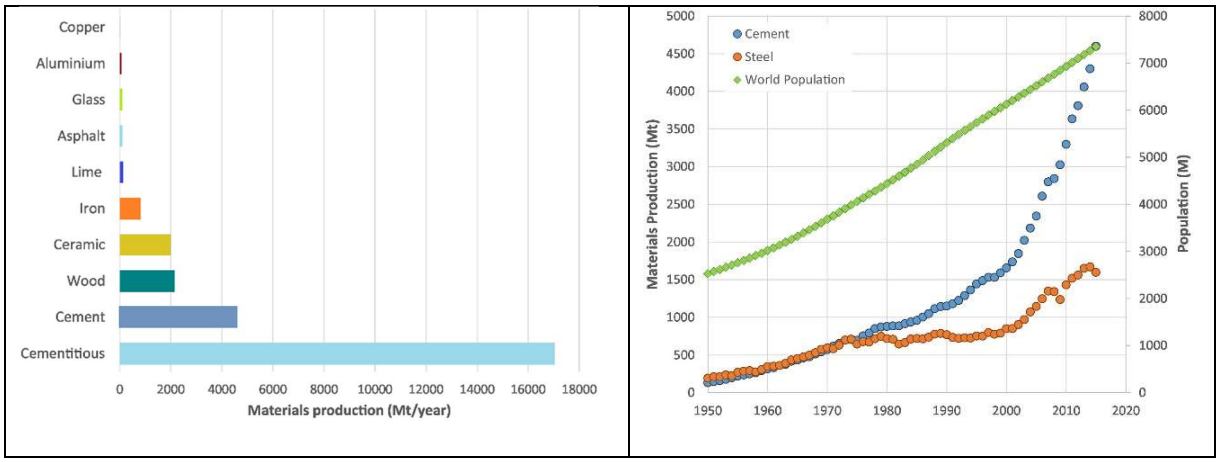

Figure 3 – Left part: Estimated consumption of common materials 2002-2005 [9]. Right part: Correlation on growth in world population and cement production 1950-2015 [9].

The World Bank estimates that around 40% of the world's population lives in low-income countries and that more than 60% of those living in slums without access to simple infrastructure like sanitation [9]. To accommodate the needs for a decent level of societal infrastructure for both the existing world population and the expected growth, the above estimate for cement consumption seems conservative. Scrivener et al. [9] showed that while the world population grew by 15% during the period 2000-2015, the cement production grew by 150% (Figure 3, right part). This unproportional growth in cement production probably illustrates welfare growth exceeding population growth.

According to CEMBUREAU [8], the cement and concrete industry generated more than 380 000 direct jobs within the EU in 2012. Also estimating indirect effects, this number grows to more than 1 million. EU is far more industrialised than most low-income countries, where concrete consumption is expected to grow. Hence, the importance of employment and economic growth is huge.

The social and economic impact stemming from the consumption of concrete seems indispensable, both due to material properties for creating necessary infrastructure and for the role of the related industry to generate personal employment, security and welfare for the citizens. Additionally, the structures being built through the concrete consumption constitute infrastructure and arenas necessary for future growth in industrial and social activities, economy and welfare.

SWOT analysis

As argued above, cement and concrete are indispensable for sustainable development of society. Consumption will grow substantially, especially in low-industrialised countries. Cementitious materials are favourable for availability, cost-effective and flexible design, simplicity of use, high strength/cost ratio and high durability. However, the concrete industry is responsible for a considerable demand for resources and greenhouse gas emissions. Production of cement is most significant, accountable for approximately 5-7% of the global anthropogenic CO_2 emissions [11-13].

A major measure to reduce CO_2 emissions would be carbon capture and storage (CCS) or even better than storage; use (CCU). A project on CCS is under development in Norway, including a full-scale pilot on Norcem's factory in Brevik expected to be realised in 2020-21. However, CCS is expensive, and unless disruptive technology is emerging, CCS/CCU is not expected to solve

the climatic challenges of the cement industry worldwide. This was the origin of a UN initiative to find alternative solutions on CO_2 reduction from the use of cementitious materials, recently reported by Scrivener et al. [9]. Mehta [1] proposes three tools for making the concrete industry more sustainable; i) consume less concrete for new structures, ii) consume less cement in concrete mixtures and iii) consume less clinker for making cement. Scrivener et al.'s conclusions are in harmony with Mehta's approach, and this logic is followed in the discussion below. Several measures are essential for global solutions, without being central to development in highly industrialised societies. A fourth tool – spanning wider than just within the cement and concrete industry is related to utilising resources that are waste from other industrial processes (often referred to as by-products) –; iv) circular economy.

i) Consume less concrete for new structures

Improved durability – reducing the need for replacement of structures – is unarguably an effective mean to reduce consumption of resources in a long-time perspective. The designed service life of infrastructure members such as bridges and tunnels in Norway is 100 years [14, 15]. The designed service life is the period a structure is expected to be in use fulfilling its intended purpose with predicted maintenance, without extensive repairs [14]. Jahren and Sui [4] emphasise that designing structures for enhanced durability has a significant positive effect on emissions when considering long-time span, but might conflict towards short time focus.

Several strategies support durability enhancement. Two of those are careful design of structures to reduce degrading loads (e.g. avoiding surface water accumulation) and careful execution of construction work (e.g. avoiding reinforcement corrosion due to lack of cover). A third measure is careful inspections and maintenance, to stop degradation before it has propagated to a level where replacement is favourable to repair.

A fourth measure – emphasised by Mehta – is using highly durable concrete materials. Ultra High Performance Concrete (UHPC) is an emerging material presently being subject to massive research efforts. In addition to having higher strength than standard concrete, UHPC is also defined by having enhanced durability. This eliminates reinforcement corrosion caused by carbonation or chloride migration [16, 17], within any service life expectancy. Pilot projects are being built worldwide, and some early design codes have even been introduced [18, 19]. Using UHPC in the rehabilitation of existing concrete bridges is also investigated by several researchers [12, 20]. Habert et al. [12] showed that it is possible to lower the impact over the life cycle by using UHPC solutions rather than traditional methods.

Design optimisation offers several strategies to reduce concrete consumption. One is designing structures with flexibility for future changes in use. Another is the optimisation of cross sections. Prefabrication might support this, e.g. by offering slender beams with optimised cross sections, that would not be economically favourable for on-site production. Traditionally, concrete design utilises the lower part of the strength span allowed by design codes such as EN 1992 (EC2) [21]. Traditional use of concrete in structural design has rarely aimed at reducing CO_2 emissions. Investigating potential in the exploitation of high strength concrete and concrete having high targeted performance in other areas, might be fruitful.

Utilising the unique mechanical properties and the possible enhanced service-life of UHPC can drastically reduce the material consumption of concrete for some types of structural members [22]. Several studies [23-25] have shown that using high and ultra high performance concrete for construction can give more environmentally friendly solutions. A study aiming at innovation in

traditional building design, focused on the utilisation of high strength concrete still within the limitation of EC2, in combination with biaxial hollow decks [26]. Potential for 60% reduction of CO_2 and at the same time 20% reduction of the cost was indicated, utilising today's formal regulations and commercially available products. Scrivener et al. [9] also concluded that using high strength concretes in suitable applications can be more efficient and decrease the total material consumption.

ii) Consume less cement in concrete mixtures

It is known that the amount of cement used to produce concretes of given strength and workability, varies enormously. Utilising pozzolans or other supplementary cementitious materials (SCM) to partly substitute cement in ready-mix production, is a well-implemented measure to use less cement. A drawback is the extended hardening time. Utilising 56- or 90-days strength instead of 28-days strength in structural design makes it possible to exploit the potential of these concretes [1]. However, this practice is often conflicting with design standards. According to the preliminary version of EC2 (2021), it will be possible to utilise 91-day compressive strength.

Another possibility to use less cement is to minimise the amount of water needed for obtaining the required consistency of fresh concrete. When keeping w/c-ratio constant, reduction of water consequently reduces the amount of cement. Superplasticisers can be utilised to reduce the amount of water required, still maintaining workability [1]. However, this strategy is well utilised in industrialised countries.

Further development to reduce water content is related to the functions of paste in concrete. The primary function is to fill the voids between aggregate particles; to envelope each particle in "glue" to obtain the required strength and durability of hardened concrete. The volume of voids is a function of particle packing. Scrivener et al. [9] claim that packing the particles of aggregate by carefully selecting the dosages of different fractions is an effective measure to reduce water and cement content in concrete. Mehta [1] also mentions the possibilities lying in optimised aggregate size and grading, without in this connection making an issue of the extra resources this would request. A secondary function of the paste in concrete is to reduce friction between aggregate particles to enhance the workability of fresh concrete. This is obtained by adding a surplus of paste exceeding the volume of voids to separate aggregate particles from each other, and hence increasing the consumption of cement. The shape of the particles also rules the friction within aggregates, as the content of flaky shaped particles creates more friction. Consequently, reducing the share of flaky shaped particles reduces the need for paste in the concrete.

Additionally, there is an emerging focus on the effect of small particles in concrete; the fillers. Scrivener et al. [9] claim that "engineering particle size distribution combined with the use of dispersants allow a binder replacement of up to 70% by inert fillers without the negative effects of dilution." Properties and grading of aggregates vary with location, which might explain variations in cement consumption. The consumption of cement, and hence also the price, can effectively be reduced by increasing focus on the composition of aggregates and the use of fillers. These measures are also location independent.

iii) Consume less clinker for making cement

Consume less clinker for making cement can be obtained by utilising other cementitious materials for partly substituting Portland clinker [1]. Depending on properties, these materials can be added into the cement production prior to, or after the calcination process – thus ending up as SCMs. Some examples are fly ash, silica fume, ground granulated blast furnace slag, rice husk ash, lime

filler and several other natural pozzolans [9, 24]. This is considered to be one of the key strategies to reduce greenhouse gas emissions from concrete production [9] having an effect both on a short time horizon and lifetime perspective [4]. The availability of these materials depends on other productions, as they are often by-products from industrial processes. Some SCMs have shown to mutually affect each other positively. These synergetic mechanisms of ternary and quaternary binder blends are not yet fully investigated. If the particle size distribution and combinations of cement, fillers and SCMs are fully optimised, an average clinker substitution level of above 40% is realistic worldwide [9].

Often, SCMs have slower strength development than cement clinker, and resistance towards migration develops correspondingly. This slower development might require intermediate measures towards the migration of harmful components into unmatured concrete. Additionally, the availability of SCMs differ locally, and some require costly processing to obtain acceptable quality [9].

iv) Circular economy

Circular economy is gaining increased attention. The aim is to improve utilisation of resources, decrease waste and improve sustainability. This philosophy has several applications within the concrete industry. The most obvious would be the reuse of structures or elements for other purposes than they were designed for. Use of SCMs stemming from industrial processes to substitute cement is another example.

The construction industry produces large amounts of materials that are presently deposited or used for landfill; some from construction works and demolition of old structures, others from excavation or blasted rock. Xuan et al. [13] suggest one way of making the concrete industry more sustainable by increasing the use of waste from ready-mix concrete plants. Another study showed that it is possible to produce UHPC with reduced cement content [27] by utilising a by-product from the production of gravel. Often, these surplus masses are produced on-site, where aggregate for concrete is required. However, they fail to fulfil quality requirements according to concrete standards. For some materials, the quality requirements can be obtained by simple processing. However, tests also show that it is possible to produce high-quality concrete from aggregates that fail to meet some standardised quality requirements.

The concrete industry is ruled by formal regulations. Severe efforts are put into harmonising standards internationally, to simplify execution and to take advantage of existing competence. The existence of clear, authoritative guidelines are guarantors for quality and safety. However, standardised solutions might prevent innovation. Scrivener et al. [9] emphasise that avoiding the prescriptive regulations in traditional standards and instead allowing for flexibility to exploit local opportunities for raw materials can only be achieved with performance standards specifying properties that must be met (like strength, E-modulus and durability).

The above findings are organised by strength, weaknesses, opportunities and threats (SWOT) and presented in Table 1.

Table 1 – SWOT sustainable use of concrete

Strengths	**Weaknesses**
• The demand is increasing and will remain so due to population growth. • No material can replace concrete, due to required volume and availability. • Several advantages, like the simplicity of use, local part materials, flexible in design, cost-effectiveness and durability.	• Resource demanding locally and globally. • Causes substantial CO_2-emissions. • Conflicting timespan considerations for varying environmental goals.
Opportunities Reduction of environmental loads through • Reduced material consumption through innovative design, prefabrication and use of HPC and UHPC. • Clinker reduction by use of SCMs and fillers. • Cement reduction by optimising grading and shape of aggregate particles. • Utilising potential in extended maturity considerations (91 days hardening time, and innovative hardening technology). • Increase the use of waste and recycled materials. • Enhancement of durability. • CCS/CCU.	**Threats** • Climatic changes. • Resource demanding. • Rigid regulations. • Availability of SCMs.

4.2 Industrialisation of the construction process

Functional refinement of the term

The term "industrialisation" is traditionally used to characterise the transition of economies from being dominated by agriculture, towards being dominated by manufacturing. Development of new technology, including the steam engine, was the vital driving force for the European transition. The term is still frequently used even in highly developed economies, now to describe the transition of industrial sectors away from craftsmanship and one-of-a-kind solutions, towards standardised and automated production. The gaining is efficiency; a higher volume of production per time and at a lower cost. Once again, new technology is a major driving force. However, the organisation of processes and data to promote human interaction is considered equally important.

The present situation

The construction industry is still dominated by one-of-a-kind design and low level of automation in management, design and production. Although changes as increased use of innovative formwork technology, self-compacting concrete, fibre reinforcement, grinding- and surface treatment machinery, and sprayed concrete robots are emerging, it is widely accepted that construction lags behind manufacturing industry on productivity. The Norwegian construction industry and the government have established a joint effort to improve productivity and sustainability, named Bygg21. In a recent report from Bygg21, the following definition is given: "Industrialising construction projects is to plan and execute processes; maximising repeated use of standardised solutions, industrial methods and digital tools" [28].

The well-known "Lean Construction" (LC) philosophy, adapted from Toyota's "Lean Production", has inspired this definition. Most major contractors have been struggling to

implement LC for many years already, often adopting company-specific names like Veidekke's "involverende planlegging" (participative planning). LC-implementation has often originated on-site to manage logistics and fabrication, but efforts are now spanning the entire process from planning and design, throughout deliverances that support operation and maintenance. Several "models" or "schools" have been developed to support these processes; like "Integrated Project Delivery" (IPD) and "Virtual Design and Construction" (VDC).

SWOT analysis

Three basic principles central to LC are: i) to improve flow in processes, ii) to reduce waste and iii) to continuously learn from experiences. These three principles are used for facilitating the SWOT analysis below.

i) Improve flow in processes

The most important "flow" in construction processes, is the flow of information relevant for each actor to execute his/her part as efficient as possible. All actors in the construction process must be involved early enough to influence actions laying premises for their own deliverance. All must also have access to correct and required information prior to executing any action, and uncertainty must be adequately handled. IPD is developed as a method utilising early involvement to focus on producing maximum value for the customer through building alliances between all people and "systems" vital for production, avoiding individual stakeholders to sub-optimise own gaining.

Though theoretical approaches to LC emphasise manual tools like "PostIt-technique", the industry soon called for computer-based LC implementations, due to the amount of information to be handled and the number of actions necessary for keeping the system updated [29]. IPD clearly defines seven sequences in a construction project, identifying vital actors in each sequence. This clear structure facilitates the use of digital solutions. Building Information Model/Modelling (BIM) is emphasized as "one of the most powerful tools supporting IPD" [30]. This is argued by BIM being able to combine all information and support all phases in a construction process, from design through the entire life-span. This is correctly the idea of BIM. However, there are still some shortcomings in the present use of BIM. Some of these are discussed in the section "Digitalisation" further down in this paper.

Another important "flow" in construction processes is the fabrication. Traditional thresholds include uncertainty; related to logistics, lack of drawings or staffing, unwanted events, etc. Prefabrication might be a strategy to reduce uncertainty. A state-of-the-art report by the Fédération Internationale du Béton (fib) from 2004 [31] reports that there are significant differences in the development and application of precast bridges in various countries. In the report, it is claimed that "Especially in the Scandinavian countries, there are few precast bridges, although the climatic conditions would logically incite to an opposite attitude". According to an investigation amongst practitioners on the use of precast bridge elements [32], there seems to be a widespread opinion that precast bridges are more prone to damage due to degradation mechanisms. These problems are recognised for bridges dated before 1990. However, in an investigation based on the NPRA database "Brutus", it was found that this is not correct – at least for bridges designed according to standards dated after 1990 [33].

Figure 4 (left part) shows the results of an investigation mapping the bridges related to four-lane national highways in the south of Norway [32]. As shown in the figure, there is a tendency that highway bridges are limited to a low number of typical lengths, clearly indicating a large potential for standardisation. NPRA has recently initiated two projects to use more prefabricated elements

in road construction. One of them has resulted in standardised solutions for prefabricated concrete culverts. The other project aims to develop new pre-accepted precast bridge solutions utilising up to 40 meter long beams [34].

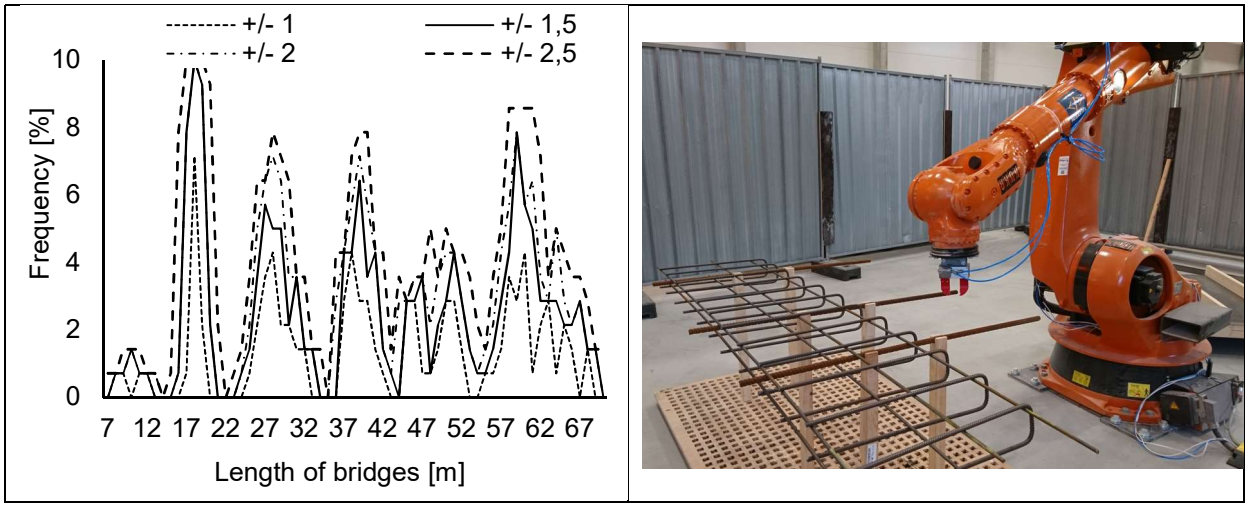

Figure 4 - Left part: Frequency of length of bridges on four-lane national highways in the south of Norway (a total of 140 bridges were included) [32].
Right part: Robotised placement and welding of prefabricated reinforcement.
Photo: Rebartek – Maximilian Trommer.

According to [32], some interviewed experts highlighted that there are challenges for precast bridges related to requirements in the regulation for bridge constructions by NPRA [14]. The Norwegian topography can also limit the use of straight precast elements. Transport on Norwegian roads can limit the span length both due to regulations and due to the road geometry (roundabouts define the maximum bridge lengths). Additionally, prefabricated (standard) elements are straight, limiting the road geometry, horizontal and vertical curvature, transverse inclination and inclining abutments. However, most agreed on the benefits of prefabrication regarding Health, Safety and Environment (HSE). Higher production speed, improved quality, reduction of traffic interrupts and potential reduction of production cost were other benefits emphasized in the interviews. These are major indicators of higher efficiency.

ii) Reduce waste

Improving flow inevitably leads to reduction of waste, as time is saved for involved personnel and equipment. Time is valuable both to business (personnel and equipment) and to the social economy (e.g. reducing traffic interruption).

Waste can also be reduced by implementing new technology like automated production of reinforcement cages (Figure 4, right part). In addition to the reduction of production time and material consumption it opens for more advanced design, e.g. by welding the minimum required the amount of reinforcement, omitting lap joints and reinforcement design optimised for production rather than structural needs. VDC is another process model heavily focusing on BIM and visualisation; including 3D models and further dimensions (time, cost, progress, risks, etc.). Once again, the primary driving force is to secure interaction and information access through organisation and the use of technology creating a work zone where all construction activities take place.

Standardisation is expected to promote industrialisation in road construction by reducing the number of alternative solutions, e.g. for fixation of railings. Reduction of the alternative solutions increases reuse of formwork, scaffolding and production techniques. Learning by repeated doing is a consequence of standardisation of production, resulting in reduction of process time, increased predictability and reduction of errors. Also, the reduction of work hours related to design processes and quality control are positive outcomes.

Standardisation inevitably leads to repetitive use of structural solutions, which might be perceived as aesthetically monotonous, limiting architectural expression. Traditionally, aesthetics is considered vital for Norwegian road infrastructure governed by an NPRA report [35]. Another drawback is that standardisation may act to conserve today's solutions. The regime of standardisation offered by today's formal regulations is frequently criticised for being conservative and counteracting new solutions and cost reductions. The urge to standardise for promoting leaner production today might prevent innovation and be a threshold to cost-efficient changes in the future. Additionally, the basic purpose is to ensure solutions that have proven their durability in practice. If opening the rigidity of standards to promote innovation, measures must be taken to make sure that the durability aspect is still attended.

iii) Continuously learning from experiences

Seen in the light of hindsight, some parts of a construction process could always have been improved. Individuals often claim to learn from experiences, however organisations like companies are known to struggle to avoid repeating mistakes. Explicit measures for organisations to learn from experiences calls for systematic registration, analysis, alternative investigation, storing and active education. Formal initiatives, processes and systems to promote this kind of organisational learning, are not always well developed. Digitalisation provides powerful tools supporting this development, but still the organisation of humans and processes is needed. One obvious reason why this is still often lacking is that these processes are time-consuming. However, the overall goal is to reduce time consumption by learning systematically from experiences.

Another measure to promote learning is the use of formerly approved solutions and practices. This might be formal standardisation through legal regulations and design codes, or restrictions given by building client (like the above-mentioned restrictions for fixation of railings along highways). However, it might also be the reuse of former design, proven to be successful. Once again, the use of digital solutions like BIM supports this kind of “standardisation” through easy access and reuse. However, also this kind of standardisation might prevent innovation.

Table 2 – SWOT industrialisation of the construction process

Strengths	**Weaknesses**
• Improved productivity by reducing the time for design and production. • Consequently, reduced cost (per unit). • Reduce climate impact (by reducing waste).	• Depending on successful implementation of interaction between numerous actors.
Opportunities	**Threats**
• Early involvement improves the possibility to influence at early stages, avoiding changes at later stages when the cost of changes rises. • Correct information required for prerequisite available for all – at any time. • Consequences of choices understood through analysis including all existing prerequisites, and easily available through visualisation. • Advanced/automated production methods open for design optimised for structural performance rather than for easy manual production. • Standardisation allows for reuse of design, equipment and production techniques. • Prefabrication allows for cost reduction, sustainable solutions and improvements on HSE. • Improved quality through systems for continuously learning.	• Aesthetics – promotes monotony. • Standard prefabricated elements limit road geometry and adaptation to terrain. • Complicated and demanding handling processes (lifting, transport and assembly).

4.3 Digitalisation of construction and management processes

Functional refinement of the term

Digitalisation is the process of using digital methods to achieve results that would not be available without these methods. The enablers are high capacity for accessing, storing, processing and presenting data. In this paper, digitalisation refers to digital information of the structure that is applied in all stages throughout the life cycle of the structure, from design until the end of service life. Digital information in the form of models including metadata may be used at the design stage, for structural analysis and dimensioning, for construction at the building site, for operation, maintenance and management and finally for demolishing, recycling and deposition of waste materials at the end of service life.

Present situation

There is an emerging interest in the opportunities related to a more digitalised construction industry. The most used development within digitalisation is BIM. By using BIM, it is possible to replace structural drawings with virtual, 3-dimensional digital models of the structure and construction site, and assign more information to the different parts than just the geometry [36]. In addition to the description of the structure and the applied materials, this may include information needed for technical and quality control, and extraction of quantities necessary for pricing. Digitalisation and BIM-models can be used throughout the life cycle of a structure. However, presently the information is often modelled in different ways and by various software tools and platforms from phase to phase, which is a serious hindrance for future development.

According to Azhar [37], BIM can be used for 3-D visualisation, fabrication of drawings, estimation of cost, automatic extraction and updates of material quantities, construction sequencing (coordinate material ordering, fabrication, and delivery schedules for all building components), conflict situations, and collision detection, to mention some. The same author also mentions that BIM may give benefits in terms of faster and more effective processes, better design (as the design of the buildings can easily be analysed and changed in the digital model), control of the lifetime costs and environmental data, and improved production quality. It is possible to achieve substantial reductions in time consumption related to generating cost estimates and utilise lifecycle data for facility management. More recently there has been increased interest in using BIM to achieve more sustainable solutions by including EPDs (Environmental Product Declaration) in the BIM-model and carry out optimum design [36].

An important part of digitalisation in the construction industry is to use modelling tools and software for structural analysis and dimensioning. Direct application of BIM and the growing sophistication of computer programs, increasing computer capacity and decreasing costs, give great possibilities for better design. Table 3 presents today's practice and two possible future scenarios for structural analyses and design, which both may facilitate more efficient material use and therefore more sustainable solutions.

Table 3 The structural design process

Solution	Date	Drawings/Design	Structural Analysis	Dimensioning/Design
I	Today	Drawings or BIM	Linear elastic methods, Finite Element Analysis (FEA) occasionally. Supported by human competence and special purpose program accounting for cracking, creep, shrinkage, relaxation and temperature effects, and construction history. Nonlinear analysis rarely used in practice.	Manually in critical sections, often using special purpose programs.
II	Future scenario, alt I	BIM	Linear elastic FEA based on the BIM, occasionally nonlinear and time-dependent. Modification of linear FEA to account for cracking, creep, shrinkage, relaxation and temperature effects, and construction history.	Computerised checks of all sections.
III	Future scenario, alt II	BIM	Numerical simulation of structural behaviour based on BIM-model. Nonlinearities and time-dependent behaviour well accounted for. Probabilistic safety-formats. Structural analysis and dimensioning fully integrated.	

In today's structural design, it is most common that the design of each structural member is done manually in critical sections using special purpose programs. This is time-consuming, and in a market with great competition and economy focus for both designers and contractors, the approach does not always give the optimal solutions and sustainable design.

Compared to today's practice, future scenario I will utilise BIM to make more accurate linear finite element analysis (FEA) of structural systems. Still, care must be taken to distribute stress concentrations, account for time-dependent effects, and in some cases also nonlinear behaviour. This, together with computerised design of all sections in a member, may contribute to more optimal and sustainable solutions. For instance, industrialising the process of prefabricating beams by placing the exact amount of shear reinforcement required by the design code, precisely fixed in position by robots. Hence, industrialising open for flexible production by standardising processes, not products.

Future scenario II assumes frequent use of advanced numerical simulations of the structural behaviour based on the BIM. The preferred method will be Non-linear Finite Element Analysis (NLFEA), including accurate material models. These tasks are challenging and require development of guidelines and regulations to be able to achieve the right structural safety concerning design resistance and robustness, and quality control of the results. NLFEA is used already today, but only in special cases, e.g. for existing structures (remaining/rest-capacity), or when there has been a structural collapse (accident) and investigations to explore the causes are required.

To fully utilise the advancement in digitalisation, to achieve future scenario II, should be one goal to achieve more sustainable solutions but, as mentioned above, further research and development of regulations and guidelines are required.

SWOT analysis

As illustrated in Figure 5, digitalisation may facilitate communication, information sharing, innovative thinking, design adjustments and construction planning. The different sub-processes work together towards a better and sustainable design.

First sub-process, denoted building opportunities (Gear 1), is constantly moving and must be checked with preliminary and advanced models to obtain the best design. This sub-process also requires feedback from the other sub-processes to improve. If one process works alone and does not communicate, it will hinder the abilities for the other sub-processes to work together.

The authors agree with the statement from Azhar [37] that BIM contributes to a better design, but the authors would like to address this broad term. Among the conclusion for a better design, one is that the building proposals can be rigorously analysed, and simulations performed quickly.

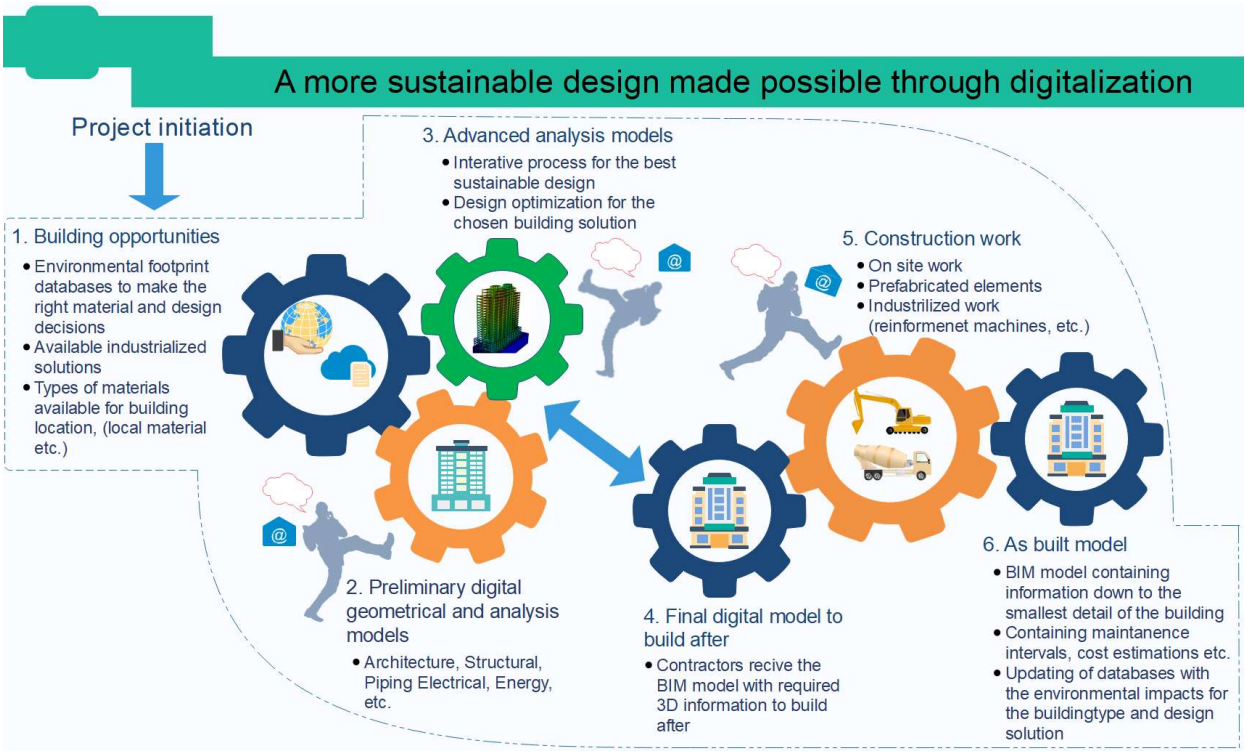

Figure 5 – A more sustainable design made possible through digitalisation (own design of illustration).

A risk when using more advanced software is that complex structures may become too simple to handle in the software's environment. In worst-case, this can lead to serious faults, and also structural failures with large consequences. Therefore, it is of vital importance that engineers understand and maintain competence within their field. Some of the advanced structural analysis programs now available for the industry were previously only available in the academic environments.

Table 4 shows the results from the SWOT analysis in digitalisation of construction and management processes.

Table 4 – SWOT Digitalisation of construction and management processes

Strengths	**Weaknesses**
• Faster and more effective processes. • More efficient design process and better quality of the design. • Faster and more correct cost estimates. • More accurate geometry and material modelling for structural analysis. • More accurate descriptions of the construction history.	• Information may be modelled in different ways and using different software tools and platforms from phase to phase. • The computer programs may use different theory and algorithms than those known to the designer, which may lead to misunderstandings and faults. • Too large amount of information creates unnecessary complexity.

Opportunities	**Threats**
• More efficient (economic and sustainable) use of materials. • Interaction of BIM and LCA-software/EPDs. • More optimal design (easier to improve the design of a structure). • More optimal and sustainable solutions.	• Changes in data-formats and platforms over time. • Robustness of systems (data storage, hacking, etc.). • Loss of competence due to phasing out valuable computer programs. • Lack of understanding of how the structural systems work – may lead to possible faults. • Import of geometrical 3D models for structural analysis– possibly wrong connections between elements due to different formats. • Too much information in the models related to the necessary task at hand.

5. DISCUSSION

The aim of this paper is to identify and discuss directions for more sustainable development of the use of concrete for road infrastructure, in an industrialised context. The term "sustainable" is defined to embrace not only environmental issues, however also the economy and social development. Hence, issues regarding HSE and productivity are included. The term "industrialised context" reflects that the discussion regards highly industrialised societies, where advancements in digitalisation and automation are natural traces of development.

Substantial growth in the use of concrete is inevitable. Consequently, measures must be taken to avoid a corresponding growth in CO_2 emissions, and to reduce the anthropogenic influence on climate change. Future solutions might involve CCS/CCU, however widespread use of these solutions requires disruptive technology that substantially reduces cost. Hence, CCS/CCU is not further discussed in this article.

The three terms sustainability (in a threefold understanding), industrialisation and digitalisation are separately discussed in SWOT analysis above. No cross-disciplinary conflicts have been identified. On the contrary, synergies are described, and simultaneous utilisation of the three considerations is necessary for realising the full potential in each. A fundamental approach to reduce the use of natural resources, emissions, time and money, is to secure flow in all processes. Flow is pursued by taking all preconditions into account in all processes and choices, including design and production. This calls for sharing information and evaluating each choice real-time, enlightened by all relevant information in the project.

Concepts like "flow", "early involvement" and "sharing information" are all vital in different approaches towards industrialisation, e.g. LC, IPD and VDC. The use of digital methods is another important measure in industrialisation; to achieve results that would not be available without these methods. Hence, further industrialisation requires both organisation of processes and the use of digital methods. Digitalisation on the other hand, will only produce gaining if all relevant information is available. Hence digitalisation requires industrialisation.

6. CONCLUSIONS AND RECOMMENDATIONS FOR FUTURE WORK

The paper considers the three frequently used catchwords; sustainability, industrialisation and digitalisation, and gives a functional refinement of them related to their application within the

construction industry. As a contribution towards more sustainable solutions within the road infrastructure a SWOT analysis is carried for each term. Several opportunities for sustainable development of the use of concrete have been identified. A prerequisite for taking advantages of these opportunities is that processes for further industrialisation and digitalisation are carefully implemented. Some of these identified opportunities are:

- More efficient use of materials through innovative design, utilisation of advanced and automated production, prefabrication and investigation into smart use of HPC/UHPC.
- More optimal design made possible by early involvement of stakeholders, the interaction of BIM and LCA software, and digital visualisation, allowing for better informed decision processes.
- Improved quality in processes, decisions and products, supported by operational systems for continuous learning; including both explicit actions and knowledge tacit in the reuse and standardisation of solutions.

Several important threats to the sustainable development of road infrastructure have also been identified:

- The main threats towards future sustainable development of the concrete infrastructure are the lack of natural resources, too rigid regulations and availability of SCMs.
- Concerning industrialisation, a threat to be avoided is making solutions that are rational when implemented but may act preservative in the longer run, preventing future innovations.
- Related to digitalisation the major threats are due to changes in data-formats and platforms over time, the robustness of systems (data storage, hacking, etc.), loss of competence due to phasing out valuable computer programs, and finally lack of understanding of how the structural systems work – which may lead to possible faults.

The paper is a part of two ongoing PhD-projects, and the findings in this paper will be followed up. One of these will focus on the development of production of Ultra High Performance Concrete (UHPC) from local constituents and investigate the structural behaviour of this material. The other one will study industrialised sustainable concrete bridges in Service Limit State (SLS). The objective is to improve structural analysis and design of concrete bridges in SLS that are adapted to new sustainability-requirements, industrialisation and digitalisation.

ACKNOWLEDGEMENTS

Two funding bodies supported this work: The Research Council of Norway (NFR) and Sørlandets Kompetansefond, through the project More Efficient and Environmental friendly Road Construction (MEERC).

REFERENCES

1. Mehta P K, "Global concrete industry sustainability," *Concrete international,* vol. 31, no. 2, pp. 45-48, 2009.
2. Pachauri R and Meyer L, "Climate change 2014 Synthesis Report-Summary for Policymakers," ed: Intergovernmental Panel on Climate Change (IPCC), 2014.

3. Samferdselsdepartement, "Meld. St. 33 Nasjonal Transportplan 2018-2029 (in Norwegian) (National Transport Plan 2018-2029)," Oslo, Norway2017.
4. Jahren P and Sui T, *Concrete and sustainability*. CRC Press, 2013.
5. Jiang R, Mao C, Hou L, Wu C, and Tan J, "A SWOT analysis for promoting off-site construction under the backdrop of China's new urbanisation," *Journal of Cleaner Production,* vol. 173, pp. 225-234, 2018/02/01/ 2018.
6. Yuan H, "A SWOT analysis of successful construction waste management," *Journal of Cleaner Production,* vol. 39, pp. 1-8, 2013/01/01/ 2013.
7. Brundtland G H, Our common future, Oxford: Oxford University Press, 1987. [Online]. Available.
8. CEMBUREAU The European Cement Association. (2016, 17.03). *Key figures*. Available: https://cembureau.eu/cement-101/key-facts-figures/
9. Scrivener K L, John V M, and Gartner E M, "Eco-efficient cements: Potential economically viable solutions for a low-CO2 cement-based materials industry," *Cement and Concrete Research,* vol. 114, pp. 2-26, 2018/12/01/ 2018.
10. United Nations. (2017, 22.03). *World Population Prospects: The 2017 Revision*. Available: https://www.un.org/development/desa/publications/world-population-prospects-the-2017-revision.html
11. Benhelal E, Zahedi G, Shamsaei E, and Bahadori A, "Global strategies and potentials to curb CO2 emissions in cement industry," *Journal of Cleaner Production,* vol. 51, pp. 142-161, 2013/07/15/ 2013.
12. Habert G, Denarié E, Šajna A, and Rossi P, "Lowering the global warming impact of bridge rehabilitations by using Ultra High Performance Fibre Reinforced Concretes," *Cement and Concrete Composites,* vol. 38, pp. 1-11, 2013/04/01/ 2013.
13. Xuan D, Poon C S, and Zheng W, "Management and sustainable utilization of processing wastes from ready-mixed concrete plants in construction: A review," *Resources, Conservation and Recycling,* vol. 136, pp. 238-247, 2018/09/01/ 2018.
14. Norwegian Public Road Administration, *Håndbok N400 Bruprosjektering (in Norwegian) (Maunal N400 Bridge design)*. Oslo: Directorate of Public Roads, 2015.
15. Norwegian Public Road Administration, *Håndbok N500 Vegtunneler (in Norwegian) (Manual N500 Road Tunnel design)*. Oslo: Directorate of Public Roads, 2016.
16. Russell H G and Graybeal B A, "Ultra-high performance concrete: A state-of-the-art report for the bridge community," 2013.
17. Thorstensen R, Larsen I, Heimdal A, and Hansen H, "LCC and carbon footprint of bridge made from locally produced UHPC, compared to standard concrete," in *Proceedings of HiPerMat 2016 4th International Symposium on Ultra-High Performance Concrete and High Performance Materials*, 2016.
18. *National addition to Eurocode 2–Design of concrete structures: Specific rules for ultra-high performance fiber-reinforced concrete (UHPFRC)*, NF P18-710, 2016.
19. *Recommendation: Ultra High Fibre Reinforced Cement-Based composites (UHPFRC): Construction material, dimensioning and application*, SIA 2052, 2016.
20. Brühwiler E, "Structural UHPFRC": Welcome to the post-concrete era," in *First International Interactive Symposium on UHPC*, 2016.
21. *Eurocode 2: design of concrete structures–part 1-1: general rules and rules for buildings*, EN 1992-1-1:2004, 2004.
22. Randl N, Steiner T, Ofner S, Baumgartner E, and Mészöly T, "Development of UHPC mixtures from an ecological point of view," *Construction and Building Materials,* vol. 67, pp. 373-378, 2014/09/30/ 2014.

23. Habert G, Arribe D, Dehove T, Espinasse L, and Le Roy R, "Reducing environmental impact by increasing the strength of concrete: quantification of the improvement to concrete bridges," *Journal of Cleaner Production,* vol. 35, pp. 250-262, 2012/11/01/ 2012.
24. Liew K M, Sojobi A O, and Zhang L W, "Green concrete: Prospects and challenges," *Construction and Building Materials,* vol. 156, pp. 1063-1095, 2017/12/15/ 2017.
25. Larsen I L, Aasbakken I G, O'Born R, Vertes K, and Thorstensen R T, "Determining the Environmental Benefits of Ultra High Performance Concrete as a Bridge Construction Material," in *IOP Conference Series: Materials Science and Engineering*, 2017, vol. 245, no. 5, p. 052096: IOP Publishing.
26. Fidjestol P and Thorstensen R T, "Improving sustainability of concrete construction - the role of high strength high performance concrete," presented at the 37th Conference on Our World in Concrete and Structures, Singapore, 2012.
27. Larsen I L, Thorstensen R T, and Vertes K, "Lowering environmental impact from UHPC, utilizing industrial by-products," in *12th fib International PhD-Symposium in Civil Engineering*, Prague, 2018, pp. 93 - 101: Federation internationale du beton (fib).
28. Bygg21, "Tenk nytt – bruk kjente løsninger (in Norwegian) (Think New - Use Known Solutions)," 2019, Available: https://www.bygg21.no/rapporter-og-veiledere/tenk-nytt-bruk-kjente-losninger/.
29. Thorstensen R T, Kalsaas B T, Skaar J, and Jensen S, "Last planner system innovation efforts on requirements for digital management system," in *Annual conference of the international group for lean construction*, 2013, vol. 21.
30. The American Institute of Architects (AIA National & AIA California Council), "Integrated Project Delivery: A guide," 2007.
31. Fédération internationale du béton (fib), *Precast Concrete Bridges: State-of-the-art report*. International Federation for Structural Concrete (fib), 2004.
32. Heimdal A, Larsen I L, and Norheim T, "Standardisering av brokonstruksjoner for nasjonale hovedveier (in Norwegian) (Standardization of bridge structures for national highways)," Engineering science, University of Agder, Grimstad, 2017.
33. Bårseth E and Birkeland K, "Bestandighet og holdninger til flerspenns prefabrikkerte brokonstruksjoner (in Norwegian) (Durability and attitudes towards multi-span prefabricated bridge structures)," BSc thesis, University of Agder, 2018.
34. Persson S, "«Brubjelkeprosjektet» (in Norwegian) ("The bridge beam project")," presented at the Brukonferansen 2017, Oslo 2017. Available: https://www.vegvesen.no/_attachment/2069373/binary/1218553?fast_title=Betongelementer.+Stian+Persson+%285+MB%29.pdf
35. Amundsen I, "Vegen i landskapet, om vakre veger (in Norwegian) (The road in the landscape, about beautiful roads)," in "Norwegian Public Roads Administration reports," No. 300, 2014.
36. Sandvik C and Fougner F, "BIM as a tool for sustainable design," in *The International Federation for Structural Concrete 5th International fib Congress, Better - Smarter - Stronger, 7 – 11 October 2018*, Melbourne, Australia, 2018, pp. 786-791: fib (Fédération internationale du béton).
37. Azhar S, "Building Information Modeling (BIM): Trends, Benefits, Risks, and Challenges for the AEC Industry," *Leadership and Management in Engineering,* vol. 11, no. 3, pp. 241-252, 2011.

Paper Ib

Application of NLFEA for crack width calculations in SLS

Terjesen, O., Kanstad, T., and Tan, R. (2022).

Computational Modelling of Concrete and Concrete Structures – Meschke, Pichler & Rots (Eds) © 2022 Copyright the Author(s), ISBN: 978-1-032-32724-2

Proceedings of the 9th EURO-C 2022 conference on computational methods and numerical models for the analysis of concrete and concrete structures DOI: https://doi.org/10.1201/9781003316404-30

Computational Modelling of Concrete and Concrete Structures – Meschke, Pichler & Rots (Eds)
© 2022 Copyright the Author(s), ISBN: 978-1-032-32724-2

Application of NLFEA for crack width calculations in SLS

O. Terjesen
Department of Structural Engineering, University of Agder, Norway

T. Kanstad & R. Tan
Department of Structural Engineering, Norwegian University of Science and Technology, Norway

ABSTRACT: In this paper, computer-based simulation is carried out using the Finite Element Analysis (FEA) package Abaqus to study crack widths in reinforced concrete beams. A set of experimentally tested beams are investigated, and measured crack widths are compared with crack widths predicted by nonlinear FEA (NLFEA) and relevant design codes. It is shown that Eurocode 2 (EC2), fib Model Code 2010 (MC2010) and the draft for new EC2 underestimates the crack widths at the outermost concrete face to different extents while they are conservative at reinforcement level. Crack widths predicted by NLFEA, on the other hand, provides good crack width predictions at the outermost concrete face for both investigated beams.

1 INTRODUCTION

Crack widths in concrete structures should be limited due to aesthetics, durability, and functional requirements (e.g., tightness). Although research related to this topic has been ongoing since modern time, large uncertainties and large need for further research remains. The large uncertainties are especially due to large scale concrete structures, the large concrete covers applied for structures in harsh environments, and introduction of more eco-friendly modern concretes (Basteskår et al. 2018). Strict crack width limits lead to increased amount of reinforcement and the economic consequences are proven to be large (Basteskår et al. 2019).

The work presented is part of the PhD-project of the first author and are related to the large research activity funded by the large Norwegian infrastructure project "Ferry-free E39" and the PhD work of Reignard Tan (Tan, Reignard 2019).

The main objective of this paper is to investigate how nonlinear finite element analysis (NLFEA) can be applied to predict maximum crackwidths, which furthermore are compared to crack widths predicted by analytical calculation methods in design codes such as Eurocode 2 (EC2) and *fib* Model Code 2010 (MC2010). The study is benchmarked against the experimental results from the comprehensive and well documented beam tests of Hognestad (1962).

2 CONCRETE DAMAGE PLASTICITY

The Concrete Damage Plasticity (CDP) model is a continuum, plasticity-based, damage model for concrete and is in Abaqus based on the models proposed by Lubliner et al. (1989) and by Lee and Fenves (1998). It is assumed that the two main failure mechanisms are tensile cracking and compressive crushing of the concrete material. The evolution of the yield (or failure) surface is controlled by two hardening variables in tension (ε_t^{pl}) and compression (ε_p^{pl}), linked to the respective failure mechanisms.

The experimental behaviour of reinforced concrete beams cannot be captured by elastic damage models or elastic-plastic constitutive laws only. Because in such models irreversible strains cannot be captured. In Figure 1b it can be noticed that a zero stress corresponds to a zero strain which makes the damage value underestimated. On the other hand, when an elastic plastic relation is adopted, the strain will be overestimated since the unloading curve will follow the elastic slope as shown in Figure 1c.

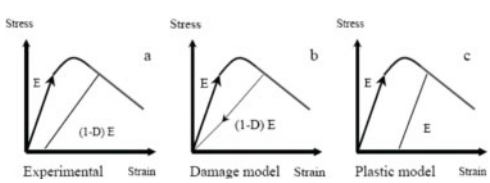

Figure 1. Elastic plastic damage law (Jason et al. 2004).

DOI 10.1201/9781003316404-30

The CDP model is combining the stress-strain curves in Figure 1b and c into Figure 1a so that we can better capture the constitutive behaviour of concrete. In SLS-design, compressive crushing of the concrete is generally not a problem and therefore the damage model for compression is excluded from the analyses described in this paper.

2.1 *Material constitutive behaviours*

The applied numerical models for the constituent material properties are described in this section

2.1.1 *Concrete model*

CDP describes the constitutive behaviour of concrete by introducing scalar damage variables. Both tensile and compressive response of concrete can be characterized by CDP, and the tensile response is depicted in Figure 2. Concrete behaviour in compression are not explained in this section due to investigated beams being within the elastic compression range.

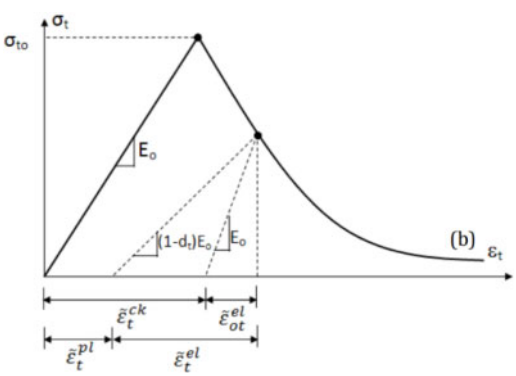

Figure 2. Behaviour of concrete under axial tension according to CDP (Abaqus User Manual 2014).

As shown in Figure 2, the unloading response of concrete specimen is weakened because the elastic stiffness of the material appears to be damaged or degraded. Damage associated with the failure mechanisms of the concrete (cracking and crushing) results in a reduction in the elastic stiffness. The CDP-model characterizes this by a scalar damage variable, d_t which can take values from zero (undamaged material) to one (fully damaged material). (Abaqus User Manual 2014). E_0 is the initial (undamaged) elastic stiffness of the material and $\tilde{\varepsilon}_t^{pl}$ and $\tilde{\varepsilon}_t^{in}$ are tensile plastic strain and inelastic strain respectively. The stress-strain relation under uniaxial tension is taken into account in Eq. (1).

$$\sigma_t = (1 - d_t) \cdot E_0 \cdot (\varepsilon_t - \tilde{\varepsilon}_t^{pl}) \tag{1}$$

A strain softening behaviour at the crack is assumed in the model. Thus, it is necessary to define the behaviour of plain concrete in tension for the CDP-model. ABAQUS allows the user to specify concrete

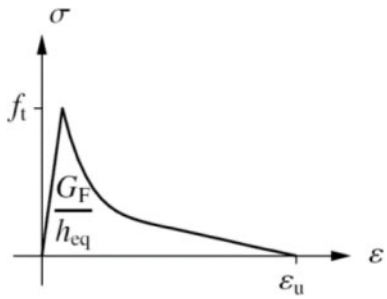

Figure 3. Hordijk softening curve (Hordijk & Dirk Arend 1991).

by post a failure stress-strain relation or by applying a fracture energy cracking criterion (Abaqus User Manual 2014) The former relation is used by the authors.

The stress strain relation for concrete in tension must be given to Abaqus in terms of the cracking strains, $\tilde{\varepsilon}_t^{ck}$, and corresponding yield stresses σ_{t0} which are determined from the nonlinear Hordijk curve (Hordijk, Dirk Arend. 1991). The exponential-type of softening diagram shown in Figure 3 will typically result in localized strains when the concrete in a structural member crack.

The area under the stress-strain curve should be equal to the fracture energy (G_f) divided by the equivalent length (h_{eq}) often called crack bandwidth. After complete softening i.e., when virtually no stresses are transmitted, the crack is said to be "fully open". The ultimate strain parameter in case of the Hordijk softening curve is given by

$$\varepsilon_u = 5.136 \frac{G_F}{h_{eq} f_t} \tag{2}$$

where f_t is the tensile strength of the concrete. The softening curve is given by

$$\sigma = \begin{cases} f_t \left(\left(1 + \left(c_1 \frac{\varepsilon^{cr}}{\varepsilon_u}\right)^3\right) \exp\left(c_2 \frac{\varepsilon^{cr}}{\varepsilon_u}\right) - \frac{\varepsilon^{cr}}{\varepsilon_u} \left(1 + c_1^3\right) \exp(-c_2) \right) & 0 \le \varepsilon^{cr} \le \varepsilon_u \\ 0 & \varepsilon^{cr} > \varepsilon_u \end{cases} \tag{3}$$

where c_1 and c_2 are parameters used to obtain the stress-crack width opening relation for concrete from deformation-controlled uniaxial tensile tests (Hordijk & Dirk Arend 1991). The recommended values are 3 and 6.93 respectively and are also applied in this study. The determination of the fracture energy G_f in tension is more complicated, and the authors have chosen this value to be as recommended by the Dutch guidelines (Hendriks 2017) and *fib* Model Code 2010 (fib 2013).

$$G_F = 0.073 f_{cm}^{0.18} \tag{4}$$

The tension softening data according to the Hordijk curve in Equation 3 are given to Abaqus in terms of

cracking strain $\varepsilon_t^{\sim ck}$ and yield stress σ_{t0} as shown in Figure 2. When the unloading data are available, the data are provided to Abaqus in terms of tensile damage curves, $d_t - \varepsilon_t^{\sim ck}$. Abaqus automatically converts the cracking strain values to plastic strain values using the relationship given by:

$$\varepsilon_t^{\sim pl} = \varepsilon_t^{\sim ck} - \frac{d_t}{(1-d_t)}\frac{\sigma_t}{E_0} \tag{5}$$

From this equation the effective tensile cohesion stress ($\bar{\sigma}_t$) determines the size of the yield (or failure) surface as:

$$\bar{\sigma}_t = \frac{\sigma_t}{(1-d_t)} = E_0(\varepsilon_t - \varepsilon_t^{\sim pl}) \tag{6}$$

In Abaqus the parameters required to define the CDP-model consists of four constitutive parameters. First the angle of internal material friction of the concrete 'ψ' measured in the p-q plane at high confining pressure, and in this study, is chosen as recommended default value. The second parameter is the eccentricity ? which defines the rate at which the hyperbolic flow potential flow potential approaches its asymptote and is chosen as default value of 0.1. The third parameter is the ratio of initial biaxial compressive yield stress to initial uniaxial compressive yield stress, 'fb0/fc0', with a default value of 1.16. The fourth parameter is the ratio of the second stress invariant on the tensile meridian to the compressive meridian at initial yield with a default value of 2/3 (Abaqus User Manual 2014).

The parameter 'Kc' should be defined based on the full triaxial tests of concrete, moreover, a biaxial laboratory test is necessary to define the value of 'fb0/fc0'. This paper does not discuss the identification procedure for parameters 'ϵ', 'fb0/fc0', 'Kc' or 'ψ' because the test series that is in this study does not have such information. Therefore, default values have been chosen.

In nonlinear finite element programs, the material models softening behaviour and stiffness degradation can often lead to severe convergence difficulties. A common technique to overcome some of these difficulties is the use of a viscoplastic regularization of the constitutive equations, which causes the consistent tangent stiffness of the softening material to become positive for sufficiently small-time increments. The CDP-model in Abaqus can be regularized by using viscoelasticity to permit stresses to be outside of the yield surface. Using a small value for the viscosity parameter (μ) (small compared to the characteristic time increment) usually helps to improve the rate of convergence of the model in the softening regime, without compromising the results (Abaqus User Manual 2014). The viscosity value used by the authors in this work was chosen as 0 and 0.0001 which is shown to be sufficiently low to give realistically results (Demir et al. 2018). The plasticity damage parameters used by the authors are shown in Table 1.

Tension stiffening is implicitly modelled by the chosen tensile softening law and corresponding chosen mesh, thus causing localization of cracking strains in the tensile zone of the investigated beams for the concrete elements. Distance between localized cracking strains becomes analogous to a crack spacing. This in turn should result in steel strains varying between the crack spacing, having its maximum at a crack and its minimum between two consecutive cracks. This also means that tension stiffening should be accounted for without having to explicitly model the bond between concrete and steel.

3 PREDICTION OF CRACK WIDTHS

The crack width calculation methods according to EC2, MC2010 and the drafts for the new versions of EC2 are briefly highlighted in the following. Chosen values for the parameters used in the subsequent crack width calculates are also addressed.

3.1 *Eurocode 2 Part 1-1*

The method for calculation of crack widths applies the following equation:

$$w = S_{r,max}(\varepsilon_{sm} - \varepsilon_{cm}) \tag{7}$$

Where $S_{r,max}$ is the maximum crack spacing for a stabilized cracking stage expressed as:

$$S_{r,max} = k_3 c + k_1 k_2 k_4 \frac{\varphi}{\rho_{s,ef}} \tag{8}$$

Here $k_1 = 0.8$, $k_2 = 0.5$, $k_3 = 3.4$ and $k_4 = 0.425$ are chosen, while φ is the diameter of longitudinal reinforcement and $\rho_{s,ef}$ is the reinforcement ratio in the effective concrete tensile zone. The difference in mean strains is calculated according to:

$$(\varepsilon_{sm} - \varepsilon_{cm}) = \frac{\sigma_s - k_t \frac{fctm}{\rho_{s,ef}}\left(1 + \alpha_e \rho_{s,ef}\right)}{E_s} \geq 0.6\frac{\sigma_{sr}}{E_s} \tag{9}$$

where σ_s is the reinforcement stress, and k_t is dependent on load duration (short- or long-term loading) and varies from 0.4 to 0.6. The authors have chosen $k_t = 0.6$ due to the probable absence of creep and shrinkage in the experimental results and applies in general as a chosen value for the other codes as well. The ratio between steel and concrete Young's modules is defined as $\alpha_e = E_s/E_{cm}$ (Eurocode 2 Part 1-1, 2004).

Table 1. Plasticity damage parameters.

Ψ	E	fb0/fc0	Kc	μ
35	0.1	1.16	0.667	0 and 0.0001

3.2 *Model Code 2010*

The maximum calculated crack width at the height of the reinforcement is found by:

$$w = 2l_{s,max}(\varepsilon_{sm} - \varepsilon_{cm}) \tag{10}$$

when the term related to shrinkage strains is neglected. Here, $l_{s,max}$ denotes the length over which slip between concrete and steel is assumed to occur and is expressed by:

$$l_{s,max} = k \cdot c + \frac{1}{4}\frac{f_{ctm}}{\tau_{bms}}\frac{\varphi_s}{p_{s,ef}} \tag{11}$$

where $k = 1$ is an empirical parameter considering the influence of the concrete cover chosen according to the recommended value and c is the concrete cover. The mean bond strength between steel and concrete is chosen as $\tau_{bms} = 1.8f_{ctm}$. The relative mean strain in Equation 10 is the same as chosen in Equation 9 but the lower bound limits between the mean strains are different.

MC2010 allows for extrapolation of the crack width at the reinforcement height given in Equation 10 by a factor (h-x)/(d-x) where, h is cross-section height, x is the height of the compressive sone, and d is the effective height. This extrapolation is valid for cover up to 75mm. For larger covers a more detailed analysis is required and procedures based on fracture mechanics approach would be appropriate.

3.3 *Draft for the new Eurocode 2, 2022 (pr EN 1992-1-1)*

In the draft for the new Eurocode 2 the calculation of crack width is expressed as:

$$w_{k,cal} = k_w S_{rm,cal}(\varepsilon_{sm} - \varepsilon_{cm}) \tag{12}$$

where $k_w = 1.7$ is a factor converting the mean crack width into a calculated crack width and is chosen according to the recommended value. $S_{rm,cal}$ is the calculated mean crack spacing assumed to be valid for both initial cracking and a stabilized crack pattern.

For elements subjected to direct loads or subjected to imposed strains $\varepsilon_{sm} - \varepsilon_{cm}$ can be expressed as:

$$\varepsilon_{sm} - \varepsilon_{cm} = k_{1/r}\frac{\sigma_s - k_t\frac{fctm}{\rho_{s,ef}}\left(1 + \alpha_e\rho_{s,ef}\right)}{E_s} \geq 0.6\frac{\sigma_{sr}}{E_s} \tag{13}$$

Where $k_{1/r}$ is a coefficient to account for the increase of crack width due to curvature which is expressed as:

$$k_{1/r} = \frac{h - x}{h - a_{y.i} - x} \tag{14}$$

Here x is the distance to the neutral axis, and $a_{y.i}$ is the cover distance plus rebar size. The mean crack spacing is:

$$S_{r,m,cal} = 1.5c + \frac{k_{fl}k_b}{7.2} \cdot \frac{\varphi}{\rho_{p,ef}} \tag{15}$$

where c is cover to the longitudinal reinforcement, φ is bar diameter, $k_b = 0.9$ is a coefficient for bond properties for ordinary reinforcement chosen according to the recommended value and $k_{fl} = (h - h_{c,eff})/h$, where h is cross-section height and $h_{c,eff}$ is the effective tension area.

3.4 *NLFEA and codes*

EC2 and MC2010 both state that SLS verifications using NLFEA can be performed a posteriori. In the case of bending cracks, the crack opening (w) may be calculated according to Dutch guidelines (Hendriks 2017):

$$w = S_{r,max} \cdot \bar{\varepsilon}_s \tag{16}$$

Where $\bar{\varepsilon}_s$ is the mean strain value of the longitudinal reinforcement in the cracked zone obtained in the analysis and $S_{r,max}$ is the maximum crack spacing according to EC2.

4 EXPERIMENTAL TEST AND FEA MODELLING

4.1 *Hognestad beam tests, control of flexural cracking*

From the established database, the investigation carried out by Hognestad (1962) was chosen as appropriate for this paper. This experimental work involved 36 rectangular beams with a length of 3429 mm. Different parameters were chosen as major variables such as bar diameter, bar type, concrete strength, reinforcement ratio, beam width and depth and thickness of cover as shown in Table 2 (Hognestad 1962). All beams were loaded by twin-loads at the third points of the span. To prevent shear failures, the outer thirds were reinforced with ø10 stirrups. The beams examined in this study are No 31 and 32, with respective properties given in Table 3. The different parameter variables shown in Table 2 are included to highlight the extensive work done by Hognestad and are relevant for further work.

Table 2. Parameter variations done by Hognestad.

Beams No.	Major Variable	Description
1–4	Bar diameter	Size and number of rebars
5–7	Bar diameter	Size and number of rebars
8–10	Bar diameter	Size and number of rebars
11–12	Bar diameter	Size and number of rebars
13–16	Bar diameter	Size and number of rebars
17–20	Bar diameter	Size and number of rebars
21–24	Beam width	Size and number of rebars
25–28	Beam depth	Size and number of rebars
29–32	Concrete cover	horizontal cover
33–36	Concrete cover	vertical and horizontal cover

* Both compressive and tensile concrete strength varied for the test series (Hognestad 1962).

Table 3. Geometrical and material properties for Beam No 31 and 32.

Description	mm	Description	MPa
Beam height*	406	fck*	25,1
Beam width*	203	fct*	2,57
Cover vertical B31	63	Es*	200.000
Cover vertical B32	112	Ec*	31.504
Cover horizontal*	25		
Effective depth B31	322		
Effective depth B32	294.5		
Beam length*	3429		
Bar size*	22		
Number of bars*	2		

* Properties shared by both beams No 31 and 32.

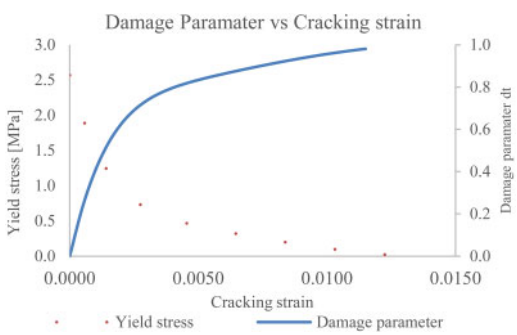

Figure 4. Softening branch of concrete in tension with corresponding damage parameter development applied by Abaqus.

Table 4. Stress-strain values for reinforcement and steel plates.

Yield Stress (σ_t) MPa	Plastic Strain $\tilde{\varepsilon}^{pl}$
Reinforcement:	
575*	0.0
Steel plates:	
275*	0.0

* Both steel plates and reinforcement never reach yielding during the analysis and plastic strains are therefore not calculated

4.2 *Finite element modelling of the RC beams*

To develop the FE models of the RC beams, steel loading- and support plates as well as the concrete cross-section were modelled using 3D brick elements. The FE models thus consist of three types of materials (concrete, steel plate, reinforcement). The embedded reinforcement technique available in ABAQUS is also used. The beams are reinforced with 22 mm rebar diameters with either 84 mm or 122.5mm distance from the outermost surface to the centroid of the reinforcement.

The elements chosen for concrete and steel plates in Abaqus is C3D20R quadratic brick elements with reduced integration (20 nodes and 8 integration points). The element size is approximately 20x20x20 mm and chosen in accordance with Dutch guidelines (Hendriks 2017) maximum element size for NLFEA. For the longitudinal reinforcement wire elements each with a length of 20 mm is used. The loading of both beams are displacement controlled.

There is a mesh sensitivity problem in cases with little or no reinforcement with the specification of a post failure stress-strain relation, in the sense that the finite element predictions do not converge to a unique solution as the mesh is refined because mesh refinement leads to narrower crack bands. In these beam models a post failure material behaviour as explained earlier with tension stiffening derived from Hordijk softening curve is applied and the cracking failure are distributed evenly and results in additional cracks and mesh sensitivity analysis with other element sizes is not performed.

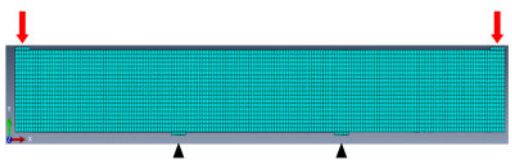

Figure 5. Model of Hognestad Beam in Abaqus.

5 RESULTS

5.1 *Load displacement behaviour*

The load displacement curves were not reported by Hognestad and therefore the FEA load-displacement is used as an indicator for crack development and used to compare when cracking occurs. Also, some sensitivity checks applying various values for the previously discussed viscosity parameter are performed. Viscosity parameters equal to 0 and 0.0001 were used, and from 5.2 we can observe that for beam No. 31 that when initial cracking occurs at approximately 20 kN loading there is a slight difference between the two solutions. This is due to that the viscosity parameter greater than 0 allows for stresses outside the yield surface but provides accurate enough results. For beam No. 32 the Viscosity parameter of 0 are not done due to the iterative process and length of the analysis required.

5.2 *Experimental crack widths*

From the Hognestad beam tests measured surface crack widths at both the height of the steel centroid and concrete top face are reported. The results for the selected beams are given in 5.3. From the measured crack widths, we notice that the crack widths at the height of reinforcement are similar regardless of concrete cover.

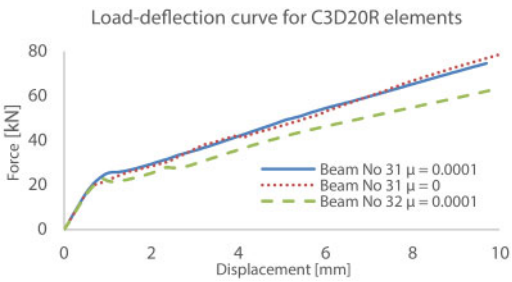

Figure 6. Load deflection curve for different viscosity parameter.

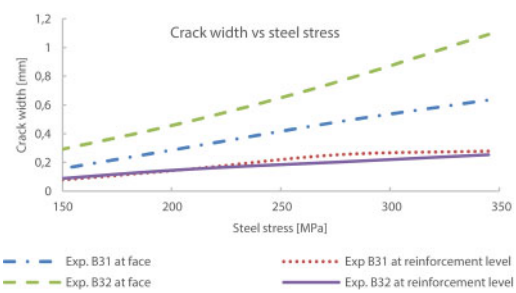

Figure 7. Experimental maximum crack widths vs steel stresses for beam No. 31 and No. 32 (Hognestad 1962).

5.3 *Maximum crack width predicted by design codes*

The predicted maximum crack widths according to EC2, MC2010 and the draft for new EC2 from equations 7,10 and 12 are compared in Figure 8.

It can be noted that for both beams the estimated crack widths are conservative at the height of reinforcement but underestimated at the outermost concrete face for EC2 and the draft for new EC2. MC2010 predict the crack width at the outermost concrete face to a good extent for 62 mm cover but underestimate it for 112 mm cover. The extrapolation of the results to get the crack width at the outermost concrete face are not valid for a larger cover than 75mm but are chosen to be included here.

The new term ($k_{1/r}$) accounting for the curvature in the new EC2 looks to provide a better result for the crack width at increased steel stresses beyond 250 MPa for both beams than the current EC2.

5.4 *Calculations of crack widths combining NLFEA and EC2*

The maximum crack width is calculated from Equation 16. Mean steel strains ($\bar{\varepsilon}_s$) for Beam No. 31 and 32 are extracted from the NLFEA. The maximum crack spacing ($S_{r,max}$) is calculated from equation 8 in accordance with EC2. In addition, the measured maximum spacing between the cracks in the constant moment zone from the Abaqus models at the stabilized cracking stage is also used (steel stress close to 350MPa).

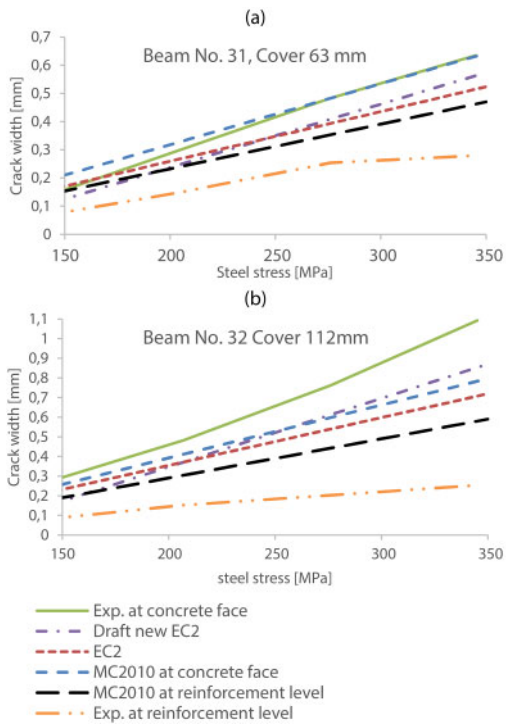

Figure 8. Crack widths predicted by design codes, (a) Beam No. 31, (b) Beam No. 32.

From Figure 9 we can determine the maximum crack spacings from where we have a stabilized cracking pattern at $\sigma_s = 350$ MPa, to (a) $S_{r,max} = 240$ mm and (b) $S_{r,max} = 300$ mm.

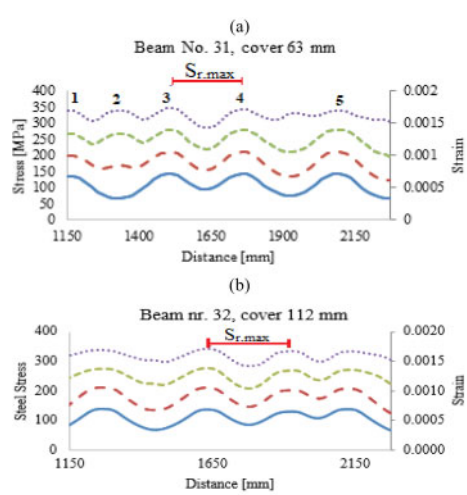

Figure 9. Steel stress levels and corresponding strains along the rebar length in the cracked concrete zone (constant moment), (a) Beam No. 31 numbers 1-5 indicate the localization of cracking strains in Figure 13, (b) Beam No. 32.

From Figure 10 the method based on extracting mean steel strains from the NLFEA and using the EC2 formulation for $S_{r,max}$ and the maximum crack spacing from the analysis shown in Figure 9 to calculate the crack widths at the reinforcement height are conservative. On the other hand, the EC2 formulation for maximum crack spacing fits better at the outmost concrete face than the maximum crack spacing from the analysis.

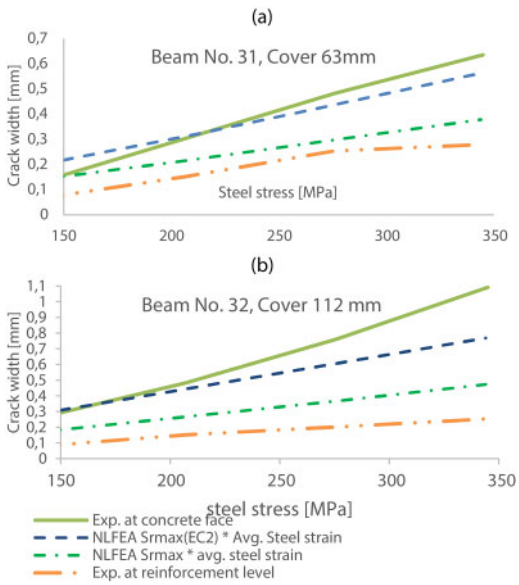

Figure 10. Crack widths estimated by extracting steel strains from NLFEA, (a) Beam No. 31, (b) Beam No. 32.

5.5 *Crack width determined by the Concrete Damage Plasticity model*

From the results in Abaqus the cracking strains are found meaning we can determine the crack width as:

$$w = \varepsilon^{cr} \cdot h_{eq} \tag{17}$$

The cracks localize within the brick elements, and at the top face of the beam the crack widths vary over the width of the beam. The crack widths are calculated by selecting the cracked elements across the beam width and using average cracking strain ε^{cr} multiplied with the crack band width (h_{eq}) which is an essential parameter in constitutive models that describe the softening stress-strain relationship. The preferred method is a method based on the initial direction of the crack and the element dimensions (Hendriks 2017). For both beams the length of the crack band width is 20mm. The development of the crack width using this method is shown in Figure 11. The crack localizations are visualized in 6.

Crack 1 in Figure 11 is selected representing the maximum crack width for both beams and compared

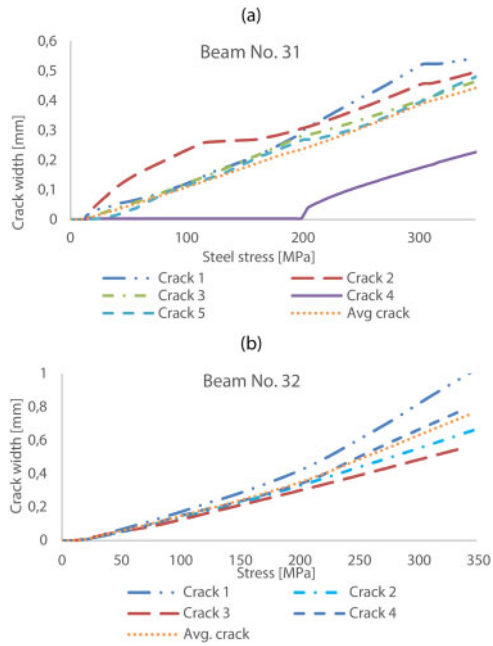

Figure 11. Crack widths of major cracks in the constant moment zone estimated by NLFEA, (a) Beam No. 31, (b) Beam No. 32.

to the reported experimental crack width values in Figure 12.

It is observed that the NLFEA with CDP-model can accurately predict the crack width at the concrete face for the two experimental beams.

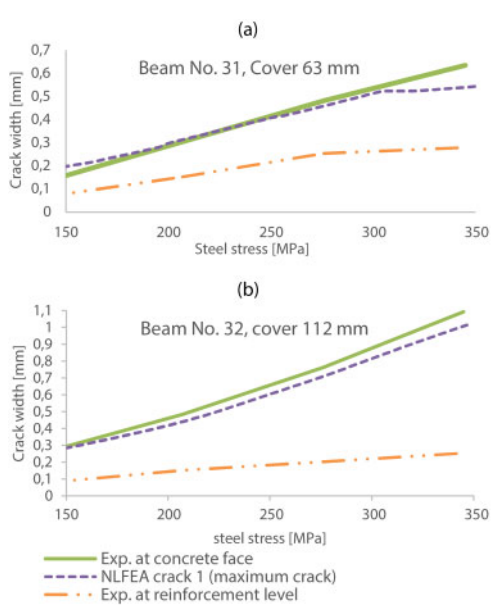

Figure 12. Maximum crack widths estimated by NLFEA CDP-model vs experimental values, (a) Beam No. 31, (b) Beam No. 32.

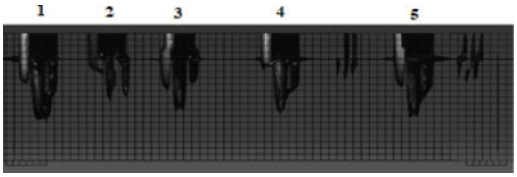

Figure 13. Visualization of localized cracking strains in between the supports for Beam No. 31 at $\sigma_{sr} = 350MPa$.

6 DISCUSSION

By applying the CDP-model with embedded reinforcement (no-slip) and calculating the crack width directly (Equation 18) by the cracking strain and the selected bandwidth as shown in Figure 14, we were able to obtain good crack width predictions of the reported experimental results at the outer most concrete face. Using the Dutch guidelines (Equation 16) with maximum crack spacing ($S_{r,max}$) defined in EC2 (Equation 8) provided also good agreement for beam No. 31 with cover 63 mm, while for beam no. 32 with cover 112 mm the results are to the unconservative side at the outermost concrete face. One reason looks to be that the maximum crack spacing ($S_{r,max}$) in EC2 does not fully consider the curvature effect for beams in bending and the impact of large concrete covers do not seem to be fully accounted for in the current code.

EC2 underestimate the maximum crack width at the outermost concrete face. In fact, it is observed that the underestimation is increasing for larger concrete cover. This seems to be addressed better in the draft for the new EC2 which introduces a coefficient ($k_{1/r}$) to account for increased crack widths due to the curvature from bending. However, it is still underestimating the crack widths at the outermost concrete face, but the results look to be more consistent in comparison with the current EC2. The need for this coefficient for concrete beams subjected to pure bending is supported by the observed results shown in Figure 7 and 14, as it is noticed that both beams have quite similar measured experimental crack widths at the reinforcement level.

MC2010 predict the crack width at the outermost concrete face for beam No. 31 to a very good extent by extrapolating the calculated crack width at reinforcement level, while being conservative at the reinforcement level. The corresponding result for Beam No. 32 by using MC2010 might be considered invalid since the distance from the reinforcement level to the outmost concrete face is larger than 75 mm. It is not clear to the first author how the code accounts for this except stating the following: *"For larger concrete cover a more detailed analysis is required. Procedures based on the fracture mechanics approach would be appropriate"*. However, it seems that methods like the CDP-model are applicable.

From the investigated beams it can be noted that a pivotal question has risen. At which location should the maximum crack width be determined? The term accounting for the curvature in the new EC2 ($k_{1/r}$) is logical, but especially for beams with large concrete cover this gives large crack widths at outermost concrete face. This increase in calculated crack width might have large economic consequences if not the allowed crack limits in the codes are adjusted to this increase. A relevant observation for this discussion is that both beams have quite similar measured experimental crack widths at the reinforcement level that we want to protect with a concrete cover.

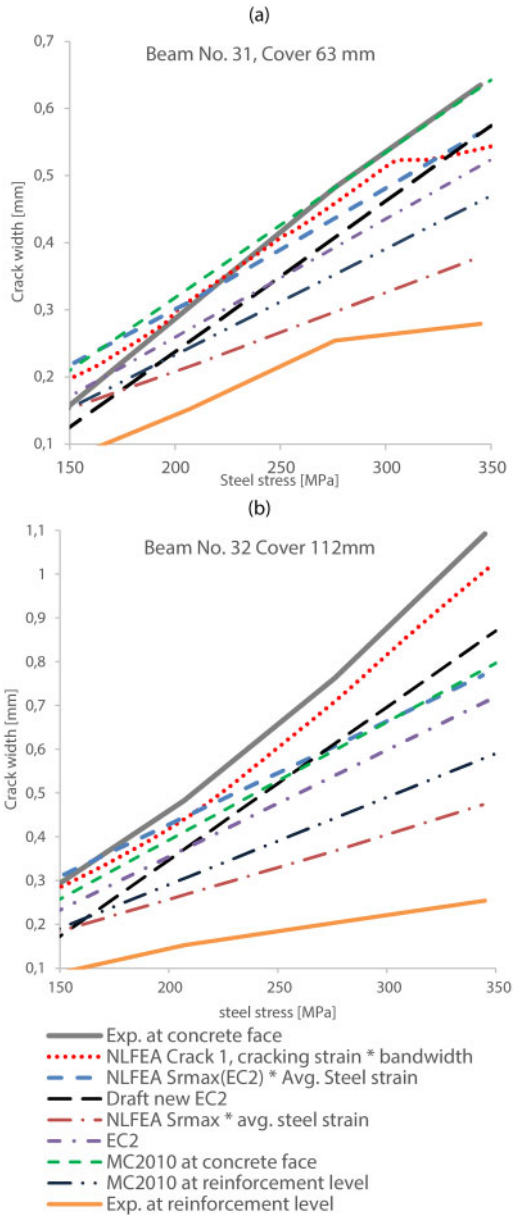

Figure 14. Crack widths vs steel stress for different approaches, (a) Beam No. 31, (b) Beam No. 32.

7 CONCLUSIONS

In this paper NLFEA with the concrete damage plasticity (CDP) model has been used to calculate the maximum crack widths in beams. The results have been compared to experimental values and results from various analytical prediction models. The results suggest that the following conclusion can be drawn:

1. 3D NLFEA analysis with the CDP model and embedded reinforcement is used to calculate the maximum crack width by multiplying the largest average cracking strain at the concrete face through the width of the beam with the selected bandwidth (Equation 18). The resulting crack widths gave predictions in good agreement with the experimental values at the outer most concrete face regardless of the cover size. This suggests that this method take the effect of cover and curvature due to bending into account better than the other NLFEA solutions and the analytical methods in the codes.
2. EC2 gave conservative results for the maximum crack width at the reinforcement level but underestimate the crack width at the outermost concrete face for the investigated beams. This suggest that the current EC2 do not correctly account for the concrete cover and the curvature effect.
3. MC2010 gave conservative results for the maximum crack width at the reinforcement level for both beams. While it gave good predictions at the experimental values at the outermost concrete face for a cover of 63 mm, the prediction was poor for cover size 112 mm. This cover size is greater than the allowed value of 75 mm and thereby clearly shows the limited validity range for beams subjected to bending in MC2010.
4. Calculating the maximum crackwidth from the draft of the new EC2, accounting for the increase in curvature by the factor $k_{1/r}$ gives better agreement than the current EC2 for crackwidth at the outermost concrete surface for increased steel stresses but is still slightly to the unconservative side. This suggests that the introduction of a curvature effect is a more correct solution for beams in bending, but this is based on only two examined beams.
5. Crackwidth calculations based on extracting the average steel strains from the NLFEA with a maximum crack spacing have been performed using two approaches:
   (a) With $S_{r,max}$ from EC2: Good agreement with crack widths at the outermost concrete face was achieved for beam no. 31 but were unconservative for beam no. 32. This suggest that the maximum crack spacing in EC2 do not fully account for the effect of large concrete covers.
   (b) The approach with $S_{r,max}$ extracted directly from the NLFEA is considerably underestimating the crackwidth at the outermost concrete face but is conservative at the reinforcement level.
6. From the conclusions in 1-5 the following can be derived:
   - Predicting crack widths at the outer most concrete face 3D NLFEA with CDP-model using cracking strains and a selected bandwidth (Equation 18) have no visible cover restrictions and gave the best results for the methods involving NLFEA.
   - From the applied codes, the draft for new EC2 seems best suited for a general crack width estimation regardless of concrete cover for beams subjected to bending.

8 FURTHER WORK

The authors are currently establishing a larger crack width database including a large number of experimental studies. Some of these will be investigated further with NLFEA to supply more raw data for recommendations on different solutions for better crack width prediction in beams subjected to bending with large concrete covers.

REFERENCES

Demir, A et al. 2018. "Effect of viscosity parameter on the numerical simulation of reinforced concrete deep beam behavior." *The Online Journal of Science and Technology*

Hordijk, Dirk Arend. 1991. "Local Approach to Fatigue of Concrete." *Delft University of Technology, The Netherlands*.

Hognestad, E. 1961 "High Strength Bars as Concrete Reinforcement Part 1. Introduction to a Series of Experimental Reports" *Journal of the PCA Research and Development Laboratories September 1961*

Hognestad, E. 1962 "High Strength Bars as Concrete Reinforcement Part 2: Control of Flexural Cracking" *Journal of the PCA Research and Development Laboratories September 1962*

M.A.N Hendriks, A. de Boer, B. Belletti, "Guidelines for Nonlinear Finite Element Analysis of Concrete Structures", *Rijkswaterstaat Centre for infrastructure, Report RTD: 1016-1:2017, 2017.*

Basteskår M, Engen M, Kanstad T, Fosså KT. *"A review of literature and code requirements for the crack width limitations for design of concrete structures in serviceability limit states" Structural Concrete. 2019;1.11.*

Basteskår, M., Engen, M., Kanstad, T., Johansen, H., Fosså, K. *"Serviceability limit state design of large concrete structures: Impact on reinforcement amounts and consequences of design code ambiguity." Engineering structures* 2019; Vol. 201.

Lubler, J., J. Oliver, S. Oller, and E. Oate, *"A Plastic-Damage Model for Concrete,"* International Journal of Solids and Structures, vol. 25, no.3, pp. 229–326, 1989.

Lee, J., and G. L. Fenves, *"Plastic-Damage Model for Cyclic Loading of Concrete Structures,"* Journal of Engineering Mechanics, vol. 124, no.8, pp. 892–900, 1998.

Tan, Reignard. 2019 "Consistent crack width calculation methods for reinforced concrete elements to 1D and 2D stress states A mixed experimental, numerical and analytical approach" Doctoral thesis, Norwegian University of Science and Technology.

Paper II

Performance study of crack width calculation methods according to Eurocodes, fib model codes and the modified tension chord model

Terjesen, O., Kanstad, T., and Tan, R. (2024).

© 2024 The Authors. Structural Concrete published by John Wiley & Sons Ltd on behalf of International Federation for Structural Concrete.

fib structural concrete 2024: DOI: https://doi.org/10.1002/suco.202300367

Check for updates

Received: 11 May 2023 | Revised: 5 December 2023 | Accepted: 15 January 2024

DOI: 10.1002/suco.202300367

ARTICLE

fib CEB-FIP WILEY

Performance study of crack width calculation methods according to Eurocodes, *fib* model codes and the modified tension chord model

Otto Terjesen[1] | **Gianclaudio Pinto**[2] | **Terje Kanstad**[3] | **Reignard Tan**[3,4]

[1]University of Agder, Grimstad, Norway
[2]Implenia Norway AS, Oslo, Norway
[3]Norwegian University of Science and Technology, Trondheim, Norway
[4]Multiconsult AS, Oslo, Norway

Correspondence
Otto Terjesen, University of Agder, Jon Lilletuns vei 9, 4879 Grimstad, Norway.
Email: otto.terjesen@uia.no

Funding information
Norges Teknisk-Naturvitenskapelige Universitet; Universitetet i Agder

Abstract

This article investigates the accuracy of various crack width prediction models and the newly proposed modified tension chord model (MTCM). A large number of experimental crack widths have been collected from the literature, including 203 specimens of reinforced concrete (RC) members subjected to bending and tension. The prediction models are described with upcoming new formulations and database validation. The modeling uncertainty is found by comparing the predicted crack widths against experimental data obtained using a log-normal distribution. The results show that fib Model Code 2010 and MTCM provide the best crack width predictions of the collected databases; MTCM has the fewest mechanical simplifications of the investigated models and no empirical modifications for fitting towards experimental databases, in contrast to the approaches in Eurocode 2 and Model Code. However, the latter do predict the crack width to a reasonably good extent and are more suited for practical dimensioning than the MTCM. The findings in this article suggest that the MTCM should serve as a point of departure for further development of crack width calculation methods, and that it may have an extensive range of possible applications in the future.

KEYWORDS

bond stress distribution, concrete cover, crack stages, crack width, effective tension area, fitting of the databases by empirical modifications

1 | INTRODUCTION

Cracks are common in reinforced concrete (RC) structures, and usually occur with irregular distribution and different crack widths along an RC member. As long as the crack width remains within an acceptable range, these cracks neither impair the serviceability or bearing capacity, nor the durability of the structure (Leonhardt[1] and Beeby[2]). Strict crack width limits in RC structures often increase reinforcement amounts, and the economic consequences are significant.[3] Extensive research has been carried out, and many approaches exist to predict the crack widths, but conversely, it is difficult to predict them consistently and accurately. This is reflected in the many techniques and methods proposed in the literature.[4] There are, however, still substantial uncertainties

This is an open access article under the terms of the Creative Commons Attribution License, which permits use, distribution and reproduction in any medium, provided the original work is properly cited.
© 2024 The Authors. *Structural Concrete* published by John Wiley & Sons Ltd on behalf of International Federation for Structural Concrete.

in the calculations, mainly due to the large-scale concrete structures, the large concrete covers applied in harsh environments, and the introduction of more eco-friendly modern concretes.[5]

The main objective of this article is to investigate the accuracy of the various calculation models and to shed light on ongoing discussions. This is performed by comparing the experimental crack widths reported with crack widths predicted by selected analytical calculation methods from design codes such as the present Eurocode 2 (EC2) and the draft for its new final version FprEC2 (2022),[6,7] fib Model Code 2010 (MC2010) and its new draft 2020 (MC2020),[8,9] the German National Annex to Eurocode 2 (DIN)[10] and the recently published MTCM by Tan et al.[11] The different strategies used by the codes are categorized by Schlicke et al.[12] as either mechanical or calibrated models. The researchers behind MC2020 and FprEC2 have made their choices to improve the models. Still, large uncertainties remain, and the CEN member states must make their national application documents to FprEC2 in the coming years, and thus, more research is needed. Therefore, a database of 203 RC specimens of reinforced concrete (RC) members subjected to bending and tension has been collected from the literature with a total of 733 data points. All of the reported data was collected from various articles and books, with validation and control checks of the data for unreasonable values. The database validation was done by two different adjustments: one due to steel stress limitation and one due to a theoretical maximum mean crack width.

The present article is part of ongoing research activity related to the "*Coastal Highway Route E39*", a project launched by the Norwegian Public Roads Administration (NPRA) and to MEERC (More Efficient and Environmental Road Construction) being carried out at the University of Agder. Furthermore, the project aims to provide guidelines and contribute to a more consistent and correct crack width prediction methodology for RC structures in Serviceability Limit States (SLS).

The main finding in this article is that MTCM, without any empirical calibration, performs as well as, or even better than, the investigated code type formulations, which all are calibrated towards similar databases as developed in this research study.

2 | ANALYTICAL CRACK WIDTH PREDICTION METHODS

In this article, the following design codes are applied to each experimental data series: Eurocode 2 (EC2),[6] the new version of Eurocode 2 (FprEC2),[7] fib Model Code 2010 (MC2010),[8] the draft for the new fib Model Code 2020 (MC2020),[9] and the German National Annex (DIN).[10] In addition, the modified tension chord model (MTCM) developed by Tan[13] is included.

All of the investigated models derive crack width formulations that, in principle, are based on the same formulae:

$$w = S(\varepsilon_{sm} - \varepsilon_{cm}) \tag{1}$$

where w is the crack width, S is the crack spacing, and $(\varepsilon_{sm} - \varepsilon_{cm})$ is the difference between the mean steel and concrete strain over the transfer lengths between cracks, that is, over the crack spacing. The models apply different simplifications to determine the parameters, and the following section provides an overview of the formulations used by each model to determine the crack spacing, while the subsequent sections present the methods used to determine the strain difference.

Classical derivations of crack width formulas mainly stem from three theories: The no-slip theory is based on the assumption of a perfect bond between reinforcement and concrete. This assumption is based on the existence of internal cracks near the steel-concrete interface, occurring due to the strain incompatibility between reinforcement and concrete. It has been shown by Terjesen et al.[14] and Cervenka et al.[15] that good agreement between nonlinear finite element analysis (NLFEA) and experimental crack widths of concrete beams can be achieved assuming a perfect bond between reinforcement and concrete. However, this is found by computational modeling with a concrete damage plasticity model where the fracture energy is the governing parameter for concrete cracking. The second theory is the bond-slip theory, in which a slip is assumed to occur between reinforcement and concrete. The slip is assumed to be at its maximum at the crack, and after a certain distance, it becomes zero, MTCM and similar models, that is, the tension chord model (TCM). However, as shown in this article, the MTCM also agrees with experimental results. The last theory combines the two theories and is applied by Eurocode 2 and fib Model Code.

In addition to the investigated models, there are other prediction models available in the literature, that is, Chavin et al.[16] proposed a crack width model representing the stabilized cracking stage which is based on Beeby et al.[17,18] who observed that the steel strain variation is linear on both sides of a crack. From tensile force equilibrium, it follows that the linear concrete strain variation is related to a constant bond-stress relation. The model by Chavin et al. applies empirical modifications to describe the increase in crack width caused by the concrete cover. The study is related to highly debated statements from Beeby[17,19] that (a) cover is a more decisive parameter for

17517648, 0, Downloaded from https://onlinelibrary.wiley.com/doi/10.1002/suco.202300367 by Otto Terjesen - Norwegian Institute Of Public Healt Invoice Receipt DFO , Wiley Online Library on [17/03/2024]. See the Terms and Conditions (https://onlinelibrary.wiley.com/terms-and-conditions) on Wiley Online Library for rules of use; OA articles are governed by the applicable Creative Commons License

the prediction of crack width than the ratio ϕ/ρ_{eff} and that (b) bond-slip conditions of reinforcement exert a nil or negligible influence on crack widths.

The crack spacing prediction is a specific reference to reality derived from experiments, whereby statistical modification may address the prediction accuracy. The various models predict either a characteristic-, mean- or maximum crack width. These design models are based on the stabilized crack stage, that is, no significant increase in the formation of new cracks or decrease in crack spacing with increased loading should occur. In design, however, an argument made by the authors in[12] is that only the maximum crack width is essential and that we should evaluate this against the experiments, thus relating the crack width to the calculated transfer length instead of a designated crack spacing formula derived empirically from experiments. This statement stems from the fact that the calculated transfer lengths to each side of a crack are more critical than the crack spacing measured itself. This calls for a calculation model that can predict cracking in both the crack formation stage and the stabilized cracking stage, thus making S in Equation (1) a *transient* parameter explicitly dependent on the load level as well as the geometrical and material parameters.[20,21] At best, determining a representative maximum crack spacing from the experiments is challenging due to the input data's range of expected sizes, such as tensile strength along the concrete member and bond properties along the rebars. It is also challenging to determine which current crack stage the RC member is in with load levels based on experimentally measured results, and reported crack spacings for members in bending are often mean values with both a mean and maximum crack width.

The MTCM proposed by (Tan)[13] is an analytical calculation model based on solving the second-order differential equation (SODE) of the slip between rebar and concrete, to which the local bond-slip law according to MC2010 with adjusted parameters to account for the mechanical behavior of RC ties is applied. It yields closed-form solutions for the so-called comparatively lightly loaded member (CLLM) behavior being analogous to the crack formation stage and non-closed form solutions for the so-called comparatively heavily loaded member (CHLM) behavior being analogous to the stabilized cracking stage. It was derived based on the mechanical behavior of RC ties and has not been calibrated towards any experimental database, aiming to not limit the range of applicability regardless of geometrical and material parameters, in contrast to EC2 and MC2010. It was demonstrated in Reference 13 that the MTCM provides excellent potential for yielding consistent crack width predictions for large-scale concrete structures, that is, large covers, large cross-section dimensions and large reinforcement amounts. However, the non-closed form solutions for the CHLM behavior cannot directly figure as a code-type replacement for EC2 or MC2010 yet. Regardless, it can be applied at the project level, or it can be included in the national application documents of a country.

2.1 | Crack spacing

The applied methods predict the maximum crack spacing assuming that the concrete stress between two cracks can never be greater than its tensile strength. As the only exceptions, FprEC2 and MC2020 predicts the mean value and applies statistical modifications to predict the maximum crack width.

In the location of the crack, with corresponding steel stress, two different crack stages may occur, namely, (a) a single crack stage occurring when the steel force in the crack can be re-transferred entirely back into the cross-section without a new crack formation and (b) stabilized crack stage occurring when crack formation has progressed to such an extent that the steel strain between two adjacent cracks is greater than the ultimate tensile strain of concrete ($\varepsilon_c = f_{ct}/E_c$). Each solution strategy is in agreement with the theoretical grounds (Equation 1) for calculating the crack width; however, models differ in estimating crack spacing and the strain difference between the concrete and reinforcement.

2.2 | Differences in steel and concrete strains

For determining the difference in mean steel and concrete strain at a stabilized crack pattern, the design codes[6–10] use the expression in Equation (2).

$$\varepsilon_{\text{sm}} - \varepsilon_{\text{cm}} = \frac{\sigma_s - k_t \frac{f_{\text{ctm}}}{\rho_{\text{eff}}}(1 + \alpha * \rho_{\text{eff}})}{E_s} \tag{2}$$

where σ_s is the stress in the tensile reinforcement assuming a cracked section; k_t is a factor describing the effect of the duration of the load (0.6 for short-term loading and 0.4 for long-term loading); f_{ctm} is the mean tensile strength of concrete; ρ_{eff} is the effective reinforcement ratio, defined as $A_s/A_{c,\text{eff}}$; $A_{c,\text{eff}}$ is the effective tension area with an effective height $h_{c,\text{eff}}$; α is the modular ratio of steel and concrete defined as $\frac{E_s}{E_{\text{cm}}}$.

The k_t factor used in this article comparing theoretical and experimental results is the short-term value;

17517648, 0, Downloaded from https://onlinelibrary.wiley.com/doi/10.1002/suco.202300367 by Otto Terjesen - Norwegian Institute Of Public Healt Invoice Receipt DFO , Wiley Online Library on [17/03/2024]. See the Terms and Conditions (https://onlinelibrary.wiley.com/terms-and-conditions) on Wiley Online Library for rules of use; OA articles are governed by the applicable Creative Commons License

however, DIN use 0.4 for both short- and long-term load cases.

For the crack formation stage, EC2 and DIN use Equation (3) below, while MC2010 and MC2020 uses Equation (4) and FprEC2 with β equal to k_t defined above. Equations (3) and (4) defines the lower boundary for the difference in mean strains.

$$\varepsilon_{sm} - \varepsilon_{cm} \geq \frac{0.6 * \sigma_s}{E_s} \tag{3}$$

$$\varepsilon_{sm} - \varepsilon_{cm} \geq \frac{(1-\beta) * \sigma_s}{E_s} \tag{4}$$

2.3 | Tension chord models

The TCM[22,23] was developed in the 1990s at ETH Zurich. It models structural elements loaded in tension, including the effect of the bond between reinforcement and concrete, that is, the tension stiffening effect with only the magnitudes of the bond stresses as empirical parameters. The bond-slip behavior $\tau_b - u$ is assumed to be rigid-perfectly plastic, with a value $\tau(u) = \tau_{b0} = 2f_{ct}$ for regions where the reinforcement stresses are below yielding and $\tau(u) = \tau_{b1} = f_{ct}$ after the onset of yielding. These regions are visualized in Figure 1.

The model assumes that the nominal bond stresses (τ_b) are independent of the slip (u) and instead step-wise dependent on steel stress (σ_s), that is, $\tau_b(\sigma_s)$. This assumption enables the kinematic relations of a differential element of a reinforcing bar embedded in concrete to be expressed as:

$$\frac{du(x)}{dx} = \varepsilon_s(x) - \varepsilon_c(x) \tag{5}$$

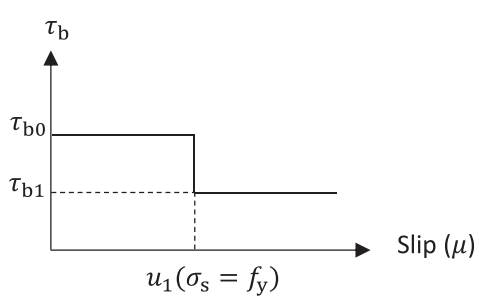

FIGURE 1 Definition of the constitutive model used in TCM before and after yielding.

Equilibrium conditions of the same element can be expressed as:

$$\frac{d\sigma_s(x)}{dx} = \frac{4\tau_b(u(x))}{\phi_s} = \frac{4\tau_b}{\phi_s} \tag{6}$$

with $\varepsilon_s(x)$, $\varepsilon_c(x)$ = steel and concrete strains along the reinforcement bar, $\sigma_s(x)$, $\tau_b(x)$ = steel stress and bond stress along the reinforcement bar, u = slip between reinforcing bar and concrete, ϕ_s = reinforcement bar diameter. With the assumption that bond stress is entirely determined by steel stress at a specific location (known by equilibrium), the steel stress can be determined by:

$$\sigma_s(x) = \sigma_{sr} - \frac{4\tau_b x}{\phi_s} \tag{7}$$

with $\sigma_{sr} = F/A_s$ = steel stress at the crack. The steel stress in Equation (7) yields a linear decrease in the steel stress from the crack to the middle of the cracked element caused by bond stresses.

The general expression for crack spacing for a stabilized crack stage is found by equilibrium considerations of a reinforced concrete tie between two cracks and is visualized in Figure 2 and deduced in the following:

$$\sigma_{sr} A_s = \sigma_s(S_r/2)A_s + f_{ctm}(A_c - A_s) \tag{8}$$

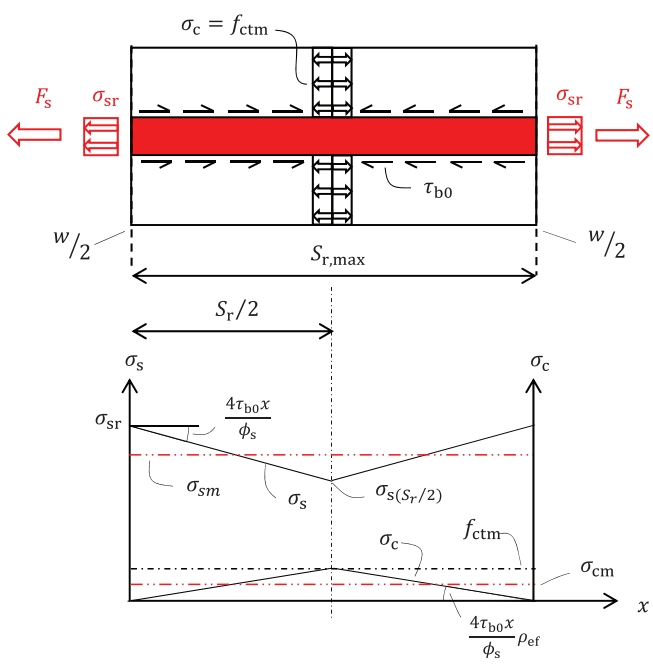

FIGURE 2 Distribution of steel and concrete stresses over the cracked RC-tie according to TCM below steel yielding for a stabilized crack pattern.

17517648, 0, Downloaded from https://onlinelibrary.wiley.com/doi/10.1002/suco.202300367 by Otto Terjesen - Norwegian Institute Of Public Healt Invoice Receipt DFO , Wiley Online Library on [17/03/2024]. See the Terms and Conditions (https://onlinelibrary.wiley.com/terms-and-conditions) on Wiley Online Library for rules of use; OA articles are governed by the applicable Creative Commons License

$$f_{\mathrm{ctm}}(A_c - A_s) = \sigma_{\mathrm{sr}} A_s - \sigma_s (S_r/2) A_s = \tau_{\mathrm{b0}} n \pi \phi_s \frac{S_r}{2} \tag{9}$$

Introducing an effective concrete area $\rho_{\mathrm{ef}} = A_s/A_c$ the concrete area can be expressed as:

$$A_c = \frac{A_s}{\rho_{\mathrm{ef}}} \tag{10}$$

where $\rho_{\mathrm{ef}} = n\phi^2\pi/4A_c$. By inserting Equation (10) into Equation (9), solving for crack spacing $S_{r,\max}$ yields the maximum crack spacing as:

$$S_{r,\max} = S_{\mathrm{TCM}} = \frac{f_{\mathrm{ctm}} \phi_s (1 - \rho_{\mathrm{ef}})}{2\tau_{\mathrm{b0}} \rho_{\mathrm{ef}}} \tag{11}$$

For a stabilized crack pattern, the maximum crack width can be expressed by the crack spacing and the difference in steel and concrete deformation. For the TCM, this yields:

$$w = \delta_s - \delta_c = S_{\mathrm{TCM}} (\varepsilon_{\mathrm{sm}} - \varepsilon_{\mathrm{cm}}) \tag{12}$$

By integrating the steel strains over the crack spacing S_{TCM} yields the mean steel strain as:

$$\varepsilon_{\mathrm{sm}} = \frac{1}{S_{\mathrm{TCM}}} \int_0^{S_{\mathrm{TCM}}} \varepsilon_s(x) dx = \frac{1}{E_s} \left(\sigma_{\mathrm{sr}} - \frac{\tau_{\mathrm{b0}} S_{\mathrm{TCM}}}{\phi_s} \right) \tag{13}$$

and mean concrete strains.

$$\varepsilon_{\mathrm{cm}} = \frac{1}{S_{\mathrm{TCM}}} \int_0^{S_{\mathrm{TCM}}} \varepsilon_c(x) dx = \frac{1}{E_c} \rho_{\mathrm{ef}} \frac{\tau_{\mathrm{b0}} S_{\mathrm{TCM}}}{\phi_s} \tag{14}$$

Furthermore, by inserting Equations (13) and (14) into Equation (12), we can now express the maximum crack width by TCM as:

$$w = S_{\mathrm{TCM}} \left[\frac{1}{E_s} \left(\sigma_{\mathrm{sr}} - \frac{\tau_{\mathrm{b0}} S_{\mathrm{TCM}}}{\phi_s} \right) - \frac{1}{E_c} \rho_{\mathrm{ef}} \frac{\tau_{\mathrm{b0}} S_{\mathrm{TCM}}}{\phi_s} \right] \tag{15}$$

The German code DIN applies the same equilibrium shown in Equations (5)–(9) but does not include the steel area in Equation (9), yielding the following expression for the maximum crack spacing.

$$S_{\mathrm{DIN}} = \frac{f_{\mathrm{ctm}} \phi_s}{2\tau_{\mathrm{b0}} \rho_{\mathrm{ef}}} \tag{16}$$

DIN then assume $\tau_{\mathrm{b0}} = 1.8 f_{\mathrm{ctm}}$ and inserting this into Equation (13) yields the maximum crack spacing shown in Table 1.

$$S_{\max} = \frac{\phi_s}{3.6 \rho_{\mathrm{ef}}} \tag{17}$$

TABLE 1 Summary of crack spacing formulae in the design codes and MTCM.

Code	Crack spacing formula	Information
EC2	$s_{r,\max} = k_3 c + k_1 k_2 k_4 \frac{\phi}{\rho_{\mathrm{eff}}}$	$k_1 = 0.8$, $k_3 = 3.4$, $k_4 = 0.425$ $k_2 = 0.5/1$ (bending/tension)
prEC2	$s_{r.m,\mathrm{cal}} = 1.5c + \frac{k_{\mathrm{fl}} k_{\mathrm{b}}}{7.2} \frac{\phi}{\rho_{\mathrm{eff}}} \leq \frac{1.3}{k_{\mathrm{w}}}(h - x)$	$k_b = 0.9$ $k_{\mathrm{fl}} = \frac{1}{2}\left(1 + \frac{h - x_{\mathrm{g}} - h_{\mathrm{c,eff}}}{h - x_{\mathrm{g}}}\right)$; $k_{\mathrm{w}} = 1.7$
MC2010	$s_{r,\max} = 2l_{s,\max} = 2\left[kc + \frac{1}{4}\frac{f_{\mathrm{ctm}}}{\tau_b}\frac{\phi}{\rho_{\mathrm{eff}}}\right]$	$k = 1$ $\tau_b = 1.8 f_{\mathrm{ctm}}$
MC2020	$s_{r,\max} = \beta_w \left(k_{\mathrm{c}} c + k_{\theta/\rho} k_{\mathrm{fl}} k_{\mathrm{b}} \frac{f_{\mathrm{ctm}} \phi}{\tau_{\mathrm{b}} \rho_{\mathrm{s,ef}}}\right)$	$k_c = 1.5$, $k_{\theta/\rho} = 0.25$, $k_b = 0.9$, $\tau_b = 1.8 f_{\mathrm{ctm}}$ $k_{\mathrm{fl}} = \frac{1}{2}\left(1 + \frac{h - x_{\mathrm{g}} - h_{\mathrm{c,eff}}}{h - x_{\mathrm{g}}}\right)$ $\beta_w = 1.7$ for stabilized cracking stage and 2.0 for the crack formation stage
DIN	$s_{r,\max} = \frac{\phi}{3.6\rho_{\mathrm{eff}}} \leq \frac{\sigma_s}{3.6 f_{\mathrm{ctm}}} \frac{\phi}{}$	
MTCM[a]	$S_{r,\mathrm{CHLM}} = \frac{1}{\delta}\left[\frac{f_{\mathrm{ctm}}}{E_{\mathrm{cm}}} \frac{1+\xi}{\xi\psi} \left(\frac{1}{2\gamma}\right)^{\frac{1}{2\delta}}\right]^{\frac{2\delta}{\beta}}$	CHLM (Maximum crack spacing in a stabilized cracking stage)
	$S_{\mathrm{r,CLLM}} = 2 \cdot \frac{1}{\delta}\left[\varepsilon_{\mathrm{sr}} \left(\frac{1}{2\gamma}\right)^{\frac{1}{2\delta}}\right]^{\frac{2\delta}{\beta}}$	CLLM (Crack formation stage where the maximum crack spacing is equal to two times the transfer length)

[a]Parameters are explained in Chapter 3.3.

17517648, 0, Downloaded from https://onlinelibrary.wiley.com/doi/10.1002/suco.202300367 by Otto Terjesen - Norwegian Institute Of Public Healt Invoice Receipt DFO , Wiley Online Library on [17/03/2024]. See the Terms and Conditions (https://onlinelibrary.wiley.com/terms-and-conditions) on Wiley Online Library for rules of use; OA articles are governed by the applicable Creative Commons License

2.3.1 | Modified tension chord model

The MTCM was developed by Tan in 2019.[13] It is based on solving the Second Order Differential Equation (SODE) for the slip in Equation (18) analytically.

$$\frac{d^2u}{dx^2} - \chi\tau(u) = 0 \tag{18}$$

where $\chi = (\sum \pi\phi_s/A_sE_s)(1+\xi)$ is a constant for equivalent cross-sections when using the SODE for the slip with the parameters ϕ_s, A_s, and E_s being the diameter, area and the Young's modulus for the rebar. Furthermore, the other constants are defined as $\xi = \alpha_E\rho_s/\psi$, $\alpha_E = E_s/E_c$, and $\rho_s = A_s/A_c$, with A_c being the sectional area of the RC tie and E_c the Young's modulus for concrete. The parameter $\psi \leq 1.0$ is a factor accounting for the fact that plane sections do not remain plane in RC ties.[24,25] It was observed by Tan et al.[11] that $\psi = 0.7$ seemed reasonably independent of geometry and load level.

The model considers the same equilibrium, compatibility and linear elastic material laws for steel and concrete as the TCM for a differential element in an RC tie. However, it assumes that the nominal bond stresses (τ_b) are directly dependent on the slip (u) as visualized in Figure 3, and not rigid-perfectly plastic as for the TCM. Solving for the slip in Equation (18) analytically requires using a local bond-slip law. The MTCM applies the local bond-slip law first proposed by Eligehausen et al.[26] and later adopted by MC2010 in Equation (19).

$$\tau(u) = \tau_{max}\left(\frac{u}{u_1}\right)^{\alpha} \tag{19}$$

where u is the slip at the load level and the empirical factors $\tau_{max} = 5\,\text{MPa}$, $u_1 = 0.1\,\text{mm}$, and $\alpha = 0.35$ are assumed to be representative of the behavior of RC ties. These factors were determined in Reference 27, with $\tau(u)$ representing a sort of the mean of local bond-slip curves for an arbitrary RC tie.

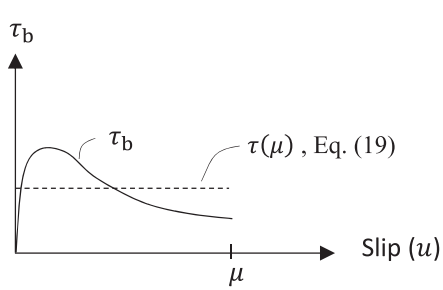

FIGURE 3 Definition of the constitutive model used in MTCM.

Inserting Equation (19) into (18) yields the SODE.

$$\frac{d^2u}{dx^2} - \chi\frac{\tau_{max}}{{u_1}^{\alpha}}u^{\alpha} = 0 \tag{20}$$

The nonlinear homogenous SODE in Equation (20) can now be solved analytically as described in Reference 11. Because the main application of the model is within SLS, the following sections focus on steel strains and stresses below yielding. In this state, the MTCM gives two sets of boundary conditions grouped by the two concepts of comparatively lightly loaded members (CLLM) and comparatively heavily loaded members (CHLM). These concepts are analogous to the crack formation stage (CLLM) and stabilized cracking stage (CHLM). The concept of CLLM is depicted in Figure 4a–c, in which the transfer length $S_{r0} = S_{r,\text{CLLM}}/2$ denotes the abscissa, where steel and concrete strains become compatible and consequently zero slip. This point moves towards the symmetry section L/2 with increasing load and a new crack is formed at the location where the concrete stresses exceed the tensile strength of the concrete, that is, $S_{r,\text{CLLM}}/2 = \text{L}/2$ if $\varepsilon_c(S_{r,\text{CLLM}}/2) = \varepsilon_{c,\max} \geq \varepsilon_{\text{ctm}} = f_{\text{ctm}}/E_c$. Afterwards, the concept of CHLM depicted in Figure 4d–f governs with $S_{r,\text{CHLM}}$ as the crack spacing. This concept now yields the response for the cracked member, in which it is observed that the distribution of steel and concrete strains remains incompatible over the entire crack spacing, and the slip is zero only at the symmetry section, as depicted in Figure 4d.

The solution of the SODE in Equation (20) can now be obtained by solving the equation for two sets of boundary conditions for the case of CLLM and CHLM. For CLLM, the slip and difference in strains are zero at the end of the transfer length s_{r0}. For CHLM, the slip is zero at the symmetry section $\frac{L}{2}$, however, the difference in strains is always larger than zero. With the chosen bond-slip law in Equation (19), the maximum slip at the loaded end in the case of CLLM Figure 4a can be found directly from the closed-form solution expressed as:

$$u_{\text{r,CLLM}} = \left(\frac{{\varepsilon_{\text{sr}}}^2}{2\gamma}\right)^{\frac{1}{\beta}} \tag{21}$$

with the constant $\gamma = \chi\tau_{max}/(\beta{u_1}^{\alpha})$, $\chi = (\sum \pi\phi_s/A_sE_s)(1+\xi)$, $\beta = 1+\alpha$ and the bond-slip parameters $u_1 = 0.1$ and $\alpha = 0.35$. For the case of CHLM, the maximum slip $u_{r,\text{CHLM}}$ depicted in Figure 4d has to be determined iteratively as a function of steel strain at the crack ($\varepsilon_{\text{sr}} = F/A_s$) due to the non-closed form solution of the SODE for this set of boundary conditions. The solution procedure for

17517648, 0, Downloaded from https://onlinelibrary.wiley.com/doi/10.1002/suco.202300367 by Otto Terjesen - Norwegian Institute Of Public Healt Invoice Receipt DFO , Wiley Online Library on [17/03/2024]. See the Terms and Conditions (https://onlinelibrary.wiley.com/terms-and-conditions) on Wiley Online Library for rules of use; OA articles are governed by the applicable Creative Commons License

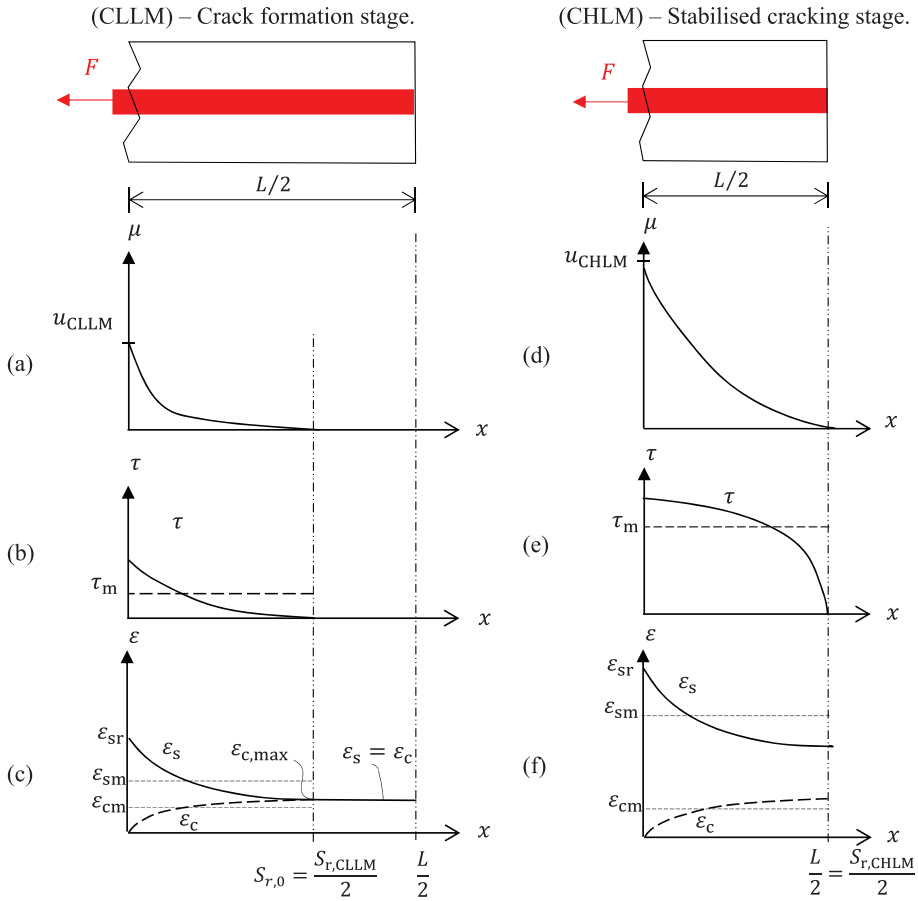

FIGURE 4 Distribution of slip, bond stress, steel and concrete strains over the cracked RC-tie for the concepts (a–c) CLLM and (b–f) CHLM.

determining the maximum slip is provided in Reference 11. Note that the slip in Equation (20) for both concepts directly depends on the reinforcement ratio and rebar size through the constant χ.

For CLLM, the crack spacing ($S_{r,\mathrm{CLLM}}$) expressed in Equation (22) is twice the theoretical transfer length of each side of a crack where steel and concrete strains become compatible in Figure 4c. The transfer length directly depends on the steel stain at the crack, which makes the transfer length transient.

$$S_{\mathrm{r,CLLM}} = 2 \cdot \left[\frac{1}{\delta} \left[\varepsilon_{\mathrm{sr}} \left(\frac{1}{2\gamma} \right)^{\frac{1}{2\delta}} \right]^{\frac{2\delta}{\beta}} \right] \tag{22}$$

In the case of CHLM, the steel and concrete strains in Figure 4f are found by integrating over the transfer length, which is defined as half the crack spacing and the maximum crack spacing ($S_{r,\mathrm{CHLM}}$) is given by:

$$S_{\mathrm{r,CHLM}} = \frac{1}{\delta} \left[\frac{f_{\mathrm{ctm}}}{E_{\mathrm{cm}}} \frac{1+\xi}{\xi\psi} \left(\frac{1}{2\gamma} \right)^{\frac{1}{2\delta}} \right]^{\frac{2\delta}{\beta}} \tag{23}$$

where $\delta = (1-\alpha)/2$.

The mean steel and concrete strains for the CLLM behavior can be expressed as:

$$\varepsilon_{\mathrm{sm}} = \frac{1}{S_{r,CLLM}} \frac{\xi \varepsilon_{\mathrm{sr}} S_{r,\mathrm{CLLM}} + 2u_{\mathrm{r,CLLM}}}{1+\xi} \tag{24}$$

$$\varepsilon_{\mathrm{cm}} = \frac{\psi\xi}{S_{r,\mathrm{CLLM}}} \frac{\varepsilon_{\mathrm{sr}} S_{r,\mathrm{CLLM}} - 2u_{\mathrm{r,CHLM}}}{1+\xi} \tag{25}$$

and for CHLM:

$$\varepsilon_{\mathrm{sm}} = \frac{1}{S_{r,\mathrm{CHLM}}} \frac{\xi \varepsilon_{\mathrm{sr}} S_{r,\mathrm{CHLM}} + 2u_{\mathrm{r,CLLM}}}{1+\xi} \tag{26}$$

$$\varepsilon_{\mathrm{cm}} = \frac{\psi\xi}{S_{r,\mathrm{CHLM}}} \frac{\varepsilon_{\mathrm{sr}} S_{r,\mathrm{CHLM}} - 2u_{\mathrm{r,CHLM}}}{1+\xi} \tag{27}$$

with the crack width for both cases expressed as:

$$w_{\mathrm{CLLM}} = S_{r,\mathrm{CLLM}} (\varepsilon_{\mathrm{sm}} - \varepsilon_{\mathrm{cm}}) \tag{28}$$

$$w_{\mathrm{CHLM}} = S_{\mathrm{r,CHLM}} (\varepsilon_{\mathrm{sm}} - \varepsilon_{\mathrm{cm}}) \tag{29}$$

17517648, 0, Downloaded from https://onlinelibrary.wiley.com/doi/10.1002/suco.202300367 by Otto Terjesen - Norwegian Institute Of Public Healt Invoice Receipt DFO , Wiley Online Library on [17/03/2024]. See the Terms and Conditions (https://onlinelibrary.wiley.com/terms-and-conditions) on Wiley Online Library for rules of use; OA articles are governed by the applicable Creative Commons License

In summary, both of the concepts of CLLM (crack formation stage) and CHLM (stabilized cracking stage) account for rebar size and reinforcement ratio for calculating the slip, which is nonlinear, as seen in Figure 4a, d. However, the main difference between the two is that the steel and concrete strains become incompatible over the entire bar length in the case of CHLM, as depicted in Figure 4f.

2.3.2 | The conceptual difference between the TCM and MTCM

The TCM assumes a simple step-wise, rigid-perfectly plastic bond-slip law that yields a slip (u) independent of the load level in regions below and above yielding in the reinforcement, as seen in Figure 1. The steel stress between two cracks is found by considering equilibrium, as shown in Equations (5)–(14), and the crack width is found as the difference between the steel and concrete deformation in Equation (15).

For the MTCM, the bond stress varies over the element length depending on the load level according to a given bond-slip relation. The maximum slip u_r, which is obtained in Equation (21) in the case of CLLM and iteratively in the case of CHLM, is required to calculate steel and concrete strains in Equations (24)–(27). The crack width is found by multiplying the strain difference with twice the transfer length for the case of CLLM or the crack spacing in CHLM, as shown in Equations (28) and (29).

The conceptual difference between TCM and MTCM is visualized in Figure 5 for steel stresses prior to yielding and a stabilized crack pattern (CHLM), in which the continuous and dashed lines represent steel strains ε_s and the corresponding concrete strains ε_c. Linear curves show that the strains vary over the bar length with a constant slope of $4\tau_{b0}/\phi_s$ for the TCM, while nonlinear strain distributions, in general, are observed for the MTCM.

2.4 | New parameters in FprEC2 and MC2020

FprEC2 and MC2020 include several modifications of both the crack width and maximum crack spacing formulas based on the work conducted by Caldentey et al.[28]

In MC2020, the factor k_{fl} is intended to account for the effect of stress distribution within the effective concrete tensile area.

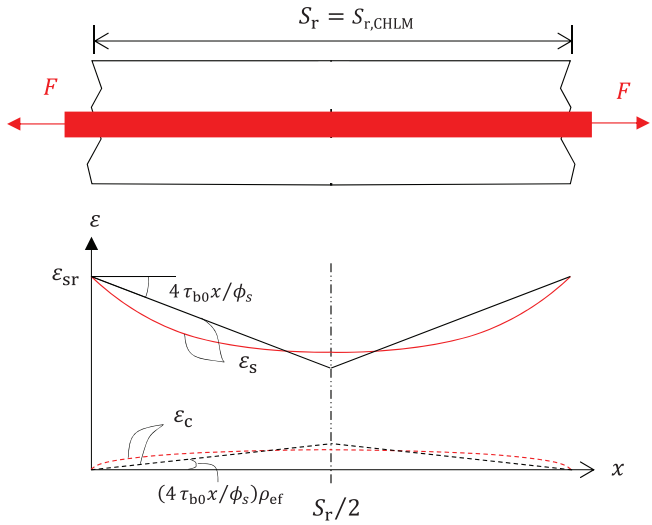

FIGURE 5 Concept of steel and concrete strain distribution over the bar length for a stabilized crack pattern below reinforcement yielding of CHLM. Linear strain distribution represents the concept of TCM, while Nonlinear distribution represents the concept of MTCM.

$$k_{fl} = \frac{1}{2}\left(1 + \frac{h - x_g - h_{c,ef}}{h - x_g}\right) \tag{30}$$

Equation (30) is valid for $h > x_g$, where x_g is the height of the compression zone of the uncracked section, and $h_{c,ef}$ is the height of the effective tensile area. The value of the expression of k_{fl} approaches 1 for pure tension (neutral axis depth $x_g = 0$) and 0.5 for bending when $h_{c,eff}$ is equal to the entire tensile zone ($h - x_g$).

Furthermore, for a rectangular cross-section under pure flexure ($x_g = h/2$) Equation (30) can be simplified to.

$$k_{fl} = \frac{h - h_{c,ef}}{h} \tag{31}$$

The factor k_b accounts for the effects of the casting process on the crack spacing, depending on whether the tensile zone is cast in a poor or good position in regard to the bond strength.

$$k_b = \begin{cases} 1.2 \text{ for poor bond conditions} \\ 0.9 \text{ for good bond conditions} \end{cases} \tag{32}$$

In the crack width formula, a new parameter introduced in FprEC2 is the curvature factor $k_{1/r}$ describing that, in bending, the value of the crack width increases proportionally with the distance from the tensile reinforcement.

17517648, 0, Downloaded from https://onlinelibrary.wiley.com/doi/10.1002/suco.202300367 by Otto Terjesen - Norwegian Institute Of Public Healt Invoice Receipt DFO , Wiley Online Library on [17/03/2024]. See the Terms and Conditions (https://onlinelibrary.wiley.com/terms-and-conditions) on Wiley Online Library for rules of use; OA articles are governed by the applicable Creative Commons License

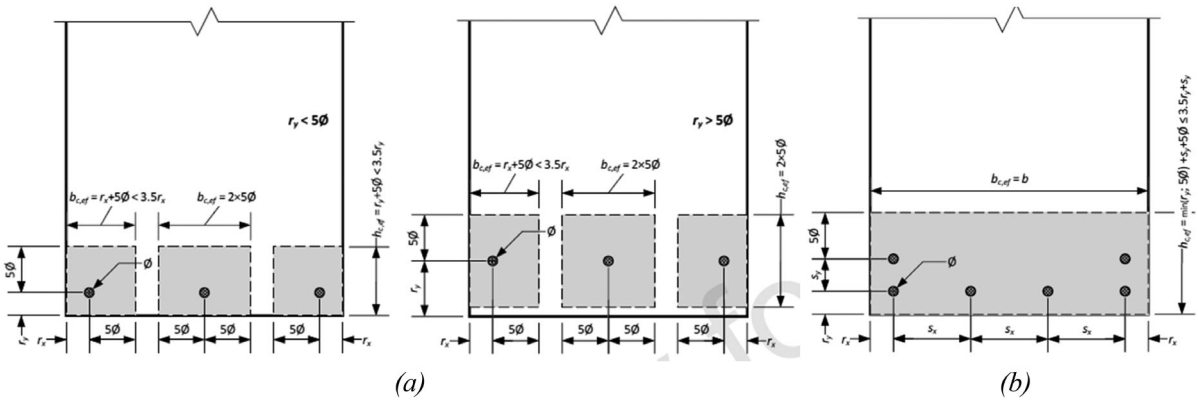

FIGURE 6 MC2020: Effective tension area of concrete (a) isolated bars and (b) group of bars.[9]

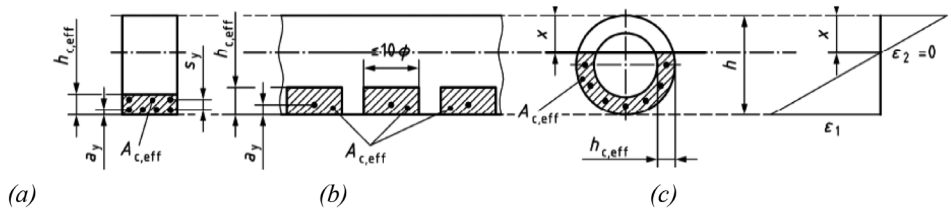

FIGURE 7 FprEC2: Effective tension area of concrete in bending (a) group of bars, (b) isolated bars and (c) circular cross-section.[29]

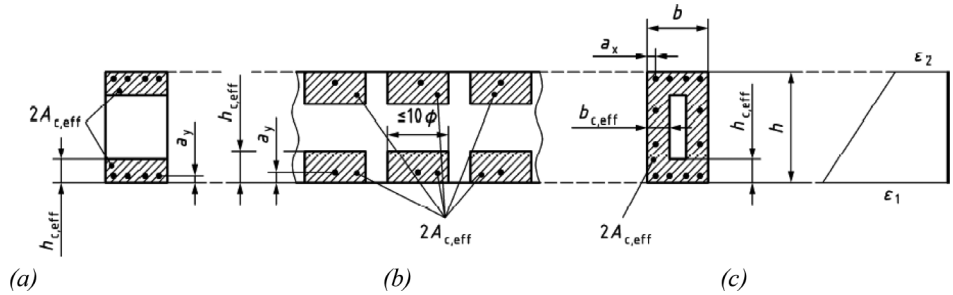

FIGURE 8 FprEC2: Effective tension area of concrete of both faces in tension (a, b) group of bars and (c) isolated bars.[29]

$$k_{1/r} = \frac{h - x_g}{d - a_{y,i} - x_g} \tag{33}$$

where d is the effective height, h is the height of the section, while $a_{y,i}$ is the cover plus half the rebar size.

Additional changes for the effective tension area ($A_{c,\mathrm{ef}}$), represented by the effective height ($h_{c,\mathrm{ef}}$) for single or layered reinforcement bars, are described by Equations (34a) and (34b) for MC2020, visualized in Figure 6 and Equations (34c) and (34d) for FprEC2, visualized in Figures 7 and 8.

$$h_{c,\mathrm{ef}} = \min\left(r_y + 5\emptyset; 10\emptyset; 3.5r_y\right) \le h - x \tag{34a}$$

$$h_{c,\mathrm{ef}} = \min\left(r_y + 5\emptyset; 10\emptyset; 3.5r_y\right) + (n_l - 1)s_y \le h - x \tag{34b}$$

$$h_{c,\mathrm{ef}} = \min\left(a_y + 5\emptyset; 10\emptyset; 3.5a_y; h - x; \frac{h}{2}\right) \tag{34c}$$

$$h_{c,\mathrm{ef}} = \min\left\{\min\left\{a_y + 5\emptyset; 10\emptyset; 3.5a_y\right\} + (n-1)s_y; h - x; \frac{h}{2}\right\} \tag{34d}$$

In which, r_y and a_y are the distance from the concrete surface to the centre of the bar in the y-direction and n_l is the number of reinforcement layers.

3 | DATABASE

An extensive database was created by collecting a large number of experimental results from the literature on reinforced concrete (RC) members subjected to bending and tension. The data was sorted into three categories before investigating the modeling uncertainties. In most references, the specimens were investigated throughout

17517648, 0, Downloaded from https://onlinelibrary.wiley.com/doi/10.1002/suco.202300367 by Otto Terjesen - Norwegian Institute Of Public Healt Invoice Receipt DFO , Wiley Online Library on [17/03/2024]. See the Terms and Conditions (https://onlinelibrary.wiley.com/terms-and-conditions) on Wiley Online Library for rules of use; OA articles are governed by the applicable Creative Commons License

TABLE 2 Overview of the databases with corresponding cross-sections.

First database: 97 experiments with beams in bending (429 data points)	
• Hognestad,[30] (35 beams) • CUR report,[31] (24 beams) • Rüsch – Rehm,[32] (14 beams) • Clark,[33] (24 beams)	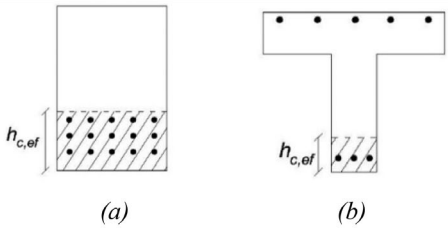
Second database: 73 experimental RC ties (104 data points) of RC ties in pure tension	
• Hartl,[34] (49 ties) • Garcia et al.[35] (4 ties) • Rimkus et al.[36] (10 RC ties) • Wu & Gilbert,[37] (2 RC ties) • Tan et al.[38] (8 RC ties)	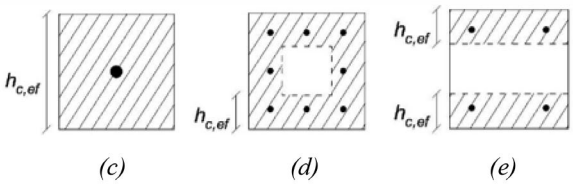
Third database: 33 experimental slabs in bending (200 data points)	
• CUR report,[31] (7 slabs) • Clark,[33] (26 slabs)	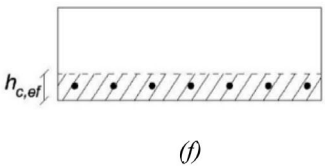

the serviceability limit state and, occasionally, until yielding or failure occurred. Stress levels and measurement results were reported, such as steel and concrete strains, mean and maximum crack widths, and average crack spacing. For several experimental investigations, results at different load steps were available from the literature.

The three databases are presented in Table 2:

1. Beams in bending
2. RC tensile ties
3. Slabs in bending

The effective heights $h_{c,ef}$ of the cross-sections were calculated following the procedures in the calculation models. For the MTCM applied to the first and third databases related to bending, the effective height was calculated according to EC2.

Figure 9 shows an overview of the databases' cross-section heights, with the first database primarily consisting of heights in the range of 500–600 mm, the second database in the range of 50–100 mm and the third database in the range of 150–200 mm. As shown in Figure 10a, the cover sizes for the first and second databases are in the range of 10–50 mm, while in the third database, the slabs have a cover in the range of 10–30 mm. Figure 10b shows that the reinforcement ratio varies significantly between 1% and 6% for all three databases.

3.1 | Adjustment of the databases

Almost no maximum crack spacings for beams and slabs in bending are reported in the database. In contrast, the average crack spacing is registered based on each author's subjective interpretation and choices. Hognestad[30] reported average crack spacing based on primary cracks and disregarded secondary cracks, that is, those close to the major cracks were excluded from the calculations. Rusch & Rehm[32] did not calculate crack spacing but made a detailed report of crack widths measured at five different points along the concrete face and their location along the beam length. From that, average crack spacing was calculated by disregarding secondary cracks. Clark[33] reported average crack widths calculated from all cracks (major and secondary) in the constant moment zone. In

17517648, 0, Downloaded from https://onlinelibrary.wiley.com/doi/10.1002/suco.202300367 by Otto Terjesen - Norwegian Institute Of Public Healt Invoice Receipt DFO , Wiley Online Library on [17/03/2024]. See the Terms and Conditions (https://onlinelibrary.wiley.com/terms-and-conditions) on Wiley Online Library for rules of use; OA articles are governed by the applicable Creative Commons License

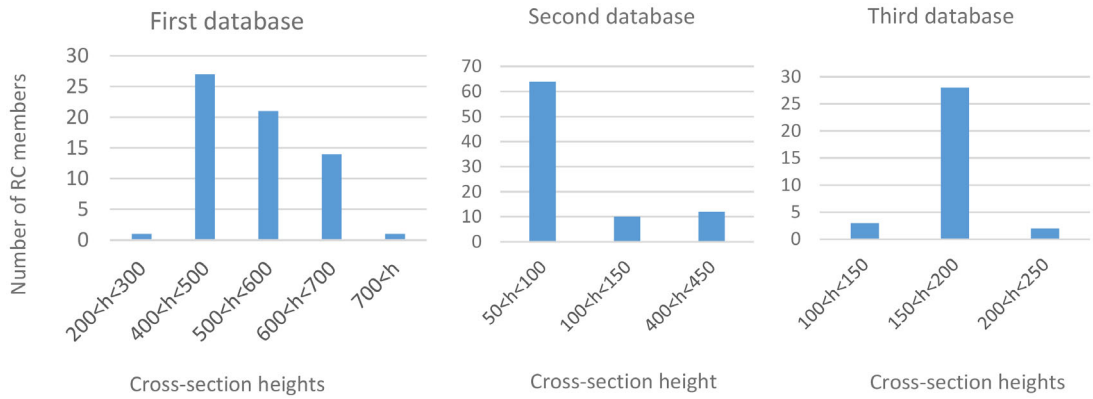

FIGURE 9 Distribution of cross-section heights in the databases.

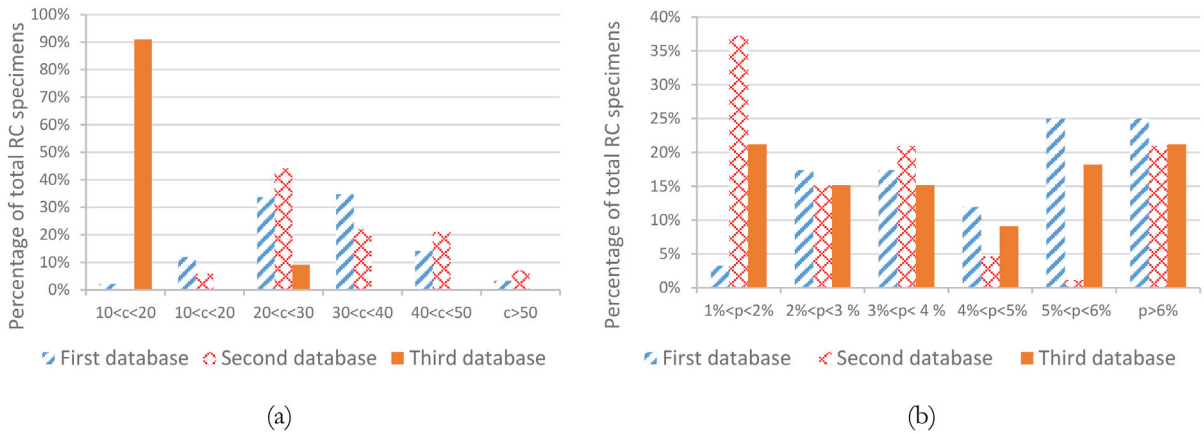

FIGURE 10 Distribution of (a) concrete cover and (b) of the reinforcement ratio, using the effective height set by EC2 for RC members in the databases.

addition, the crack widths and spacing in the location for bending and shear cracks were included if the crack spacing was less or equal to 6 inches (152.4 mm) in this zone. Therefore, verifying which cracks (major and secondary) are included or excluded is difficult due to limited information or lack thereof. There are also uncertainties regarding how the measured crack widths and spacings were found across the RC member's width and length. In some cases, it is also uncertain if the reported crack width is a single point or an average of more readings, that is, across the member's width at the bottom outermost concrete face. Hence, database adjustments are performed to obtain consistent comparisons of predictions from calculation models with experimental results.

3.1.1 | First adjustment

In SLS, it is uncommon to have reinforcement stress above 300 MPa; therefore, the first adjustment was excluding data with stresses larger than this. This requirement results into a reduction of data on 27%, 41%, and 55%for the three respective databases.

3.1.2 | Second adjustment

A second adjustment was performed to further benchmark the experimental results by considering mean crack width and spacings, and investigating if they were unreasonably large. The focus on mean values is due to the literature's lack of reported maximum crack spacings. Using the theoretical framework of all the investigated methods described by Equation (1), we should be able to predict an upper limit of the mean crack width by neglecting bond stresses between steel and concrete or, more rigorously, the tension stiffening effect, as given in Equation (35).

$$w_{\text{mean,max}} = \varepsilon_{\text{sr}} S_{\text{exp,mean}} \tag{35}$$

17517648, 0, Downloaded from https://onlinelibrary.wiley.com/doi/10.1002/suco.202300367 by Otto Terjesen - Norwegian Institute Of Public Healt Invoice Receipt DFO , Wiley Online Library on [17/03/2024]. See the Terms and Conditions (https://onlinelibrary.wiley.com/terms-and-conditions) on Wiley Online Library for rules of use; OA articles are governed by the applicable Creative Commons License

TABLE 3 Modeling uncertainty.

Model	θ_{mean}	θ_{var}	θ_{SD}	θ_{COV}	θ_{min}	θ_{max}	n (θ > 1)	(θ > 1) %
(a) Beams subjected to bending, 429 data points								
MTCM	1.05	0.083	0.309	0.294	0.433	3836	225	52.4
EC2	1.31	0.073	0.360	0.275	0.598	4857	361	84.1
FprEC2	1.34	0.060	0.335	0.250	0.651	4043	368	85.8
MC2010	1.11	0.065	0.286	0.258	0.439	3653	253	59.0
MC2020	1.33	0.059	0.327	0.246	0.651	4043	366	85.3
DIN	1.81	0.116	0.634	0.351	0.586	4852	417	97.2
(b) 315 data points, $\sigma_{sr} \leq 300$ Mpa								
MTCM	1.02	0.074	0.284	0.278	0.375	2199	155	49.2
EC2	1.30	0.073	0.358	0.276	0.598	4794	262	83.2
FprEC2	1.36	0.063	0.345	0.255	0.651	3359	270	85.7
MC2010	1.11	0.066	0.288	0.261	0.439	2734	187	59.4
MC2020	1.34	0.061	0.336	0.251	0.651	3359	268	85.1
DIN	1.83	0.123	0.663	0.362	0.586	4649	304	96.5
(c) 227 data points, results included if $w_{mean.exp} < S_{mean}\varepsilon_{sr}$								
MTCM	0.98	0.075	0.278	0.278	0.433	2187	98	43.3
EC2	1.27	0.080	0.369	0.290	0.598	4794	178	79.5
FprEC2	1.40	0.069	0.374	0.266	0.746	3605	194	86.6
MC2010	1.10	0.074	0.304	0.277	0.439	2734	128	57.1
MC2020	1.36	0.064	0.349	0.257	0.651	3359	191	85.3
DIN	1.69	0.116	0.592	0.350	0.586	4522	213	95.1

where ε_{sr} is the steel strain at the load level of the reported mean crack spacing $S_{exp,mean}$. Data points which had measured mean crack widths larger than $w_{mean,max}$ were excluded from the database. An aspect of this adjustment is due to uncertainties if shrinkage could have affected the experiments. Significant shrinkage might result in a negative tension stiffening, but by excluding tests with reported mean crack widths larger than Equation (35), the tension stiffening (TS) factor is always ≤1.0, and the shrinkage problem is assumed to be accounted for.

4 | RESULTS

The accuracy of the investigated crack width prediction models was determined by applying the concept of modeling uncertainty according to the method provided by Engen et al.[38] and Tan et al.[37] The method assumes a log-normal distribution, according to the guidelines of the JCSS Probabilistic Model Code[39] and is thereby considering the natural logarithm of theta (θ) as a normal distribution and is determined as:

$$\theta = \frac{w_{exp}}{w_{cal}} \tag{36}$$

where w_{exp} is the experimental crack width reported from the experiments and w_{cal} the crack width calculated by the various methods. The uncertainty, determined by the quality of a model, represents the lack of knowledge and is called epistemic uncertainty. The best agreement between the prediction models and the experiment is obtained when θ is close to 1.0. Tables 3–5 show the statistical properties of the modeling uncertainty for each calculation model for the databases previously described and are graphically presented in Figures 12–16 with the mean value (θ_{mean}), the variance (θ_{var}), the standard deviation (θ_{SD}), the coefficient of variation (θ_{COV}), the minimum (θ_{min}) and maximum (θ_{min}) values of θ, and the number of observations n for which the crack widths measured exceed the maximum crack widths predicted (θ > 1).

- Table 3(a) shows the statistical properties of the modeling uncertainty from the first database consisting of 92 RC beams and 429 data points.

17517648, 0, Downloaded from https://onlinelibrary.wiley.com/doi/10.1002/suco.202300367 by Otto Terjesen - Norwegian Institute Of Public Healt Invoice Receipt DFO , Wiley Online Library on [17/03/2024]. See the Terms and Conditions (https://onlinelibrary.wiley.com/terms-and-conditions) on Wiley Online Library for rules of use; OA articles are governed by the applicable Creative Commons License

TABLE 4 Modeling uncertainty.

Model	θ_{mean}	θ_{var}	θ_{SD}	θ_{COV}	θ_{min}	θ_{max}	$n(\theta > 1)$	$(\theta > 1)$ %
(a) RC ties in tension 104 data points								
MTCM	0.86	0.131	0.320	0.374	0.17	2.04	18	17.3
EC2	0.64	0.113	0.221	0.345	0.10	1.62	2	1.9
FprEC2	1.03	0.093	0.321	0.312	0.23	2.34	34	32.7
MC2010	0.96	0.110	0.327	0.340	0.20	2.58	27	26.0
MC2020	1.01	0.108	0.342	0.338	0.19	3.01	33	31.7
DIN	1.18	0.140	0.459	0.388	0.19	2.29	51	49.0
(b) 61 data points, $\sigma_{sr} \leq$ 300 Mpa								
MTCM	0.92	0.152	0.372	0.405	0.17	2.04	16	26.2
EC2	0.73	0.153	0.298	0.406	0.10	1.61	2	3.3
FprEC2	1.07	0.106	0.358	0.335	0.23	2.32	31	50.8
MC2010	1.01	0.124	0.368	0.363	0.20	2.57	25	41.0
MC2020	1.08	0.119	0.386	0.356	0.23	2.99	31	50.8
DIN	1.17	0.144	0.459	0.394	0.19	2.28	38	62.3

TABLE 5 Modeling uncertainty.

Model	θ_{mean}	θ_{var}	θ_{SD}	θ_{COV}	θ_{min}	θ_{max}	$n(\theta > 1)$	$(\theta > 1)$ %
(a) Slabs subjected to bending, 200 data points								
MTCM	0.90	0.113	0.313	0.346	0.21	2.14	63	31.5
EC2	1.80	0.189	0.823	0.456	0.32	5.43	178	89.0
prEC2	1.59	0.163	0.667	0.421	0.30	4.39	174	87.0
MC2010	1.20	0.165	0.508	0.423	0.29	3.31	128	64.0
MC2020	1.72	0.152	0.698	0.405	0.34	4.39	182	91.0
DIN	1.75	0.255	0.943	0.539	0.25	5.09	156	78.0
(b) 90 data points, results included if $\sigma_{sr} \leq$ 300 MPa and $w_{mean.exp} \leq S_{mean}\varepsilon_{sr}$								
MTCM	0.82	0.125	0.299	0.365	0.21	1.37	17	18.9
EC2	1.54	0.197	0.719	0.467	0.32	2.90	72	80.0
prEC2	1.35	0.176	0.592	0.439	0.30	2.55	68	75.6
MC2010	1.05	0.160	0.436	0.416	0.29	1.92	47	52.2
MC2020	1.59	0.186	0.721	0.452	0.34	3.19	77	85.6
DIN	1.41	0.248	0.749	0.530	0.25	3.25	59	65.6

- Table 3(b) shows the statistical properties after the first adjustment.
- Table 3(c) shows the statistical properties after the second adjustment.

- Table 4(a) shows the results from the second database consisting of 73 experimental RC ties and 104 data points.
  - Table 4(b) shows the statistical properties after the first adjustment.
- Table 5(a) shows the results from the third database consisting of 33 experimental slabs in bending and 200 data points.
  - Table 5(b) shows the statistical properties after the first and second adjustments.

4.1 | First database (beams subjected to bending)

Table 3(a) shows the modeling uncertainty for all 92 RC beams included in the reviewed literature with 429 data points. After the first adjustment, as shown in Table 3(b), and the second adjustment in Table 3(c) of the database,

17517648, 0, Downloaded from https://onlinelibrary.wiley.com/doi/10.1002/suco.202300367 by Otto Terjesen - Norwegian Institute Of Public Healt Invoice Receipt DFO , Wiley Online Library on [17/03/2024]. See the Terms and Conditions (https://onlinelibrary.wiley.com/terms-and-conditions) on Wiley Online Library for rules of use; OA articles are governed by the applicable Creative Commons License

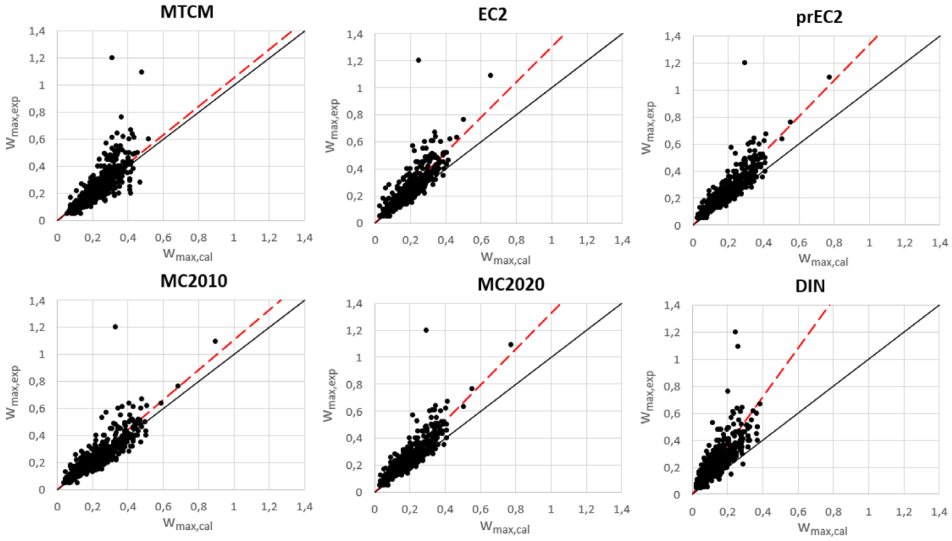

FIGURE 11 Modeling uncertainty from Table 3(a) with the long dash line (red) as the mean value (θ_{mean}), while the solid line is the 1 to 1 line.

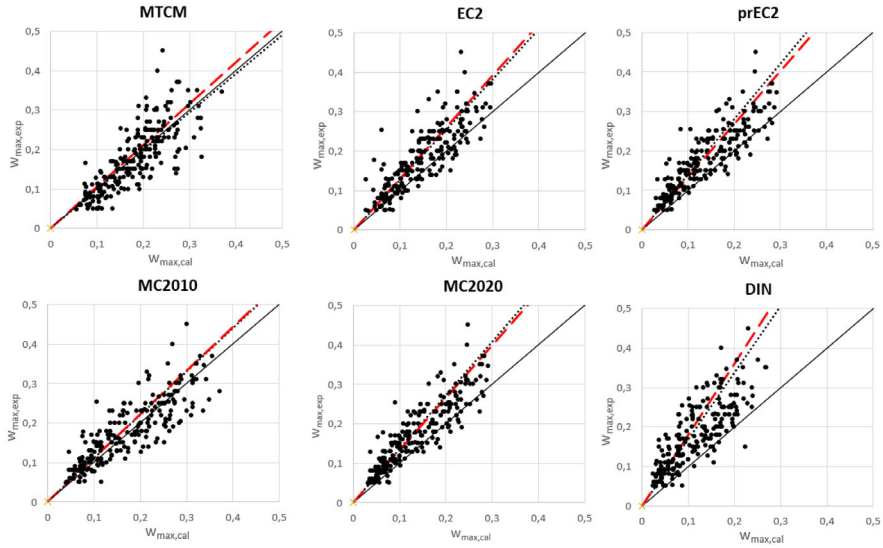

FIGURE 12 Modeling uncertainty from Table 3(c), black dotted line as the mean value, long dash line (red) as the global mean value from Table 3(a) and solid line as 1 to 1 line.

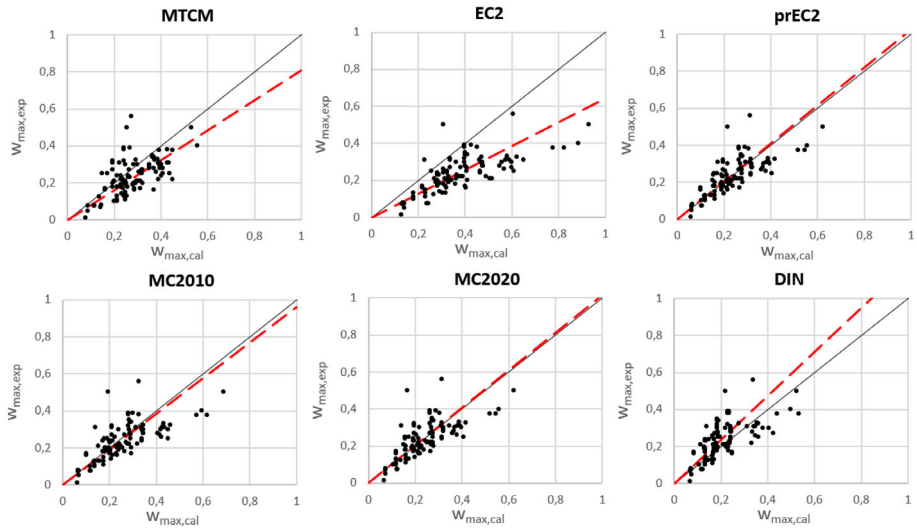

FIGURE 13 Modeling uncertainty from Table 4(a) with the red long dash line as the global mean value and solid black line as the 1 to 1 line.

17517648, 0, Downloaded from https://onlinelibrary.wiley.com/doi/10.1002/suco.202300367 by Otto Terjesen - Norwegian Institute Of Public Healt Invoice Receipt DFO , Wiley Online Library on [17/03/2024]. See the Terms and Conditions (https://onlinelibrary.wiley.com/terms-and-conditions) on Wiley Online Library for rules of use; OA articles are governed by the applicable Creative Commons License

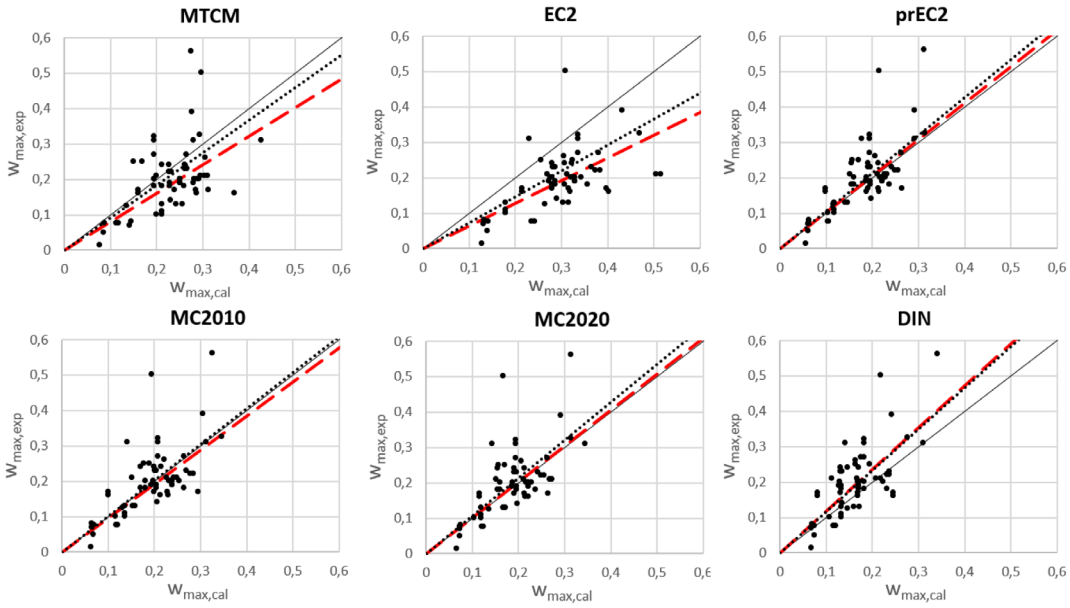

FIGURE 14 Modeling uncertainty from Table 4(b), black dotted line as the mean value, long dash line (red) as the global mean value from Table 6 and solid line as 1 to 1 line.

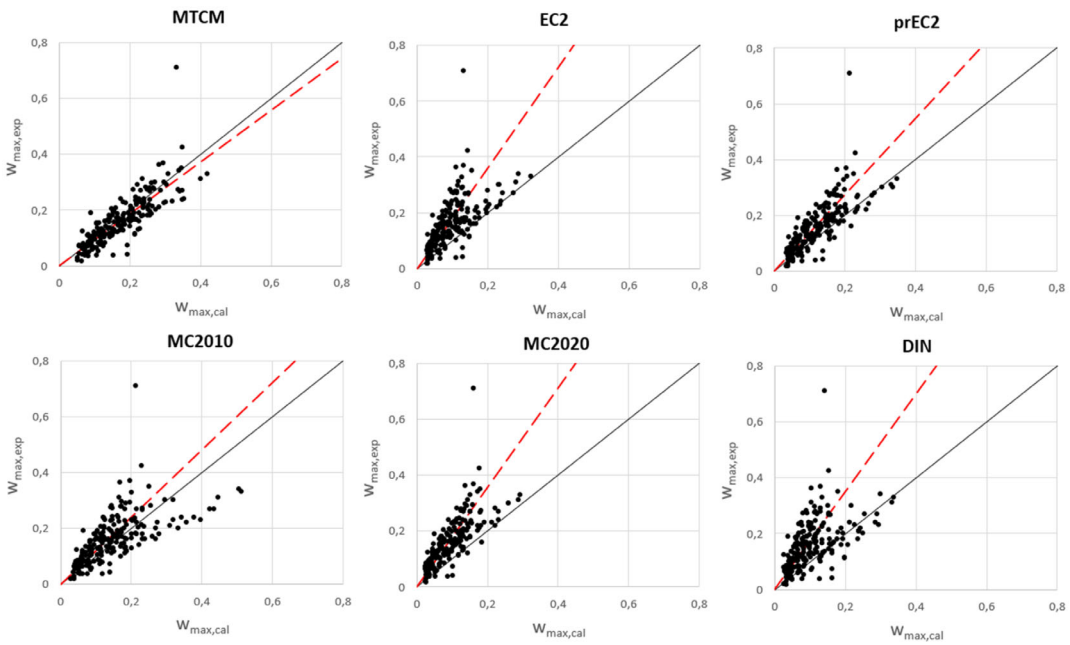

FIGURE 15 Modeling uncertainty from Table 5(a) with the long dash line (red) as the global mean value and the solid black line as 1 to 1.

we can see the change in the model uncertainties. The best agreement between the prediction models and the experiment (θ) is achieved by the MTCM and MC2010 described by θ_{mean} of 0.98 and 1.10, with an underestimated crack width in 43.3% and 57.1% of the cases. The rest of the codes has a θ_{mean} between 1.27 and 1.69 with an underestimated crack width in 79.5–95.1% of the cases. The scatter of the prediction models and the experiment expressed by the coefficient of variation (θ_{cov}) are lowest for FprEC2 ($\theta_{cov} = 0.266$) and MC2020 ($\theta_{cov} = 0.257$) while the largest are EC2 ($\theta_{cov} = 0.29$), MTCM ($\theta_{cov} = 0.293$), and DIN ($\theta_{cov} = 0.35$). These changes are graphically illustrated in Figures 11 and 12.

17517648, 0, Downloaded from https://onlinelibrary.wiley.com/doi/10.1002/suco.202300367 by Otto Terjesen - Norwegian Institute Of Public Healt Invoice Receipt DFO , Wiley Online Library on [17/03/2024]. See the Terms and Conditions (https://onlinelibrary.wiley.com/terms-and-conditions) on Wiley Online Library for rules of use; OA articles are governed by the applicable Creative Commons License

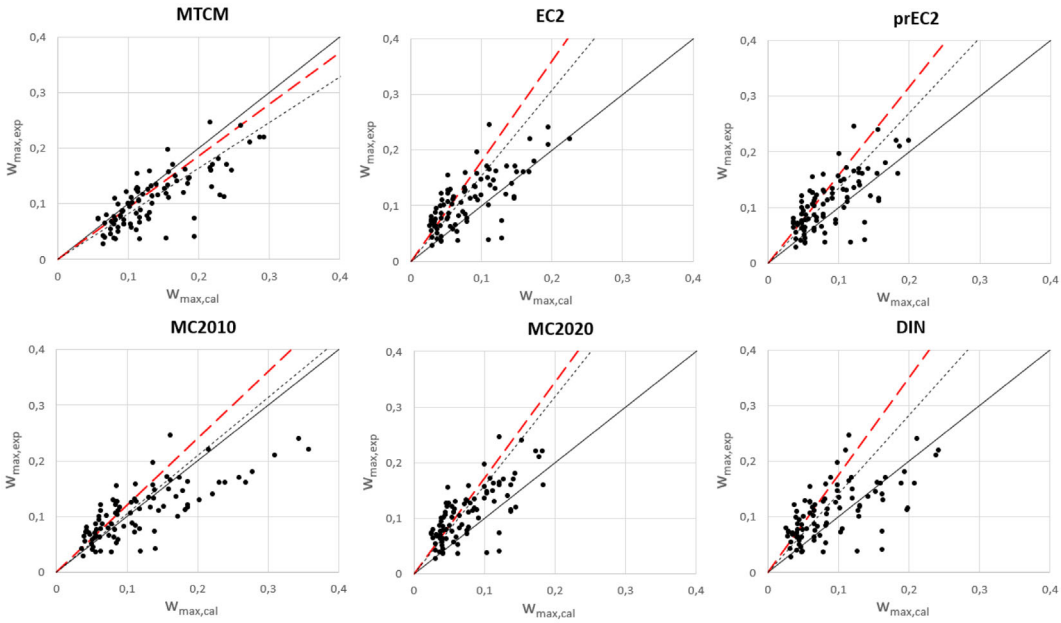

FIGURE 16 Modeling uncertainty from Table 5(b) black dotted line as the mean value, long dash line (red) as the global mean value from Table 6 and solid black line as 1 to 1.

Table 3(b) shows the modeling uncertainty after disregarding steel stresses >300 Mpa from Table 3(a).

Table 3(c) shows the modeling uncertainty after the second adjustment, disregarding the tension-stiffening effect described in Equation (28) in Table 3(b).

4.2 | Second database (RC ties in tension)

Table 4(a) shows the modeling uncertainty for all 73 RC ties included in the reviewed literature with 104 data points. After the first adjustment of the database shown in Table 4(b), we can see an improvement for almost all prediction models except for DIN, which has an increase in all statistical uncertainties except θ_{mean}. However, the reported crack spacing is the maximum at the last load level, and no other spacing was reported; therefore, the second adjustment by neglecting concrete strains, that is, tension stiffening, was not performed. The best agreement between the prediction models and the experiment (θ) expressed by θ_{mean} are MTCM, FprEC2, MC2010 and MC2020 with 0.92, 1.00, 1.07 and 1.08, respectively. The scatter of the prediction models and the experiment expressed by the coefficient of variation (θ_{cov}) are higher than for all the models in the first database with RC beams in bending with a θ_{cov} between 0.358 and 0.406. These changes are graphically illustrated in Figures 13 and 14.

Table 4(b) shows the modeling uncertainty after the first adjustment, excluding data with stresses larger than 300 MPa.

4.3 | Third database (slabs in bending)

Table 5(a) shows the modeling uncertainty for all 33 RC slabs included in the reviewed literature with 200 data points. After the first and second adjustments of the database, we can see a change in the model uncertainties, presented in Table 5(b). The best agreement between the prediction models and the experiments (θ) are MTCM and MC2010, described by θ_{mean} of 0.82 and 1.05, while the rest of the codes has a θ_{mean} between 1.27 and 1.59. The scatter of the prediction models described by the coefficient of variation (θ_{cov}) are best for MTCM with 0.365, and the other design codes vary between 0.42 and 0.53. These changes are graphically illustrated in Figures 15 and 16.

Table 5(b) shows the modeling uncertainty after the first and second adjustments, excluding data with stresses larger than 300 MPa and disregarding the tension-stiffening effect described in Equation (28) from Table 5(a).

17517648, 0, Downloaded from https://onlinelibrary.wiley.com/doi/10.1002/suco.202300367 by Otto Terjesen - Norwegian Institute Of Public Healt Invoice Receipt DFO , Wiley Online Library on [17/03/2024]. See the Terms and Conditions (https://onlinelibrary.wiley.com/terms-and-conditions) on Wiley Online Library for rules of use; OA articles are governed by the applicable Creative Commons License

5 | DISCUSSION

Established databases with crack width measurements can be complicated to use for benchmarking purposes, and misinterpretations are bound to occur if special care is not taken. The complexity stems mainly from the lack of homogeneity in the measurement criteria used in different laboratories, and also because test reports are not always well documented, so it is complicated to understand the measuring procedures. In the case of crack width measurement, subjective factors may play a major role. Therefore, evaluating calculation models towards experimental results should be done with a critical view. There could be grounds for confusion between the experimental results and the analytical prediction models, as stated by Schlicke et al.[12] Therefore, the correlation between theoretical formulations and their reference to reality is necessary, and combining experimental data from various sources might be especially challenging.

5.1 | Adjustment of the database

The content and methods used to establish a comprehensive database like this could influence the results due to the nature and properties of the input data (random products), even though the statistical properties are almost homogenous for all the codes. As noted from Table 3, all models show large numbers of observations n for which the crack widths measured exceed the predicted crack width ($\theta > 1$). Such population behavior might lead to thinking that the predicted crack widths are too small or incorrect, and that the crack width values measured experimentally are too large or inconsistent. There is generally a large scatter from all models, which can be related to the aleatory uncertainties and the subjective interpretations and choices made by the reporting authors. Observing that the statistical properties for the model uncertainties of the calculation models are in the same order of magnitude justifies these viewpoints.

Several experimental tests reported large crack widths, such as Rüsch & Rehm[32]: For Beam No R-69, a maximum crack width of 1.2 mm at 390 MPa was reported, while the average crack width from the prediction models was 0.27 mm. The reported reinforcement yield stress was 400 MPa. Therefore, plastic deformation in the steel could have affected the crack and supported the choice for the first adjustment. Even if the difference in terms of maximum crack width given by the prediction model was irrelevant, it is evident how such outliers can affect the modeling uncertainty; hence, the need to benchmark the models.

Table 6 shows that 28 data points from 14 beams tested by Rüsch & Rehm[32] exceed the theoretical maximum mean crack width given in Equation (35), and 90 data points by Clark,[33] as shown in Table 7.

As seen in Table 8 and Figures 17 and 18, it is complicated to interpret crack spacings from the experimental tests consistently. To improve the accuracy of the second adjustment for Rüsch & Rehm, the experimental results would require detailed interpretations of the crack patterns. A solution strategy could be to determine maximum- and average crack widths and spacings based on their size and crack propagation into the effective tensile sone, that is, if a crack width is constant and not increasing its propagation in the beam height with increased reinforcement stress, the crack would be disregarded as a secondary crack. Different interpretations of crack spacings may not be wrong, but to achieve consistent results, the same basis of interpretation should be used for all experimental tests.

TABLE 6 Number of experimental data points exceeding the mean crack width criterion (neglecting tension stiffening).

Criteria	Hognestad	CUR-report	Rusch-Rehm	Clark	Total numbers
$w_{k,\text{mean}} < \varepsilon_{\text{sr}} S_{r,\text{mean,exp}}$	114	92	41	64	311
$w_{k,\text{mean}} > \varepsilon_{\text{sr}} S_{r,\text{mean,exp}}$	0	0	28	90	118

Note: $S_{r,\text{mean,exp}}$ is based on different interpretations of crack spacings for each database.

TABLE 7 Number of experimental beams where the mean crack width requirement is exceeded for at least one data point.

Criteria	Hognestad	CUR-report	Rusch-Rehm	Clark	Total numbers
$w_{\text{k,exp}} < \varepsilon_{\text{sr}} S_{r,\text{mean,exp}}$	30	24	4	1	59
$w_{\text{k,exp}} > \varepsilon_{\text{sr}} S_{r,\text{mean,exp}}$	0	0	10	23	33

Note: $S_{r,\text{mean,exp}}$ is based on different interpretations of crack spacings for each database.

17517648, 0, Downloaded from https://onlinelibrary.wiley.com/doi/10.1002/suco.202300367 by Otto Terjesen - Norwegian Institute Of Public Healt Invoice Receipt DFO , Wiley Online Library on [17/03/2024]. See the Terms and Conditions (https://onlinelibrary.wiley.com/terms-and-conditions) on Wiley Online Library for rules of use; OA articles are governed by the applicable Creative Commons License

TABLE 8 Experimental Beam R-69 by Rüsch & Rehm.

Beam	MTCM	EC2	prEC2	MC2010	MC2020	DIN	Experimental results Reported				Conservative mean
R-69	w_k (mm)						$S_{r.\text{mean}}$ mm	σ_{sr} MPa	$w_{k.\max}$ mm	w_{mean} mm	$w_{k.\text{mean}} = \varepsilon_{\text{sr}} S_{r.\text{mean}}$
	0.14	0.12	0.14	0.14	0.14	0.12	150	200	0.15	0.07	0.15
	0.18	0.15	0.18	0.18	0.18	0.15	115	250	0.23	0.11	0.14
	0.22	0.19	0.22	0.23	0.22	0.19	105	300	0.25	0.13	0.16
	0.26	0.22	0.26	0.27	0.26	0.22	102	350	0.3	0.16	0.18
	0.29	0.25	0.30	0.30	0.30	0.25	100	390	1.2	0.23	0.20

Note: $w_{k.\max}$ is the maximum crack width at the bottom face by the average value of five measured points I, II, III, IV, and V.

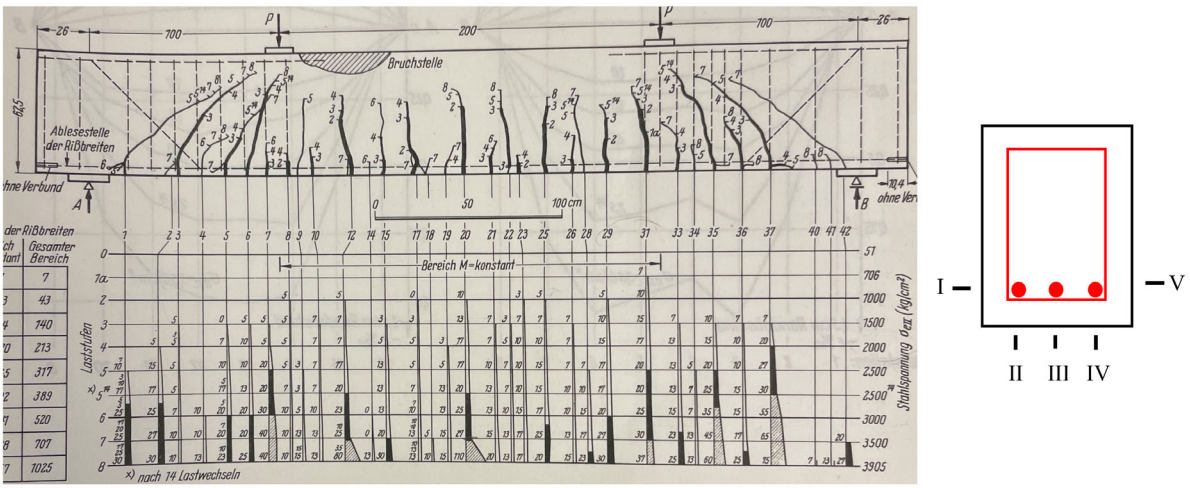

FIGURE 17 Crack widths for R-69 (in 1/100 mm) with corresponding load intensity on one side of the beam with the crack width reading at point V.

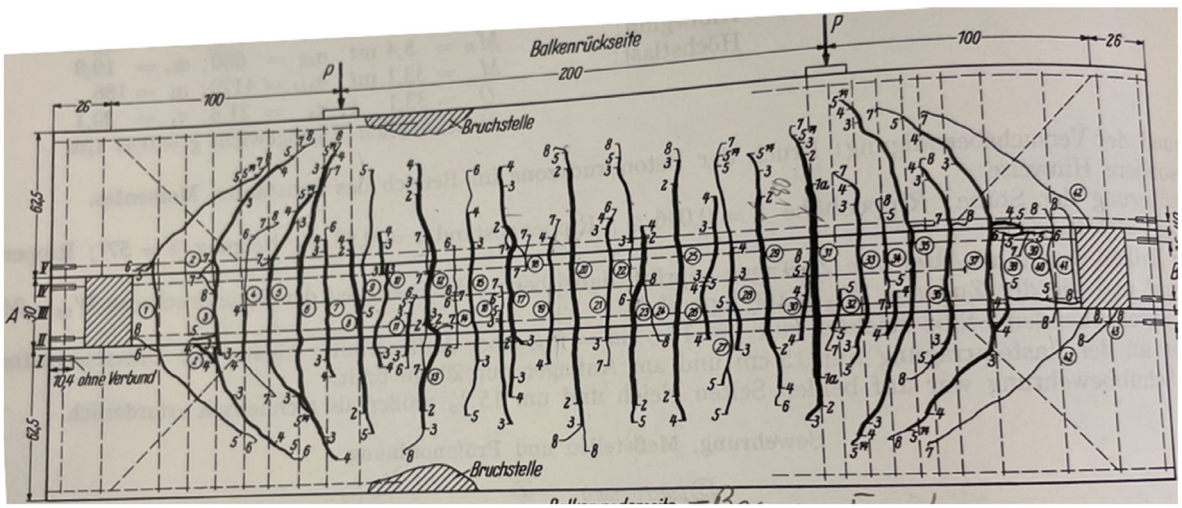

FIGURE 18 Illustration of cracks on the beam faces of R-69, crack number and load intensity 1–8.

17517648, 0, Downloaded from https://onlinelibrary.wiley.com/doi/10.1002/suco.202300367 by Otto Terjesen - Norwegian Institute Of Public Healt Invoice Receipt DFO , Wiley Online Library on [17/03/2024]. See the Terms and Conditions (https://onlinelibrary.wiley.com/terms-and-conditions) on Wiley Online Library for rules of use; OA articles are governed by the applicable Creative Commons License

TABLE 9 Predicted crack width location.

Model	Description	
EC2	w_2	At the outermost concrete face
FprEC2	w_2	At the outermost concrete face
MC2010	w_1, w_2	At reinforcement height and outermost concrete face.
MC2020	w_2	At reinforcement height and outermost concrete face.
MTCM	–	Representative crack width over the surface of the effective tensile area
DIN	–	Representative crack width over the surface of the effective tensile area

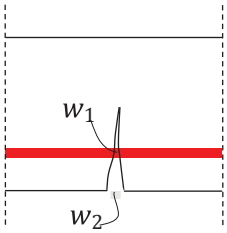

5.2 | Crack width location

The crack width predicted by the investigated models does not represent the crack width at the same location, as seen in Table 9. MC2010 determines the crack width at the reinforcement height with the option to extrapolate to the outermost concrete surface. The current EC2 does not directly state the predicted crack width location; however, the work described in fib bulletin 92[40] supports that the predicted crack width is at the outermost concrete face. In FprEC2, it is now directly stated that the crack width is at the outermost concrete face. The German annexe to EC2 (DIN) is based on Model Code 1990,[41] which takes no explicit account of cover and is based primarily on defining the transfer length based on rebar size and reinforcement ratio, which includes no explicit empirical cover term like the formulations in the TCM and MTCM. The predicted crack width by DIN and MTCM is a representative maximum crack width over the effective tensile area.

5.3 | Effective concrete area

For beams in bending, EC2 and MC2010 define the effective height as.

$$h_{\mathrm{ef}} = \min\left(2.5(h-d); \frac{h-x}{3}\right) \tag{37}$$

In both cases, the effective height limitation $(h-x)/3$ is included to distinguish between elements in bending and tension. The explanation for this limitation is based on the stress distribution over the cross-section height in bending; however, as pointed out by Reference 42, there seems to be no published justification for this factor which seems to be originating from curve fitting to test data. Therefore, when calculating the effective height by MTCM, the effective height was defined as $h_{\mathrm{ef}} = 2.5(h-d)$ for beams and slabs in bending.

For RC ties in tension, MTCM applies the EC2 and MC2010 definitions:

$$h_{\mathrm{ef}} = \min\left(2.5(h-d); 2.5\left(c+\frac{\phi_{\mathrm{s}}}{2}\right); \frac{h}{2}\right) \tag{38}$$

5.4 | The difference in bond stress and crack spacing formulas by the models

The applied codes EC2, Model Codes and DIN assume that the bond stresses are proportional to the concrete's tensile strength with the assumption of a perfectly plastic bond-slip relation, as shown in Figure 1. MC2010 and DIN apply constant mean bond stresses equal to 1.8 times the tensile strength of concrete ($\tau_{\mathrm{sm}} = 1.8 f_{\mathrm{ctm}}$), while EC2 applies 2.5 or 1.25 depending on if deformed or smooth bars are used. This assumption means that the bond stress is independent of the slip between rebar and concrete, and the effects of geometry and stress level are not directly considered. In contrast, MTCM yields different mean bond stresses directly dependent on the slip where geometry and stress level are accounted for. This effect is illustrated in Figure 19 for constant reinforcement ratio versus increasing rebar stress and different rebar sizes.

Another major difference between MTCM and the code formulations that should be highlighted is how the transfer length in the crack formation stage is accounted for. No explicit term is provided for the code formulations, while MTCM provides a solution method by means of the CLLM behavior. Capturing this behavior has previously proven essential for sections with large covers, as stabilized cracking might not be obtained even for relatively large steel stresses.[30] The transfer lengths

17517648, 0, Downloaded from https://onlinelibrary.wiley.com/doi/10.1002/suco.202300367 by Otto Terjesen - Norwegian Institute Of Public Healt Invoice Receipt DFO , Wiley Online Library on [17/03/2024]. See the Terms and Conditions (https://onlinelibrary.wiley.com/terms-and-conditions) on Wiley Online Library for rules of use; OA articles are governed by the applicable Creative Commons License

between formed cracks will not overlap and interfere in such cases. This will, for instance, lead to incorrect and inconsistent calibration of code formulations if such spacing between cracks is interpreted as a specific maximum crack spacing. Unlike the code formulations, MTCM does not use the crack spacing as a primary variable determined a priory to calculate the crack width but rather deduced from the calculations as a state variable. This means that only the maximum crack width is the primary variable returned from an MTCM calculation. The authors are thus of the opinion that the calculated transfer lengths of each side of a crack are more critical than the crack spacing measured itself. Two further develop this opinion, two parametric studies were carried out for Hognestad B-5, the first shown in Table 10, with increased concrete cover as the only variable. The results for predicted crack spacing are shown in Figure 20 for MTCM and EC2.

The second study was performed for the same beam with increased cover sizes and keeping the reinforcement ratio constant by increasing the reinforcement diameter, as shown in Table 11. The results for predicted crack spacing are shown in Figure 21 for MTCM and EC2.

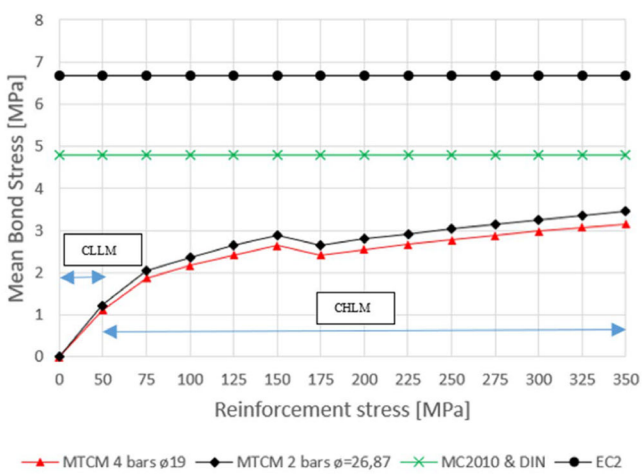

FIGURE 19 Bond stresses for different rebar sizes with constant reinforcement ratio between MTCM, EC2, MC2010 and DIN for Hognestad Beam No 5.

Figures 20 and 21 show that the crack formation stage (CLLM) and the stabilized cracking stage (CHLM) in MTCM heavily depend on the reinforcement ratio and rebar size. The difference between predicted crack spacing in the stabilized cracking stage of MTCM and Eurocode 2 is even more significant for large-scale concrete structures, which could yield maximum crack spacing up to over 1 m with large covers, small rebars and a low reinforcement ratio. This would, in practice, never be the case as crack spacing for stabilized cracking rarely becomes larger than half a meter, justifying the code formulation's inconsistency.

The aforementioned oversimplifications made by the codes result in the effect of cracking only being captured by empirical calibration of the predicted crack spacing. Considering that the empirical calibration is performed with respect to a specific database suggests that the code formulation cannot capture the cracking behavior of an arbitrary section properly judged from a mechanical viewpoint. This further implies that the formulation in the codes should have a strictly limited range of applications and that care should be taken when applying the calculations, in particular to cross-sections with properties deviating from those in the database, for example, cross-sections with large heights, covers, rebars or the combination of them. Figures 22 and 23 compare measured crack width versus calculated crack widths for databases 1 and 2 when the data are separated into normal and large covers.

In the case of MTCM, for beams in bending with cover in the range of 38–48 mm, shown in Figure 22, the predicted crack width is in good agreement with experimental data. However, with larger concrete covers in the 51–102 mm range, the predicted crack width is underestimated. Both DIN and MTCM transform an arbitrary cross-section into an equivalent cross-section. Furthermore, DIN solves this problem by assuming a constant bond stress distribution while MTCM acknowledges that

TABLE 10 Parametric study of increased cover with effective depth kept constant for Hognestad B-5 beam.

Hognestad B-5, 4ø19					
Width (mm)	Height (mm)	Effective depth (mm)	$h_{ef} = 2.5(h-d)$ (mm)	Cover (mm)	ρ_{ef} (%)
203	406[a]	360	115	25	4.86
	430		174	50	3.22
	455		236	75	2.46
	480		299	100	2.33
	505		361	125	2.21

[a]Tested beam.

17517648, 0, Downloaded from https://onlinelibrary.wiley.com/doi/10.1002/suco.202300367 by Otto Terjesen - Norwegian Institute Of Public Healt Invoice Receipt DFO , Wiley Online Library on [17/03/2024]. See the Terms and Conditions (https://onlinelibrary.wiley.com/terms-and-conditions) on Wiley Online Library for rules of use; OA articles are governed by the applicable Creative Commons License

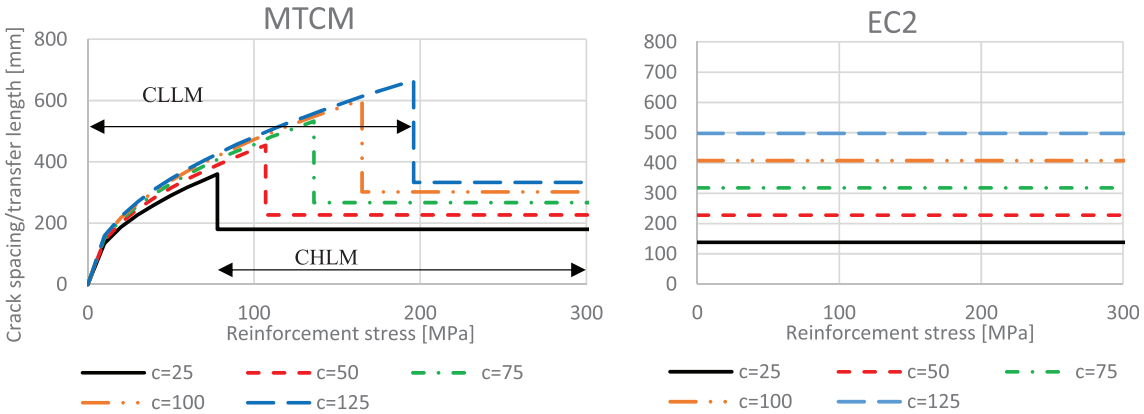

FIGURE 20 Crack spacing/transfer length for MTCM and EC2 for different cover sizes of Hognestad B-5 beam with values from Table 10.

TABLE 11 Parametric study of increased cover with effective depth and reinforcement ratio kept constant with different rebar sizes for Hognestad B-5 beam.

Hognestad B-5, constant reinforcement ratio, $n = 4$						
Width (mm)	Height (mm)	Effective depth (mm)	$h_{ef} = 2.5(h - d)$ (mm)	Cover (mm)	$\varnothing_s$ (mm)	ρ_{ef} (%)
203	406[a]	360	115	25	19.00	4.86
	432		180	50	23.76	
	459		247	75	27.86	
	486		314	100	31.43	
	512		381	125	34.58	

[a]Tested beam.

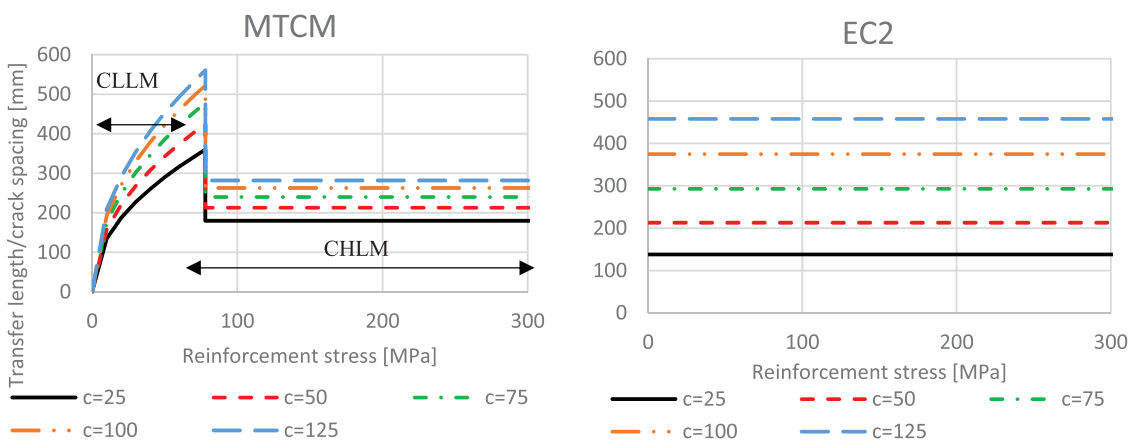

FIGURE 21 Crack spacing/transfer length for MTCM and EC2 for different cover sizes of Hognestad B-5 beam with values from Table 11.

the bond stress distribution around the rebar is not uniform in a non-symmetric RC tie by applying the parameter $\psi = 0.7$. However, a considerable difference between the vertical and horizontal concrete cover, which was 25 mm for the case of 63 and 102 mm vertical cover, is a natural explanation for the considerable underestimation of the crack width in these cases for both DIN and MTCM. It is also seen that MTCM performs well in cases of a relatively small difference in vertical and horizontal covers. For the RC ties in tension shown in Figure 23,

17517648, 0, Downloaded from https://onlinelibrary.wiley.com/doi/10.1002/suco.202300367 by Otto Terjesen - Norwegian Institute Of Public Healt Invoice Receipt DFO , Wiley Online Library on [17/03/2024]. See the Terms and Conditions (https://onlinelibrary.wiley.com/terms-and-conditions) on Wiley Online Library for rules of use; OA articles are governed by the applicable Creative Commons License

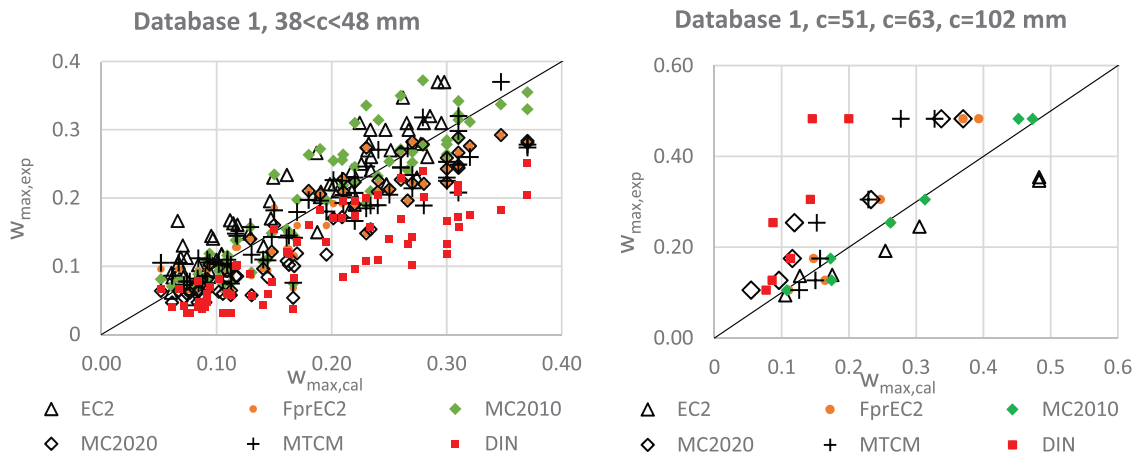

FIGURE 22 Comparison of measured crack width with calculated crack width for Database 1 with different concrete covers.

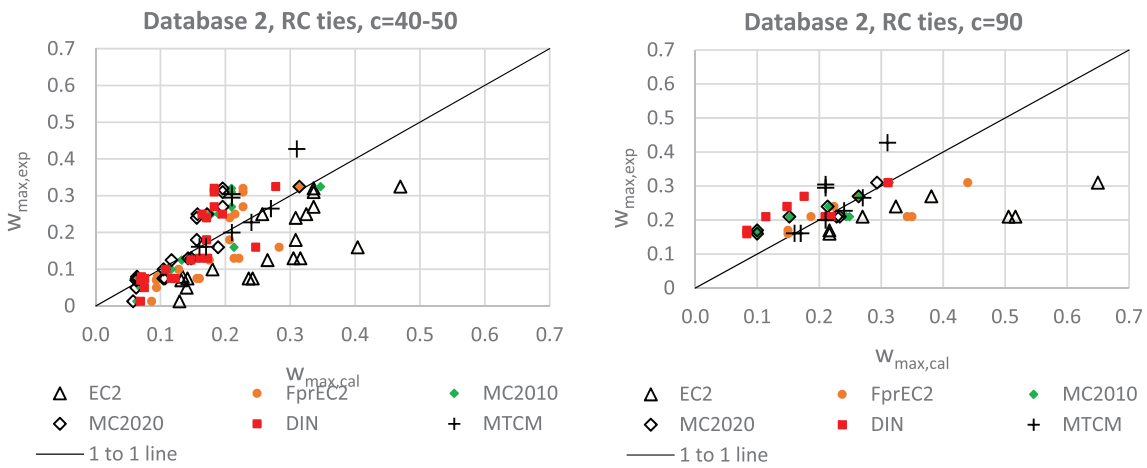

FIGURE 23 Comparison of measured crack width with calculated crack width for Database 2 with different concrete covers.

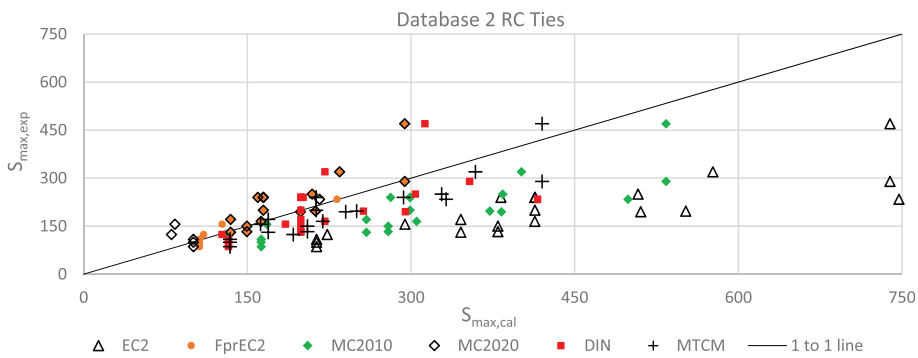

FIGURE 24 Measured maximum crack spacing versus calculated maximum crack spacing for reported values in Database 2 cover sizes of 20–90 mm.

there is perfect symmetry in all cases regarding vertical and horizontal cover, and both DIN and MTCM are in good agreement with the experimental results for both normal and large concrete covers.

Figure 24 shows the maximum measured crack spacing versus calculated crack spacing with clear indications that EC2 and MC2010 overestimate the crack spacing for RC ties. The MTCM predict the crack width and spacing for RC ties to a good extent, even though the crack spacing is not a primary variable in the MTCM.

The MTCM is purely based on a mechanical formulation and has not been calibrated towards any

17517648, 0, Downloaded from https://onlinelibrary.wiley.com/doi/10.1002/suco.202300367 by Otto Terjesen - Norwegian Institute Of Public Healt Invoice Receipt DFO , Wiley Online Library on [17/03/2024]. See the Terms and Conditions (https://onlinelibrary.wiley.com/terms-and-conditions) on Wiley Online Library for rules of use; OA articles are governed by the applicable Creative Commons License

experimental databases at all. Observing that it performs as well as the code formulations, not to say even better, suggests that it (i) offers a wider range of applications and, thus, (ii) shows greater potential for development than the codes. The current drawback is that the MTCM calls for a numerical solution procedure, which makes it more complicated to handle for a code type formulation and daily use for design purposes. This also makes sense since it is a refined calculation model compared to the code formulations. Hence, this calls for the development of a simplified version of the MTCM, which can be compressed to a code-type formulation for the purpose of becoming a direct competitor to the current code formulations. This can be obtained by applying the mechanical basis in the MTCM to formulate a closed-form solution for the CHLM case instead of a non-closed solution. The authors of this article are currently working on developing such a model.

6 | CONCLUSIONS

This article shows the performance of the crack width calculation methods according to Eurocodes (EC2, FPrEC2), *fib* Model Codes, German Annex to Eurocode 2 and the new MTCM, applying the principles of model uncertainty. The calculation methods are benchmarked against experiments performed by various authors in the literature, which further was collected into a comprehensive database consisting of 429 data points obtained from bending tests of beams, 104 data points obtained from tensile tests of RC ties and 200 data points obtained from bending tests of slabs. The modeling uncertainty shows that the MTCM performs best for beams in bending with $\theta_{\text{mean}} = 0.98$, for MC2010 RC ties in tension with $\theta_{\text{mean}} = 1.0$ and for slabs in bending with $\theta_{\text{mean}} = 1.05$. DIN underestimate the crack width to a relatively large extent for beams in bending with $\theta_{\text{mean}} = 1.69$. The majority of the experimental tests in the database have already been used to develop the code formulations by means of empirical calibration.

The crack width models compared are based on the same theoretical framework expressing the crack width as a product of crack spacing and strain difference between reinforcement and concrete. However, the models incorporate mechanical properties such as bond stress distribution, effective tension area, strain gradients and consideration of the crack stages differently. In addition, Eurocode 2 and Model Code use empirical modifications to adjust the calculated crack width, that is, cover term in the crack spacing formulas. The reason behind this is justified from an empirical standpoint in the literature,[43–47] which clearly shows that cover is a significant factor in crack spacing. The proposed changes from EC2 to FpEC2 are well documented by Caldentey et al.[42] The first and third databases have a majority of the experimental members with relatively small covers of 20–30 mm and 10–20 mm which do not favor the new empirical k_{fl} factor in MC2020 and FprEC2 intended to account for the effect of stress distribution within the effective concrete tensile area. Therefore, the authors of this article find it challenging to conclude the general effect of the new empirical and mechanical modifications from the results included in the existing databases. It can however be argued, from a mechanical viewpoint, that the largest inconsistencies in the code formulations stem from the oversimplifications of (i) an excessive focus on crack spacing rather than the maximum crack width itself and (ii) assuming constant bond stress regardless of geometry and stress level. The lack of mechanical understanding and interpretation in the code formulation is compensated for by experimental calibration against a chosen database. This will provide a strict range of applicability. In contrast, the results in this article show that the MTCM performs as well as the code formulations without calibration towards a specific database.

7 | SUGGESTIONS FOR FURTHER RESEARCH

The findings in this article suggest that a simplified version of the MTCM should be developed to obtain a code-type formulation that can challenge the current code formulations investigated in this study. The first step in this approach would be to obtain a closed-form solution in the case of CHLM in the MTCM. The authors are currently working on such a calculation model.

DATA AVAILABILITY STATEMENT

The data that support the findings of this study are available from the corresponding author upon reasonable request.

ORCID

Reignard Tan https://orcid.org/0000-0001-8190-6215

REFERENCES

1. Leonhardt F. Zur Behandlung von Rissen im Beton in den deutschen Vorschriften (Teil 1). Ther Ber. 1985;80:179–84.
2. Beeby AW. Corrosion of reinforcing steel in concrete and its relation to cracking, vol. 56A. London: Institution of Structural Engineers; 1978. p. 77–81. https://trid.trb.org/view/78946
3. Basteskår M, Engen M, Kanstad T, Fosså KT. A review of literature and code requirements for the crack width limitations for design of concrete structures in serviceability limit states. Struct

17517648, 0, Downloaded from https://onlinelibrary.wiley.com/doi/10.1002/suco.202300367 by Otto Terjesen - Norwegian Institute Of Public Healt Invoice Receipt DFO , Wiley Online Library on [17/03/2024]. See the Terms and Conditions (https://onlinelibrary.wiley.com/terms-and-conditions) on Wiley Online Library for rules of use; OA articles are governed by the applicable Creative Commons License

Concr. 2019;20(2):678–88. Portico. https://doi.org/10.1002/suco.201800183
4. Borosnyói A, Balázs GL. Models for flexural cracking in concrete: the state of the art. Struct Concr. 2005;6(2):53–62. https://doi.org/10.1680/stco.2005.6.2.53
5. Basteskår M, Engen M, Kanstad T, Johansen H, Fosså KT. Serviceability limit state design of large concrete structures: impact on reinforcement amounts and consequences of design code ambiguity. Eng Struct. 2019;201:109816. https://doi.org/10.1016/j.engstruct.2019.109816
6. CEN. EN 1992-1-1, Eurocode 2: Design of Concrete Structures—Part 1–1: general rules and rules for buildings. Brussels: European Committee for Standardization; 2004.
7. CEN-TC250-SC2-WG1_N1296_FprEN_1992-1-1_e_stf_2022-07-24 FIN clean. 2022.
8. fib. Model Code for Concrete Structures 2010. Berlin: International Federation for structural concrete; 2013.
9. 2nd Draft of ModelCode 2020—December. 2022.
10. DIN: EN-1992-1-1/NA. 2011-01, National Annex—Nationally determined parameters—Eurocode 2: Design of concrete structures—Part 1-1: General rules and rules for buildings. 2011.
11. Tan R, Hendriks MAN, Geiker M, Kanstad T. Analytical calculation model for predicting cracking behavior of reinforced concrete ties. J Struct Eng. 2020;146(2):04019206. https://doi.org/10.1061/%28ASCE%29ST.1943-541X.0002510
12. Schlicke D, Dorfmann EM, Fehling E, Tue NV. Calculation of maximum crack width for practical design of reinforced concrete. Civ Eng Des. 2021;3(3):45–61. https://doi.org/10.1002/cend.202100004
13. Tan R. Consistent crack width calculation methods for reinforced concrete elements subjected to 1D and 2D stress states a mixed experimental, numerical and analytical approach, Philosophiae Doctor, Department of Structural Engineering, Norwegian University of Science and Technology. 2019 http://hdl.handle.net/11250/2607051
14. Terjesen O, Kanstad T, Tan R. Application of NLFEA for crack width calculations in SLS. In: Meschke G, Pichler B, Rots JG, editors. Computational modelling of concrete and concrete structures. 1st ed. Vienna: Routledge Taylor & Francis Group; 2022. p. 246–54. https://www.routledge.com/Computational-Modelling-of-Concrete-and-Concrete-Structures/Meschke-Pichler-Rots/p/book/9781032327242#
15. Cervenka V, Rimkus A, Gribniak V, Cervenka J. Simulation of the crack width in reinforced concrete beams based on concrete fracture. Theor Appl Fract Mech. 2022;121:103428. https://doi.org/10.1016/j.tafmec.2022.103428
16. Naotunna CN, Samarakoon SMSMK, Fosså KT. Experimental investigation of crack width variation along the concrete cover depth in reinforced concrete specimens with ribbed bars and smooth bars. Case Stud Construct Mater. 2021;15:e00593. https://doi.org/10.1016/j.cscm.2021.e00593
17. Beeby AW, Scott RH. Cracking and deformation of axially reinforced members subjected to pure tension. Magaz Concr Res. 2005;57(10):611–21. https://doi.org/10.1680/macr.2005.57.10.611
18. Beeby RHSAW. Influence of tension stiffening on deflection of reinforced concrete structures: report of a concrete society. Sandhurst, Berkshire: Concr Soc; 2004.
19. Beeby AW. The influence of the parameter φ/ρeff on crack widths. Struct Concr. 2005;6:155–65. https://doi.org/10.1680/stco.2005.6.4.155
20. Russo G, Romano F. Cracking response of RC members subjected to uniaxial tension. J Struct Eng. 1992;118(5):1172–90. https://doi.org/10.1061/(ASCE)0733-9445(1992)118:5(1172)
21. fib. Bond of reinforcement in concrete: state-of-art report fib bulletin No. 10. Lausanne, Switzerland: Sprint-Druck Stuttgart; 2000.
22. Marti P, Alvarez M, Kaufmann W, Sigrist V. Tension chord model for structural concrete. Struct Eng Int. 1998;8(4):287–98. https://doi.org/10.2749/101686698780488875
23. Alvarez M. Einfluss des Verbundverhaltens auf das Verformungsvermögen von Stahlbeton. Birkhäuser. 1998;236:3-7643-5993-5.
24. Edwards AD, Picard A. Theory of cracking in concrete members. Proc ASCE J Struct Div. 1972;98(12):2687–700.
25. Tan R, Hendriks MAN, Kanstad T. An investigation of the strain profile over the cover in reinforced concrete elements subjected to tension. 5th *fib* Congress in Melbourne, Australia (2018) proceedings, 7-11 October, Melbourne Australia; 2019. p. 1784–91.
26. Eligehausen R, Popov EP, Bertero VV. Local bond stressslip relationships of deformed bars under generalised excitations: experimental results and analytical model. Rep. No. UCB/EERC 83/23. Berkeley, CA: University of California. 1983.
27. Tan R, Hendriks MAN, Geiker M, Kanstad T. A numerical investigation of the cracking behaviour of reinforced-concrete tie elements. Mag Concr Res. 2020;72(3):109–21. https://doi.org/10.1680/jmacr.18.00156
28. Caldentey AP, García R, Gribniak V, Rimkus A. Tension versus flexure: reasons to modify the formulation of MC 2010 for cracking. Struct. Concr. 2020;21(5):2101–23. https://doi.org/10.1002/suco.202000279
29. Stable version CEN-TC250-SC2-WG 102_N0321_CENTC_250SC_2WG_1_N_1143_-_Stable_version_of_prEN_1992-1-12021-09. 2022.
30. Hognestad. Journal of PCI Research and Development Laboratories. 1962. 1962.
31. CUR. Dutch centre for civil engineering, Research and Codes Report no. 37 (Out of print). 1994.
32. Rüsch EH, Rhem G. Versuche mit BetonformStählen. (1963), pt. II (1963), pt. III (1964). Deutscher Ausschuss für Stahlbeton, No. 140. 1963–1964.
33. Clark AP. Cracking in reinforced concrete flexural members. ACI J, Proc. 1956;27(8):851–62.
34. Hartl G. Die Arbeitslinie " eingebetteter Stähle" bei Erst- und Kurzzeitbelastung Dissertation, University of Innsbruck. 1977.
35. Rimkus A. Effects of Bar reinforcement arrangement on deformations and cracking of concrete elements. Doctoral Dissertation. Vilnius: Technika, 2017. 143 p. 2017.
36. Wu H, Gilbert R. An experimental study of tension stiffening in reinforced concrete members under short-term and long-term loads. 2008.
37. Tan R, Eileraas K, Opkvitne O, Žirgulis G, Hendriks MAN, Geiker M, et al. Experimental and theoretical investigation of crack width calculation methods for RC ties. Struct Concr. 2018;19(5):1436–47. https://doi.org/10.1002/suco.201700237."
38. Engen M, Hendriks MAN, Köhler J, Øverli JA, Åldstedt E. A quantification of the modelling uncertainty of nonlinear finite element analyses of large concrete structures. Struct Saf. 2017;64:1–8. https://doi.org/10.1016/j.strusafe.2016.08.003

17517648, 0, Downloaded from https://onlinelibrary.wiley.com/doi/10.1002/suco.202300367 by Otto Terjesen - Norwegian Institute Of Public Healt Invoice Receipt DFO , Wiley Online Library on [17/03/2024]. See the Terms and Conditions (https://onlinelibrary.wiley.com/terms-and-conditions) on Wiley Online Library for rules of use; OA articles are governed by the applicable Creative Commons License

39. JCSS. Probabilistic model code, 12th draft. joint committee on Structural Safety. 2001.
40. Serviceability limit state of concrete structures: Techincal report fib bulletin 92. 2019.
41. Euro-International Committee for Concrete. Ceb-Fip model code 1990: design code. Thomas Telford. 1991.
42. Caldentey A, Bellod J, Torres L, Kanstad T. Serviceability limit states according to the new Eurocode 2 proposal: description and justifications of the proposed changes. Hormigón y Acero. 2023;71:91–108. https://doi.org/10.33586/hya.2023.3104
43. Guedes F, and Vaz Rodrigues R, The effect of concrete cover on the crack width in reinforced concrete members-a code perspective. 2nd International Conference on Recent Advances in Nonlinear Models-Design and Rehabilitation of Structures, Coimbra, Portugal 2017. https://www.uc.pt/fctuc/dec/destaques_historico/CoRASS
44. Naotunna C, Samarakoon S, Fosså K. A new crack spacing model for reinforced concrete specimens with multiple bars subjected to axial tension using 3D nonlinear FEM simulations. Struct Concr. 2021;22:3241–54. https://doi.org/10.1002/suco.202100025
45. Naotunna C, Samarakoon S, Fosså K. Influence of concrete cover thickness and clear distance between tensile bars on crack spacing behavior of large-scale reinforced concrete members. Fatigue Fract Eng Mater Struct. 2022;45:1052–64. https://doi.org/10.1111/ffe.13650
46. Gribniak V, Rimkus A, Pérez Caldentey A, Sokolov A. Cracking of concrete prisms reinforced with multiple bars in tension: the cover effect. Eng Struct. 2020;220:110979. https://doi.org/10.1016/j.engstruct.2020.110979
47. Pérez Caldentey A, Corres Peiretti H, Peset Iribarren J, Giraldo Soto A. Cracking of RC members revisited: influence of cover, ϕ/ρs, ef and stirrup spacing: an experimental and theoretical study. Struct Concr. 2013;14(1):69–78. https://doi.org/10.1002/suco.201200016

AUTHOR BIOGRAPHIES

Otto Terjesen, M.Sc. PhD Research Fellow, University of Agder, Jon Lilletuns vei 9, 4879 Grimstad, Norway.
Email: otto.terjesen@uia.no

Gianclaudio Pinto, M.Sc. Civil Engineer, Implenia Norway AS, Fornebuveien 11, 1366, Oslo, Norway.
Email: gianclaudio.pinto@implenia.com

Terje Kanstad, Ph.D., M.Sc, Professor, Norwegian University of Science and Technology, Richard Birkelands vei 1A, 7491 Trondheim, Norway.
Email: terje.kanstand@ntnu.no

Reignard Tan, Ph.D., M.Sc. Associate Professor, Norwegian University of Science and Technology, Richard Birkelands vei 1A, 7491 Trondheim. Multiconsult AS, Postboks 265 Skøyen, 0213 Oslo, Norway.
Email: reignard.tan@multiconsult.no

How to cite this article: Terjesen O, Pinto G, Kanstad T, Tan R. Performance study of crack width calculation methods according to Eurocodes, *fib* model codes and the modified tension chord model. Structural Concrete. 2024. https://doi.org/10.1002/suco.202300367

17517648, 0, Downloaded from https://onlinelibrary.wiley.com/doi/10.1002/suco.202300367 by Otto Terjesen - Norwegian Institute Of Public Healt Invoice Receipt DFO , Wiley Online Library on [17/03/2024]. See the Terms and Conditions (https://onlinelibrary.wiley.com/terms-and-conditions) on Wiley Online Library for rules of use; OA articles are governed by the applicable Creative Commons License

Paper III

Simplified Modified Tension Chord Model – an alternative crack width calculation model to Eurocode 2 and fib Model Codes

Terjesen, O., Kanstad, T., and Tan, R. (2024).

Version is submitted to *fib* Structural Concrete March 2024:

Simplified Modified Tension Chord Model – an alternative crack width calculation model to Eurocode 2 and *fib* Model Codes

	Otto Terjesen, M.Sc. PhD Research Fellow, University of Agder Jon Lilletuns vei 9, 4879 Grimstad otto.terjesen@uia.no Phone: +47 95 90 44 54
	Terje Kanstad, Ph.D., M.Sc Professor, Norwegian University of Science and Technology Richard Birkelands vei 1A, 7491 Trondheim terje.kanstand@ntnu.no
	Reignard Tan, Ph.D., M.Sc. Associate Professor, Norwegian University of Science and Technology Richard Birkelands vei 1A, 7491 Trondheim. Multiconsult AS, Postboks 265 Skøyen, 0213 Oslo, Norway reignard.tan@multiconsult.no

1 Abstract

This paper proposes a new design code formulation for calculating crack widths for regular and more special reinforced concrete (RC) members. The more comprehensive Modified Tension Chord Model (MTCM) has been simplified (SMTCM) to facilitate an alternative method for calculating crack widths to Eurocode 2 and *fib* Model Codes. The model is based on mechanical principles without empirical modifications and is benchmarked against a previously published experimental crack width database. The SMTCM predicts crack widths quite as accurately as the MTCM and provides a broader range of applicability, such as for large covers and RC ties having arbitrary rebar configurations and thus a better crack width model than the current design codes for RC ties. In addition, there are no openings for ambiguous interpretations of the calculations, which can increase the risk of obtaining two different crack widths from two different designers. To further justify the SMTCM code formulation and concept, several RC ties with experimental crack width profiles were used and discussed. The results show a considerable difference between the crack width profile at the surface and at the reinforcement location, depending on the concrete cover and rebar size. These observations are interesting regarding durability design and requirements and show that the approach using a maximum design crack width at a specific surface as a decisive parameter should be further investigated, especially for large concrete covers.

2 Introduction

Cracks in reinforced concrete (RC) structures usually occur with irregular distribution and different crack widths along the members. Despite a century of research, predicting them accurately and consistently is still difficult, as shown by Terjesen et al. [1]. On the other hand, the consequences of cracks related to functionality, durability, aesthetics, and economy are large, and discussions in the research environments are ongoing [2, 3]

It was shown by Terjesen et al. [1] that the Modified Tension Chord Model (MTCM) proposed by Tan [4] predicts crack widths for RC beams, slabs and ties close to reality without any empirical adjustments towards an experimental database whatsoever. The MTCM also yields a consistent formulation for when the member is in a crack formation or stabilized cracking stage by applying the two solution schemes: Comparatively Lightly Loaded Member (CLLM) and Comparatively Heavily Loaded Member (CHLM). However, the model offers non-closed form analytical solutions to the

second-order differential equation for the slip and is thus not applicable in a design code format. Therefore, the main objective of this paper is to formulate a simplified version of the MTCM in a design code format as an alternative crack width calculation method to Eurocode 2 [5, 6] and *fib* Model Codes [7, 8], and which covers both the crack formation and the stabilized crack stage in a mechanical consistent manner. Figure 1 illustrates the generic behaviour of tensioned RC members by the force-deformation relation of a symmetrically reinforced tie and its relation to the two solution schemes in the MTCM and SMTCM.

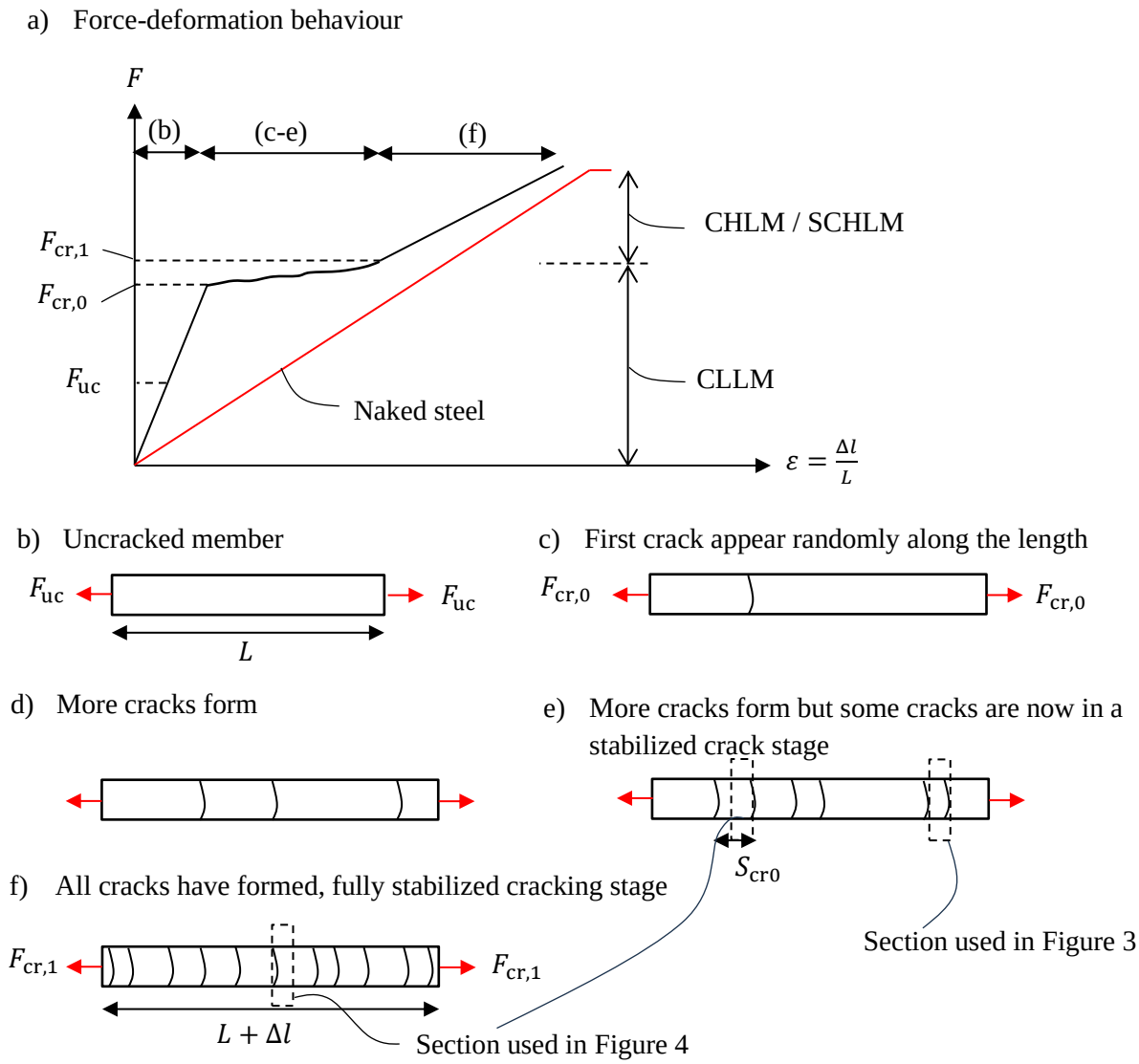

Figure 1 (a) Force-deformation and a crack development of a symmetric RC-tie for (b) Uncracked, (c-d) Crack formation stage, (f) A fully stabilized cracking stage

Figure 1 c) illustrates that at an arbitrary location, a crack is formed when the tensile stress in the concrete exceeds the tensile strength and initiates the crack formation phase. By increasing the loading again, as shown in Figure 1 d-e), more cracks will

form, while the location of new cracks will still occur randomly. However, in the case of Figure 1 e), they will now also form close to the existing cracks, but the entire member is still in a crack formation phase because the formation of new cracks influences the existing cracks upon further loading, as shown in Figure 1 f), where all the major cracks have formed the crack width is now influenced by the opening of existing cracks, i.e., a fully stabilized cracking stage.

The current Eurocode 2 (EC2) [5], the new version of Eurocode 2 (FprEC2) [6], and *fib* Model Code 2010 (MC2010) [7] calculate the crack width as a product of crack spacing and the strain difference between steel and concrete. These crack width formulas are based on a combination of two alternative theories:

a. The bond-slip theory assumes a slip between the reinforcement and the surrounding concrete; however, the slip is assumed independent of load level and rebar size since constant bond stress is applied.
b. The no-slip theory assumes that internal cracking along the rebar surface represents the strain incompatibility between reinforcement and concrete; however, at the rebar level, there is strain compatibility, and thus, perfect bond is assumed. Theoretically, a crack is of no width at the rebar.

While the crack spacing and the mean steel and concrete strains in the design codes are calculated assuming *constant* bond stress distribution over the transfer length, the crack spacing is calculated with an additional empirical cover term according to the no-slip theory. The cover effect is justified by experimental results showing increased crack width due to increased concrete cover, often identified as a shear-lag effect in the literature [7, 9, 10] because the concrete within the cover depth is subjected to shear stresses. Consequently, the crack spacing in Eq. (1) by FprEC2 [6] contains empirical modifications used to calculate the crack width for the three cases shown in Figure 2.

$$S_{\mathrm{r,m,cal}} = 1.5c + \frac{k_{\mathrm{fl}} k_{\mathrm{b}}}{7.2} \frac{\phi}{\rho_{\mathrm{p,eff}}} \leq 1.3(h - x) \tag{1}$$

Eq. (1) represents the mean crack spacing when all cracks have formed in the stabilized crack stage but is also applied in the crack formation stage, where it is assumed to represent the maximum length along the reinforcement with slip between the concrete and the reinforcement. Physically, the second term represents a tension chord model with a bond slip theory assuming constant bond stresses, while the first term represents the effect of cover by the no-slip theory first proposed in 1965 by Broms [11] and is

calibrated as shown by Perez et al. [12] and Rasmussen [13]. However, this is considered mechanically inconsistent since the length of the zone with slip between the concrete and reinforcement (transfer length) may vary significantly in the crack formation stage.

Generally, in the design of a reinforced concrete structure, external loads and/or imposed deformations (creep, shrinkage and temperature) are applied, and consequently, the steel stress or strain is found by structural analysis and stress calculations. However, different procedures for external load and imposed deformations might be required to achieve accurate solutions. An additional obstacle is that external loads usually require a solution in the stabilized cracking stage, while imposed deformations should be handled more often in the crack formation stage. Figure 2 illustrates how the difference between the mean steel ($\varepsilon_{\mathrm{sm}}$) and concrete strain ($\varepsilon_{\mathrm{cm}}$) are calculated and intended to be handled according to FprEC2 [6] from (a) external loads and (b-c) imposed deformation.

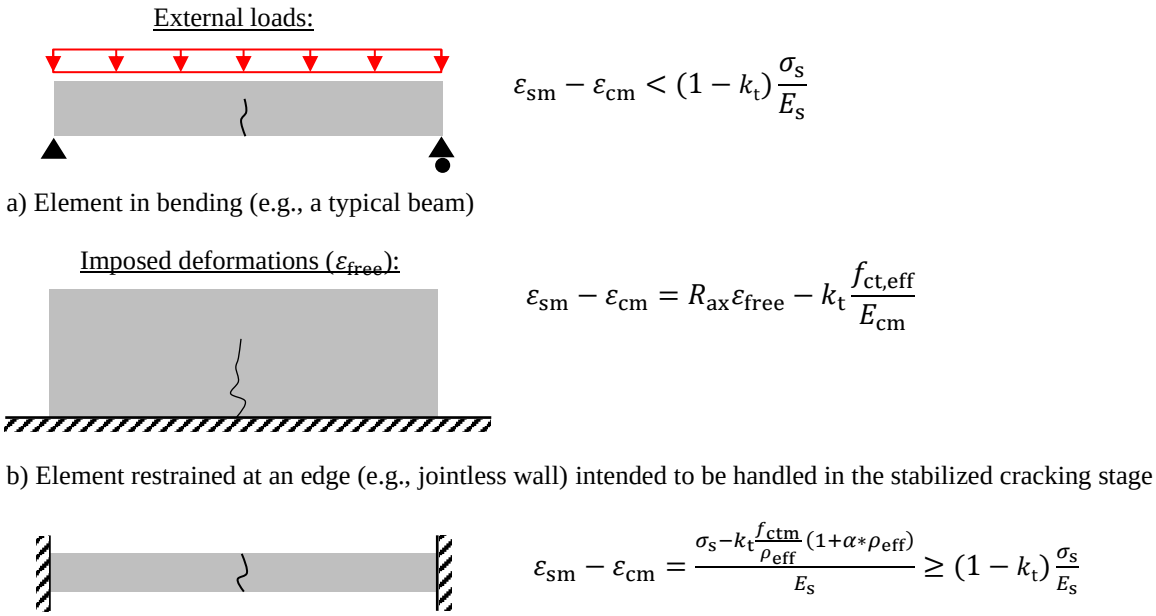

Figure 2 Definitions of when a member is assumed to be in a crack formation stage according to FprEC2 [6].

3 Simplified Modified Tension Chord Model

3.1 General

The Simplified Modified Tension Chord Model (SMTCM) is based on the MTCM developed by Tan in 2019 [14]. It is based on solving the Second Order Differential Equation (SODE) for the slip in a cracked RC tie representing the tensile zone of structural members expressed analytically by Eq. (2). The calculated slip is the decisive parameter for the crack width in the crack formation stage when the model represents a tie with one crack as shown in Figure 1c-e. In the stabilized cracking stage, the model represents a tie limited by two cracks and one crack in the middle, as shown in Figure 1e-f.

$$\frac{d^2u}{dx^2} - \chi\tau(u) = 0 \tag{2}$$

The two variables, bond stress (τ) and slip (u), are both dependent on the applied reinforcement force in the crack as input to the crack width calculations, while $\chi = (\sum \pi\phi_s/A_sE_s)(1+\xi)$ is a parameter representing equivalent tensile cross-sections with ϕ_s, A_s and E_s being the diameter, area and Young's modulus for the rebar. Furthermore, the other parameters are defined as $\xi = \alpha_E\rho_s/\psi$, $\alpha_E = E_s/E_c$ and $\rho_s = A_s/A_c$, with A_c being the sectional area of the RC tie and E_c Young's modulus for concrete. The parameter $\psi \leq 1.0$ is a factor accounting for the fact that plane sections do not remain plane in RC ties [15], i.e., it accounts for the fact that the strain profile over the cover is not constant [16]. It was observed by Tan et al. [4] that a value of 0.7 for ψ seemed reasonable, independent of geometry and load level.

The model expresses that the nominal bond stresses (τ) depend on the slip (u). Solving for the slip in Eq. (2) analytically requires using a local bond-slip law, and the MTCM applies the local bond-slip law first proposed by Eligehausen et al. [17] and later adopted by MC2010 [7].

$$\tau(\mu) = \tau_{\max}\left(\frac{u}{u_1}\right)^{\alpha} \tag{3}$$

where the parameter u is the slip at the actual load level, and the chosen empirical factors are $\tau_{\max} = 5\ MPa,\ u_1 = 0.1$, and $\alpha = 0.35$. These factors were determined in

[18], representing the mean of local bond-slip curves for an arbitrary RC tie. Inserting Eq. (3) into Eq. (2) yields the SODE expressed as:

$$\frac{d^2u}{dx^2} - \chi \frac{\tau_{\max}}{{\mu_1}^{\alpha}} u^{\alpha} = 0 \tag{4}$$

The SODE can now be solved analytically, as described in [4]. In this state, the MTCM gives two sets of boundary conditions and solutions grouped by the concepts of comparatively lightly loaded members (CLLM) and comparatively heavily loaded members (CHLM). These concepts are analogous to the crack formation stage (CLLM) and stabilized cracking stage (CHLM). It is worth mentioning that Debernardi et al. [19] recently proposed a new theoretical formulation of a new bond-slip law based on an RC tie with a length equal to the crack spacing. The solution is proposed through two constitutive relationships with origins at zero slip and maximum slip sections. The work indicates an opportunity to replace the bond law in Eq (3) with one based on experimental works that represent the real situations of reinforced concrete structures and not pull-out tests.

In the case of CLLM, steel and concrete strains become compatible at the distance S_{r0} from the loaded end, expressed as the *transfer length*, see Figure 3a. Upon further loading S_{r0} moves towards the symmetry section, $L/2$, as long as the maximum concrete stresses are below the tensile strength limit, i.e., $\varepsilon_{\mathrm{c,max}} < \varepsilon_{\mathrm{ctm}} = f_{\mathrm{ctm}}/E_{\mathrm{cm}}$. In contrast, if the maximum concrete stresses at any abscissa x reaches the tensile strength, i.e. $\varepsilon_{\mathrm{c,max}} = \varepsilon_{\mathrm{ctm}}$, a new crack is formed at this location, denoted as S_{cr0}, which expressed more rigorously becomes the *crack spacing*. The steel strain at the loaded end that causes a new crack to form at S_{cr0} is denoted $\varepsilon_{\mathrm{s,cr}}$ and is shown in Figure 3b is deduced from axial equilibrium and can be expressed as [4]:

$$\varepsilon_{\mathrm{s,cr}} = \varepsilon_{\mathrm{ctm}} \frac{1+\xi}{\psi\xi} \tag{5}$$

where $\xi = \alpha_{\mathrm{E}}\rho_{\mathrm{s}}/\psi$, $\alpha_{\mathrm{E}} = E_{\mathrm{s}}/E_{\mathrm{c}}$, $\rho_{\mathrm{s}} = A_{\mathrm{s}}/A_{\mathrm{c}}$ and the parameter $\psi = 0{,}7$. Afterwards, the response should be determined according to the new member length $L = S_{\mathrm{cr0}}$, see Figure 4a. For further loading, it is noticed that steel and concrete strains, in general, remain incompatible over the entire crack spacing, which means that the concept of

CHLM governs when the steel strain in the crack $\varepsilon_s > \varepsilon_{s,cr}$. The CHLM behaviour is in the simplified approach (SCHLM) discretized as a linear interpolation between the points for the mean steel strains at load levels at crack formation ($\varepsilon_s = \varepsilon_{s,cr}$), and when the steel strain reaches yielding ($\varepsilon_s = \varepsilon_{s,y}$), Figure 5a.

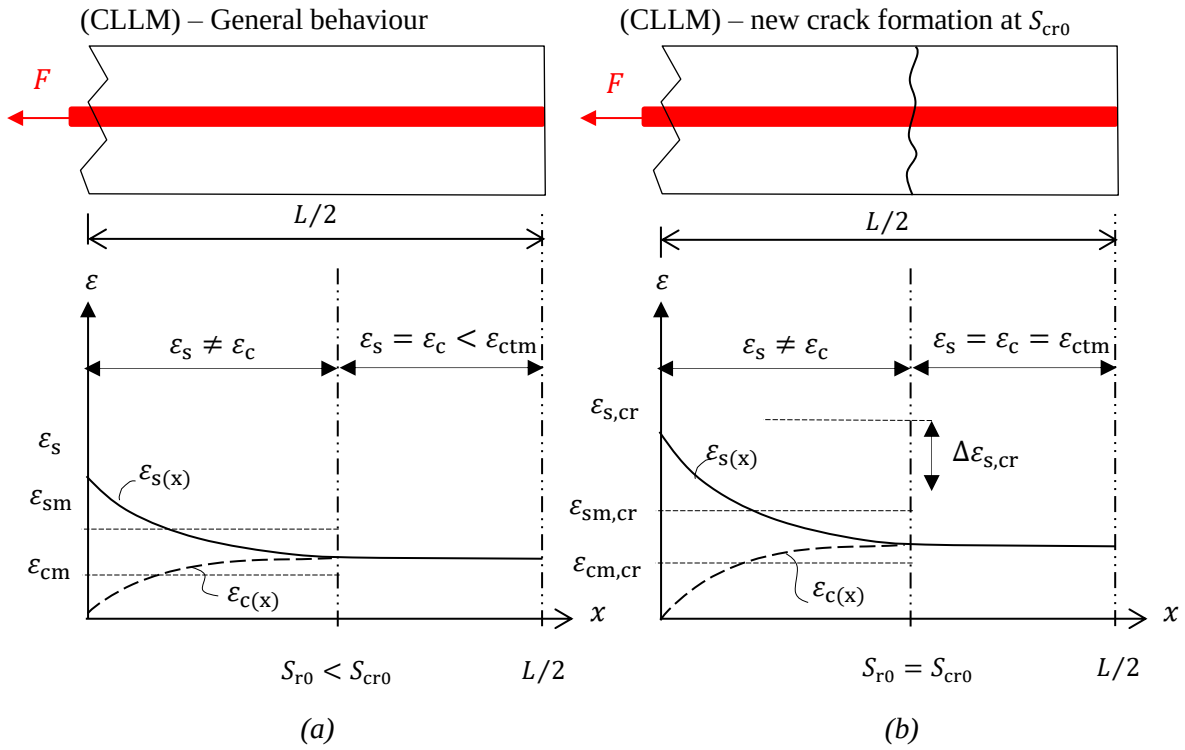

Figure 3 Distribution of steel and concrete strains over the cracked RC-tie for CLLM (a) general behaviour and (b) at the crack formation

3.2 Solution for comparatively lightly loaded members (CLLM)

The CLLM behaviour governs as long as the steel strain in the crack $\varepsilon_s < \varepsilon_{s,cr}$, and the solution of the SODE for the slip at the loaded end from MTCM is applied:

$$u_r = \left(\frac{{\varepsilon_s}^2}{2\gamma}\right)^{\frac{1}{\beta}} \tag{6}$$

Where $\gamma = \chi\tau_{max}/(\beta {u_1}^{\alpha})$, $\chi = (\sum \pi\phi_s/A_s E_s)(1+\xi)$, $\beta = 1+\alpha$ and the bond-slip parameters are defined as $u_1 = 0.1$ and $\alpha = 0.35$. The transfer length is dependent on the steel strain at the crack and is obtained as:

$$S_{r0} = \frac{1}{\delta}\left[\varepsilon_s\left(\frac{1}{2\gamma}\right)^{\frac{1}{2\delta}}\right]^{\frac{2\delta}{\beta}} \tag{7}$$

where $\delta = (1-\alpha)/2$

The mean steel and concrete strains are obtained as

$$\varepsilon_{\mathrm{sm.CLLM}} = \frac{1}{S_{r0}} \frac{\xi \varepsilon_{\mathrm{s}} S_{r0} + u_{\mathrm{r}}}{1+\xi} \tag{8}$$

$$\varepsilon_{\mathrm{cm.CLLM}} = \frac{\psi\xi}{S_{r0}} \frac{\varepsilon_{\mathrm{s}} S_{r0} - u_{\mathrm{r}}}{1+\xi} \tag{9}$$

Finally, the crack width is expressed as a product of the difference in average strains and the transfer length as:

$$w_{\mathrm{cr}} = 2S_{r0}(\varepsilon_{\mathrm{sm.CLLM}} - \varepsilon_{\mathrm{cm.CLLM}}) \tag{10}$$

3.3 Solution at crack formation

At the formation of a new crack, as shown in Figure 3b, the transfer length (S_{cr0}) becomes analogue to the crack spacing initiating the CHLM behaviour after this point. The transfer length S_{cr0} was found by substituting ε_{s} with $\varepsilon_{\mathrm{s,cr}}$ determined from Eq. (5) in Eqs. (6) and (7), and the maximum slip at the loaded end at cracking then becomes.

$$u_{\mathrm{r,cr}} = \left(\frac{\varepsilon_{\mathrm{s,cr}}^2}{2\gamma}\right)^{\frac{1}{\beta}} \tag{11}$$

whereas the transfer length at cracking becomes the crack spacing:

$$S_{\mathrm{cr0}} = \frac{1}{\delta}\left[\varepsilon_{\mathrm{s,cr}}\left(\frac{1}{2\gamma}\right)^{\frac{1}{2\delta}}\right]^{\frac{2\delta}{\beta}} \tag{12}$$

where $\delta = (1-\alpha)/2$.

The mean steel strains and concrete strains are obtained as

$$\varepsilon_{\mathrm{sm,cr}} = \frac{1}{S_{\mathrm{cr0}}} \frac{\xi \varepsilon_{\mathrm{s,cr}} S_{\mathrm{cr0}} + u_{\mathrm{r,cr}}}{1+\xi} \tag{13}$$

$$\varepsilon_{\mathrm{cm,cr}} = \frac{\psi\xi}{S_{\mathrm{cr0}}} \frac{\varepsilon_{\mathrm{s,cr}} S_{\mathrm{cr0}} - u_{\mathrm{r,cr}}}{1+\xi} \tag{14}$$

The difference between the steel strain ($\varepsilon_{\mathrm{s,cr}}$) for when a crack forms at the end of the transfer length (S_{cr0}) and the mean steel strains ($\varepsilon_{\mathrm{sm,cr}}$) is then expressed as:

$$\Delta\varepsilon_{\mathrm{s,cr}} = \varepsilon_{\mathrm{s,cr}} - \varepsilon_{\mathrm{sm,cr}} \tag{15}$$

The relation is depicted in Figure 5a.

3.4 Solution for simplified comparatively heavily loaded members (SCHLM)

3.4.1 Strains at steel yielding

The strains at reinforcement yielding are determined by a procedure starting with the strain state at the initiation of CHLM; however, still having strain compatibility at the symmetry section for a member length $L = S_{\mathrm{cr0}}$ as shown in Figure 4b. This means that the solution of a CLLM-behaviour still governs and can be applied.

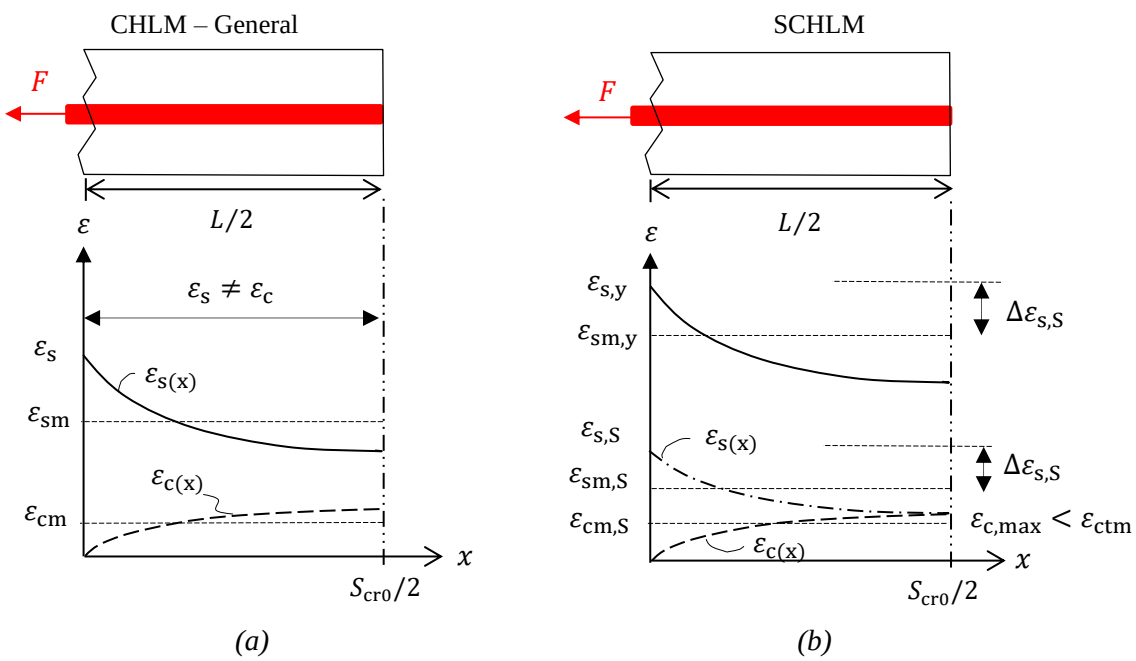

Figure 4 Distribution of steel and concrete strains along the cracked RC-tie for the concepts CHLM (a) general behaviour and (b) simplified behaviour (SCHLM)

The steel strain that moves the transfer length s_{r0} to the symmetry section for an RC tie having the member length S_{cr0}, as shown in Figure 4b, is expressed as [4]

$$\varepsilon_{\mathrm{s,S}} = (2\gamma)^{\frac{1}{2\delta}} \left(\frac{S_{\mathrm{cr0}}}{2}\delta\right)^{\frac{\beta}{2\delta}} \tag{16}$$

While the slip at the loaded end for this steel strain is

$$u_{\mathrm{r,S}} = \left(\frac{\varepsilon_{\mathrm{s,S}}^2}{2\gamma}\right)^{\frac{1}{\beta}} \tag{17}$$

Furthermore, the corresponding mean strain values are obtained by modifying Eq. (13) and (14) as:

$$\varepsilon_{\mathrm{sm,S}} = \frac{1}{\frac{S_{\mathrm{cr0}}}{2}} \frac{\xi \varepsilon_{\mathrm{s.S}} \frac{S_{\mathrm{cr0}}}{2} + u_{\mathrm{r,S}}}{1+\xi} \tag{18}$$

$$\varepsilon_{\mathrm{cm,S}} = \frac{\psi\xi}{\frac{S_{\mathrm{cr0}}}{2}} \frac{\varepsilon_{\mathrm{s.S}} \frac{S_{\mathrm{cr0}}}{2} - u_{\mathrm{r,S}}}{1+\xi} \tag{19}$$

The difference between the steel strain at the loaded end ($\varepsilon_{\mathrm{s,S}}$) and the mean strain ($\varepsilon_{\mathrm{sm,S}}$) can now be expressed as

$$\Delta\varepsilon_{\mathrm{s,S}} = \varepsilon_{\mathrm{s,S}} - \varepsilon_{\mathrm{sm,S}} \tag{20}$$

Then, the mean strains at yielding are taken as

$$\varepsilon_{\mathrm{sm,y}} = \varepsilon_{\mathrm{s,y}} - \Delta\varepsilon_{\mathrm{s,S}} \tag{21}$$

$$\varepsilon_{\mathrm{cm,y}} = \varepsilon_{\mathrm{cm,S}} \tag{22}$$

The chosen formulation is at yielding on the conservative side compared to the MTCM, which is appreciated from an engineering viewpoint since the SMTCM is a simplified version.

3.4.2 Strains for SCHLM

The SMTCM applies formulae (6)-(10) for the crack formation stage, while it predicts the CHLM behaviour shown in Figure 4a using a simplified (SCHLM) approach. This solution assumes a linear interpolation between the points for mean steel strains at a load level corresponding to the crack formation $\varepsilon_s = \varepsilon_{s,cr}$ (Figure 3b), and the steel strain at yielding $\varepsilon_s = \varepsilon_{s,y} = f_y/E_s$ as shown in

Figure 4b and Figure 5, where f_y is the yield strength of the reinforcement. The two stages represent the initiation and the end of the stabilized cracking stage. The slope a of the curve is thus determined from the two-point form as:

$$a = \frac{\varepsilon_{s,y} - \varepsilon_{s,cr}}{\varepsilon_{sm,y} - \varepsilon_{sm,cr}} \tag{23}$$

The expression for the mean strains for the SCHLM behaviour then becomes

$$\varepsilon_{sm,SCHLM} = \varepsilon_{sm,cr} + \frac{\varepsilon_s - \varepsilon_{s,cr}}{a} \tag{24}$$

$$\varepsilon_{cm,SCHLM} = \varepsilon_{cm,S} \tag{25}$$

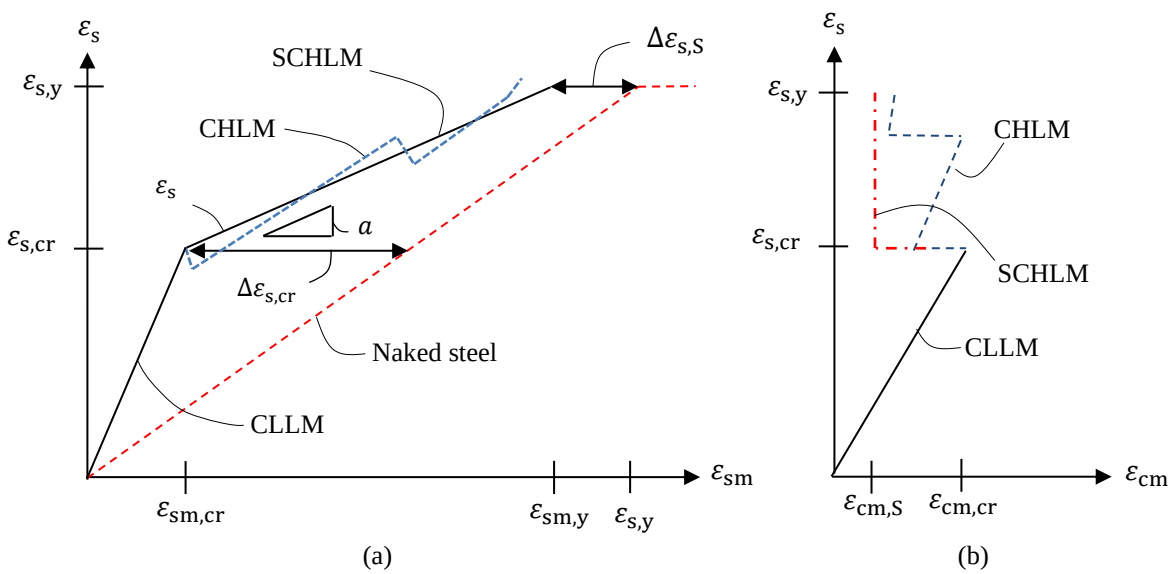

Figure 5 Steel strains at crack vs (a) mean steel strains and (b) mean concrete strains between two cracks.

In summary, the main difference between the two concepts is that the strains remain compatible in the case of CLLM, while the strains are incompatible in the case of CHLM. The SMTCM utilizes the closed-form solutions for the case of CLLM to predict

the CHLM behaviour using a simplified approach. The relations between CLLM, CHLM and SCHLM are illustrated in Figure 5 and later discussed in section 4.3.1.

4 Design code format by SMTCM

4.1 General

The SMTCM is now formulated in a design code format for practical application. In this format, the primary input to the model is the stress in the tensile reinforcement found from structural and cross-sectional analysis, in addition to material parameters and the geometry of an RC tie. The method offers two solutions depending on whether the RC tie is in the crack formation stage (CLLM-behaviour) or the stabilized cracking stage (SCHLM-behaviour). Furthermore, it should be noted that the model's underlying assumptions provide the maximum crack width. w_{cal}.

4.2 Calculation of crack width

Depending on the steel strain ε_{s} $(\sigma_{\mathrm{s}}/E_{\mathrm{s}})$ the structure is in a crack formation stage when $\varepsilon_{\mathrm{s}} < \varepsilon_{\mathrm{s,cr}}$ and in the stabilized cracking stage, when $\varepsilon_{\mathrm{s,cr}} \leq \varepsilon_{\mathrm{s}} \leq \varepsilon_{\mathrm{s,y}}$ where:

$\varepsilon_{\mathrm{s,cr}}$ is the steel strain at cracking determined as $\varepsilon_{\mathrm{ctm}}(1+\xi)/\psi\xi$.
$\varepsilon_{\mathrm{ctm}}$ is the mean concrete tensile strain limit determined as $f_{\mathrm{ctm}}/E_{\mathrm{cm}}$
$\varepsilon_{\mathrm{s,y}}$ is the characteristic yielding strain for the reinforcement determined as $f_{\mathrm{yk}}/E_{\mathrm{s}}$.

The calculated surface crack width may be determined as:

$$w_{\mathrm{cal}} = S_{\mathrm{r}}(\varepsilon_{\mathrm{sm}} - \varepsilon_{\mathrm{cm}}) \tag{26}$$

Expressions for the transfer length S_{r} and the difference in mean strains $(\varepsilon_{\mathrm{sm}} - \varepsilon_{\mathrm{cm}})$ are calculated for the respective cracking regimes and are provided in the following subchapters. The parameters needed are given in Table 1 and the text below:

Table 1 Bond slip parameters

$\boldsymbol{\tau_{\max}}$	$\mathbf{5}\ \boldsymbol{MPa}$
$\boldsymbol{\beta}$	$1+\alpha$
$\boldsymbol{\alpha}$	0,35
$\boldsymbol{u_1}$	0,1 mm

ξ is the ratio $\alpha_{\mathrm{e}}\rho_{\mathrm{s,ef}}/\psi$.

ψ is a constant for the relation between mean concrete strains over the concrete cover height and concrete strains at the steel bar surface at an arbitrary section over the bar length and can be set as 0.7.

α_{e} is the modular ratio $E_{\mathrm{s}}/E_{\mathrm{cm}}$.

$\rho_{\mathrm{s,ef}}$ is the effective reinforcement ratio $A_{\mathrm{s}}/A_{\mathrm{c,ef}}$.

$A_{\mathrm{c,ef}}$ is the effective concrete in the RC-tie in tension defined in Figure 6

δ is a constant $(1-\alpha)/2$

ζ is a constant, taking into account the bond stress not being constant around the circumference of the rebar in nonaxisymmetric cases. A factor 1.0 can be used for practical application.

γ is the coefficient to account for the stress distribution around each rebar determined as

$$\gamma = \frac{\tau_{\max}\chi}{\beta {u_1}^{\alpha}} \tag{27}$$

χ is a constant to transform the cross-section to an equivalent cross-section and acknowledge that the bond stress is not uniformly distributed over the concrete cover.

$$\chi = \frac{\zeta \sum \pi\phi_{\mathrm{s}}}{A_{\mathrm{s}}E_{\mathrm{s}}}(1+\xi) \tag{28}$$

ϕ_{s} is the bar diameter as defined in FprEC2 [6]. For a section with n_1 bars of diameter ϕ_1 and n_2 bars of diameter ϕ_2, an equivalent bar diameter ϕ_{eq} according to formula (33a), should be used instead of ϕ_{s}. For bundled bars, an equivalent diameter ϕ_b can be used according to equation (33b).

$$\phi_{\mathrm{eq}} = \frac{n_1{\phi_1}^2 + n_2{\phi_2}^2}{n_1\phi_1 + n_2\phi_2} \tag{29a}$$

$$\phi_b = \phi_s\sqrt{n_i} \tag{33b}$$

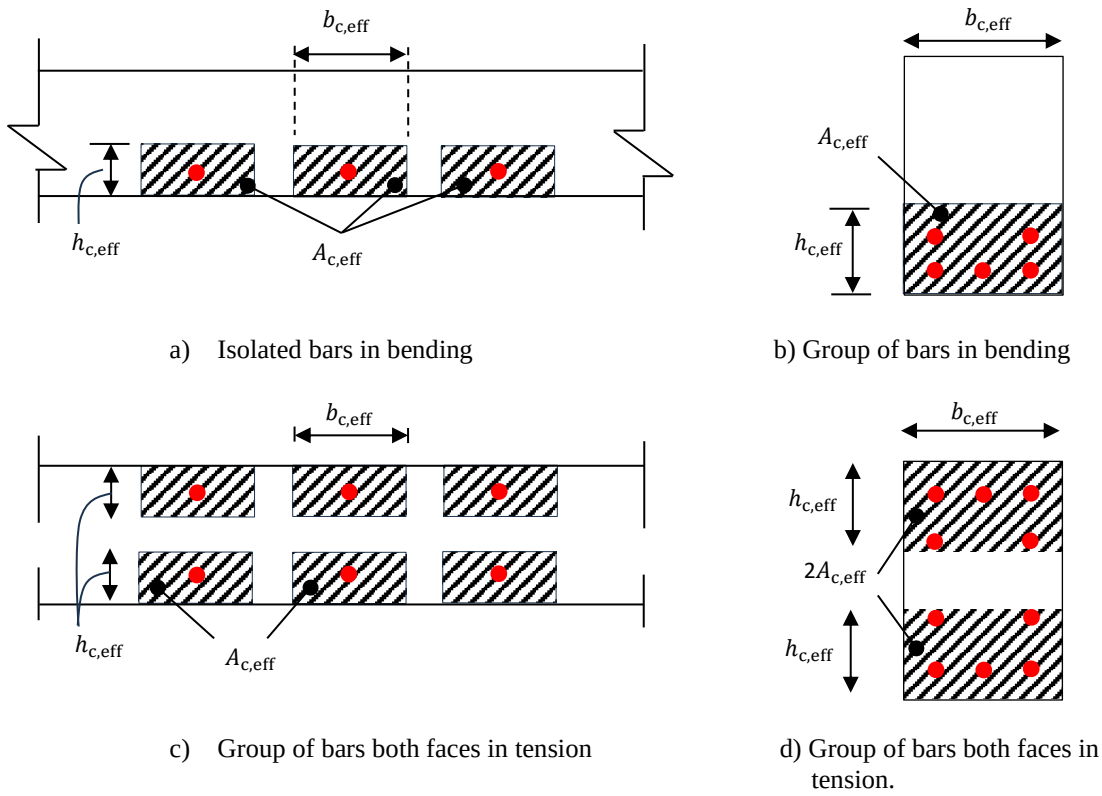

Figure 6 Effective tension area by SMTCM

According to Figure 6 a) and b), the effective height of the concrete area in tension is calculated as

$$h_{\mathrm{ef}} = min(2{,}5(h-d)\,;h-x\,) \tag{30}$$

And for Figure 6 c) and d)

$$h_{\mathrm{ef}} = min\left(2{,}5\left(c+\frac{\phi_{\mathrm{s}}}{2}\right)\,;\,\frac{h}{2}\right) \tag{31}$$

For Figure 6b) and d), the effective width of the tensile area is calculated as $b_{\mathrm{ef}} = b$ and Figure 6a) and c), the effective width of the tensile area is calculated as FprEC2 [6]:

$$b_{\mathrm{ef}} = min\left(c+\frac{\phi_{\mathrm{s}}}{2}+5\phi_{\mathrm{s}}\,;10\phi_{\mathrm{s}}\,;3{,}5\left(c+\frac{\phi_{\mathrm{s}}}{2}\right);cc\right) \tag{32}$$

Where cc is the rebar spacing

4.2.1 Crack formation stage

For cases where the steel strain at the crack $\varepsilon_{\mathrm{s}} < \varepsilon_{\mathrm{s,cr}}$ the transfer length is calculated as

$$S_{\mathrm{r}} = 2S_{\mathrm{r0}} = 2\frac{1}{\delta}\left[\varepsilon_{\mathrm{s}}\left(\frac{1}{2\gamma}\right)^{\frac{1}{2\delta}}\right]^{\frac{2\delta}{\beta}} \tag{33}$$

where the mean strains are calculated as

$$\varepsilon_{\mathrm{sm}} = \frac{1}{\frac{S_{\mathrm{r0}}}{2}}\frac{\xi\varepsilon_{\mathrm{s}}\frac{S_{\mathrm{r0}}}{2} + \left(\frac{\varepsilon_{\mathrm{s}}^2}{2\gamma}\right)^{\frac{1}{\beta}}}{1+\xi} \tag{34}$$

$$\varepsilon_{\mathrm{cm}} = \frac{\psi\xi}{\frac{S_{\mathrm{r0}}}{2}}\frac{\varepsilon_{\mathrm{s}}\frac{S_{\mathrm{r0}}}{2} - \left(\frac{\varepsilon_{\mathrm{s}}^2}{2\gamma}\right)^{\frac{1}{\beta}}}{1+\xi} \tag{35}$$

Note that the upper bound for the crack width in a crack formation stage is obtained when $\varepsilon_{\mathrm{s}} = \varepsilon_{\mathrm{s,cr}}$.

4.2.2 Stabilized cracking stage

For cases where $\varepsilon_{\mathrm{s,cr}} < \varepsilon_{\mathrm{s}} \leq \varepsilon_{\mathrm{s,y}}$ the transfer length is calculated as

$$S_{\mathrm{r}} = S_{\mathrm{cr0}} = \frac{1}{\delta}\left[\varepsilon_{\mathrm{s,cr}}\left(\frac{1}{2\gamma}\right)^{\frac{1}{2\delta}}\right]^{\frac{2\delta}{\beta}} \tag{36}$$

The mean steel strain is calculated as

$$\varepsilon_{\mathrm{sm}} = \frac{\varepsilon_{\mathrm{s}} - \varepsilon_{\mathrm{s,cr}}}{\left(\frac{\varepsilon_{\mathrm{s,y}} - \varepsilon_{\mathrm{s,cr}}}{\varepsilon_{\mathrm{sm,y}} - \varepsilon_{\mathrm{sm,cr}}}\right)} + \varepsilon_{\mathrm{sm,cr}} \tag{37}$$

While the mean concrete strains are taken as

$$\varepsilon_{\mathrm{cm}} = \frac{\psi\xi}{\frac{S_{\mathrm{cr0}}}{2}} \frac{\varepsilon_{\mathrm{s,S}} \frac{S_{\mathrm{cr0}}}{2} - \left(\frac{\varepsilon_{\mathrm{s,S}}^2}{2\gamma}\right)^{\frac{1}{\beta}}}{1+\xi} \tag{38}$$

where

$$\varepsilon_{\mathrm{s,S}} = (2\gamma)^{\frac{1}{2\delta}} \left(\frac{S_{\mathrm{cr0}}}{2}\delta\right)^{\frac{\beta}{2\delta}} \tag{39}$$

$$\varepsilon_{\mathrm{sm,cr}} = \frac{1}{S_{\mathrm{cr0}}} \frac{\xi\varepsilon_{\mathrm{s,cr}} S_{\mathrm{cr0}} + \left(\frac{\varepsilon_{\mathrm{s,cr}}^2}{2\gamma}\right)^{\frac{1}{\beta}}}{1+\xi} \tag{40}$$

$$\varepsilon_{\mathrm{sm,y}} = \frac{f_{\mathrm{s,y}}}{E_{\mathrm{s}}} - \varepsilon_{\mathrm{s,S}} + \varepsilon_{\mathrm{sm,S}} \tag{41}$$

$$\varepsilon_{\mathrm{sm,S}} = \frac{1}{\frac{S_{\mathrm{cr0}}}{2}} \frac{\xi\varepsilon_{\mathrm{s.S}} \frac{S_{\mathrm{cr0}}}{2} + \left(\frac{\varepsilon_{\mathrm{s,S}}^2}{2\gamma}\right)^{\frac{1}{\beta}}}{1+\xi} \tag{42}$$

Note that the crack width in a stabilized crack stage should never be less than the upper bound for the crack formation stage, i.e., $2S_{\mathrm{cr0}}\left(\varepsilon_{\mathrm{sm,cr}} - \varepsilon_{\mathrm{cm,cr}}\right)$ where the mean steel strain is calculated by equation (41) and the mean concrete strain by equation (43).

$$\varepsilon_{\mathrm{cm,cr}} = \frac{\psi\xi}{S_{\mathrm{cr0}}} \frac{\varepsilon_{\mathrm{s,cr}} S_{\mathrm{cr0}} - \left(\frac{\varepsilon_{\mathrm{s,cr}}^2}{2\gamma}\right)^{\frac{1}{\beta}}}{1+\xi} \tag{43}$$

4.3 Benchmarking

To benchmark the alternative crack width method SMTCM towards the more comprehensive MTCM, the experimental database by Terjesen et al. [1] was used. The model uncertainties representing the crack widths vs experimental crack widths calculated by the MTCM and SMTCM are shown in Table 2-Table 4 and visualized in Figure 7-9.

The first benchmarking is done against the database containing reinforced concrete (RC) beams provided by Terjesen et al. [1], and the results are shown in Table 2. The model uncertainty by predicted crack widths and the experiments (θ) is described by θ_{mean} and is 0.98 by MTCM and 1.0 by SMTCM, with an underestimated crack width in 43,3 and 47.8% of the cases. The scatter of the predicted and the experimental crack width expressed by the coefficient of variation (θ_{cov}) is slightly larger for the SMTCM ($\theta_{\text{cov}} = 0{,}283$) than for the MTCM ($\theta_{\text{cov}} = 0{,}278$). The model uncertainties are shown in Figure 7.

Table 2 Modelling uncertainty of calculated crack widths vs experimental result

Model	$\boldsymbol{\theta}_{\text{mean}}$	$\boldsymbol{\theta}_{\text{var}}$	$\boldsymbol{\theta}_{\text{SD}}$	$\boldsymbol{\theta}_{\text{COV}}$	$\boldsymbol{\theta}_{\text{min}}$	$\boldsymbol{\theta}_{\text{max}}$	***n*(θ>1)**	**(θ>1) %**
SMTCM	1,00	0,077	0,283	0,283	0,375	2,326	107	47,8 %
MTCM*	0,98	0,075	0,278	0,278	0,433	2,187	98	43,3 %
EC2*	1,27	0,080	0,369	0,290	0,598	4,794	178	79,5 %
FprEC2*	1,40	0,069	0,374	0,266	0,746	3,605	194	86,6 %
MC2010*	1,10	0,074	0,304	0,277	0,439	2,734	128	57,1 %
MC2020*	1,36	0,064	0,349	0,257	0,651	3,359	191	85,3 %
DIN*	1,69	0,116	0,592	0,350	0,586	4,522	213	95,1 %

** Modelling uncertainties by the MTCM and design codes are given in Terjesen et al. [1] Table 3(c)*

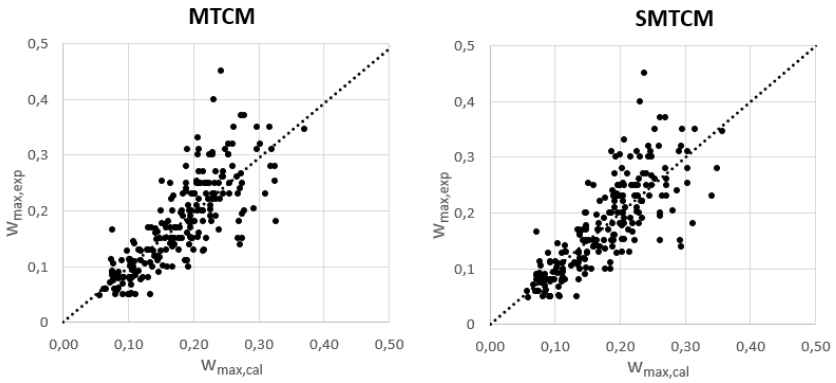

Figure 7 Modelling uncertainties from Table 2 with the dotted line as the mean value

The second benchmarking is done against the database containing RC tension ties provided by Terjesen et al. [1], and the results are shown in Table 3. The model uncertainty by predicted crack widths and the experiments (θ) is described by θ_{mean} and is 0.92 by MTCM and 0.95 by SMTCM, with an underestimated crack width in 26.2 and 27.9% of the cases. The scatter of the predicted and the experimental crack width expressed by the coefficient of variation (θ_{cov}) is slightly larger for the SMTCM ($\theta_{\text{cov}} = 0{,}425$) than for the MTCM ($\theta_{\text{cov}} = 0{,}405$). The model uncertainties are shown in Figure 8.

Table 3 Modelling uncertainty – RC ties in tension (61 data points, $\sigma_s \leq 300$ MPa)

Model	θ_{mean}	θ_{var}	θ_{SD}	θ_{COV}	θ_{min}	θ_{max}	$n(\theta>1)$	$(\theta>1)$ %
SMTCM	0,95	0,166	0,404	0,425	0,17	2,14	17	27,9 %
MTCM*	0,92	0,152	0,372	0,405	0,17	2,04	16	26,2 %
EC2*	0,73	0,153	0,298	0,406	0,10	1,61	2	3,3 %
FprEC2*	1,07	0,106	0,358	0,335	0,23	2,32	31	50,8 %
MC2010*	1,01	0,124	0,368	0,363	0,20	2,57	25	41,0 %
MC2020*	1,08	0,119	0,386	0,356	0,23	2,99	31	50,8 %
DIN*	1,17	0,144	0,459	0,394	0,19	2,28	38	62,3 %

** Modelling uncertainties by the MTCM and design codes are given in Terjesen et al. [1] Table 4(b)*

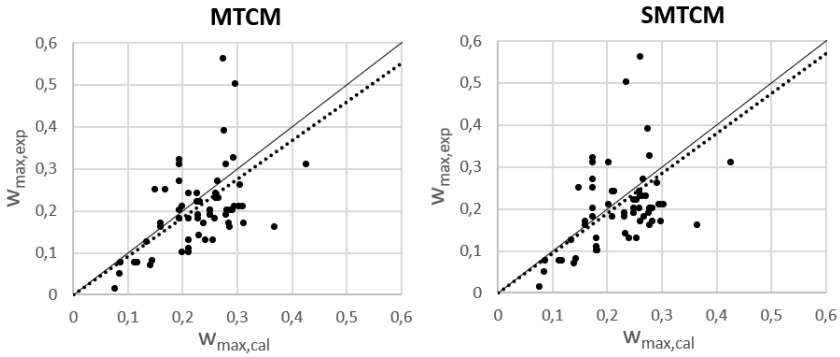

Figure 8 Modelling uncertainties from Table 3 with dotted line as mean and solid line as 1 to 1

The third benchmarking is done against the database, including experimental tests of slabs in bending provided by Terjesen et al. [1], and the results are shown in Table 4. The model uncertainty by predicted crack widths and the experiments (θ) is described by θ_{mean} and is 0.82 by MTCM and 0.92 by SMTCM, with an underestimated crack width in 18.9 and 40.0 % of the cases. The scatter of the predicted and the experimental crack width expressed by the coefficient of variation (θ_{cov}) is smaller for the SMTCM ($\theta_{\text{cov}} = 0{,}3$) than for the MTCM ($\theta_{\text{cov}} = 0{,}365$). These changes are graphically illustrated in Figure 8.

Table 4 Modelling uncertainty – (90 data points, results included if $\sigma_{sr} \leq$ 300 MPa and $w_{mean.exp} \leq S_{mean}\varepsilon_{sr}$)

Model	θ_{mean}	θ_{var}	θ_{SD}	θ_{COV}	θ_{min}	θ_{max}	$n(\theta>1)$	$(\theta>1)$ %
SMTCM	0,94	0,112	0,282	0,300	0,28	1,60	36	40,0 %
MTCM*	0,82	0,125	0,299	0,365	0,21	1,37	17	18,9 %
EC2*	1,54	0,197	0,719	0,467	0,32	2,90	72	80,0 %
prEC2*	1,35	0,176	0,592	0,439	0,30	2,55	68	75,6 %
MC2010*	1,05	0,160	0,436	0,416	0,29	1,92	47	52,2 %
MC2020*	1,59	0,186	0,721	0,452	0,34	3,19	77	85,6 %
DIN*	1,41	0,248	0,749	0,530	0,25	3,25	59	65,6 %

** Modelling uncertainties by the MTCM and the design codes are given in Terjesen et al. [1] Table 5(b)*

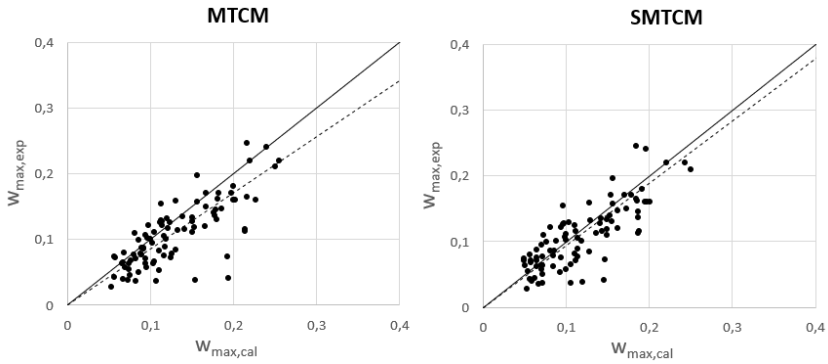

Figure 9 Modelling uncertainty from Table 4 with dotted line as mean and solid line as 1 to 1

4.3.1 The difference in crack widths between MTCM and SMTCM

The linear interpolation of strains by SMTCM, as shown in Figure 5, yields a discrepancy in the calculated crack width for a small interval in the case of the stabilized cracking stage, as shown in Figure 10. This difference can be attributed to the fact that i) there is a difference in solutions to the equations for CHLM and SCHLM and ii) the MTCM allows for a new crack to form at the symmetry section even in the case of CHLM, meaning that the member length for this condition becomes $L = S_{\mathrm{cr0}}/2$. So although both MTCM and SMTCM provide similar transfer lengths, the discrepancy in crack widths is owing to the slight difference in tension stiffening for CHLM and SCHLM, at which SCHLM tends to predict a certain mean behaviour of the CHLM, see Figure 5 and Figure 10.

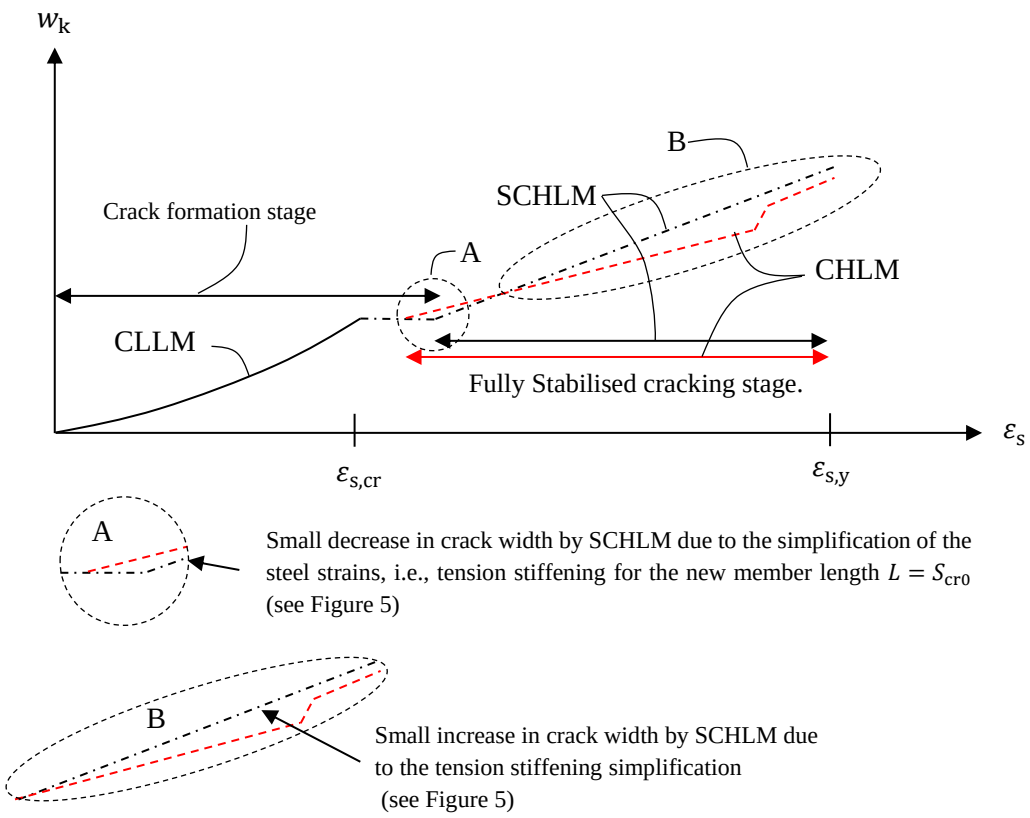

Figure 10 Design crack width vs steel strain illustrated for CLLM, CHLM, and SCHLM at one crack location along an RC member.

5 Experimental studies of RC-ties

5.1 Geometry, material properties and test setup of RC-ties

Tan et al. [20] tested eight 3m long RC-ties with a square cross-section (400x400 mm) reinforced with eight deformed steel bars in axial tension. The bar diameter was either 20 or 32 mm, while the cover was 40 or 90 mm; thus, four alternative reinforcement solutions presented in Table 5 were tested. Chavin et al. [21] tested RC-ties with three alternative square cross-sections reinforced with a central deformed steel bar with a diameter of 16 mm and 40, 60 and 80mm cover, as shown in Table 5. These RC ties were also pulled in axial tension and had a length of 0,65m.

The motivation for including the two experimental series in this paper is twofold. First of all, they are included to verify the SMTCM, considering the crack widths recorded at the concrete surfaces. Secondly, both investigations include crack width profiles accurately recorded over the cover thickness, although the crack width profiles from

Tan et al. [20] have not previously been published. These results establish and enlighten a basis for a discussion and an evaluation of the relevance of large concrete covers and crack width limitations at the concrete surface to achieve good durability, as other researchers have [9, 22-26].

Table 5 Geometrical properties in millimetres for the investigated RC-ties

Author	Specimen	Rebar size	Number of rebars	Cover	Height	Width	Member length
Chavin et al.	R-c40	16	1	40	96	96	650
	R-c60			60	136	136	
	R-c80			80	176	176	
Tan et al.	F-20-c40	20	8	40	400	400	2000
	S-20-c40						
	F-32-c40	32					
	S-32-c40						
	F-20-c90	20		90			
	S-20-c90						
	F-32-c90	32					
	S-32-c90						

SR-c40	**SR-c60**	**SR-c80**
	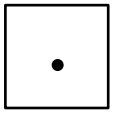	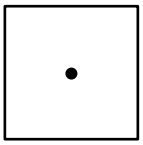

F/S-20c40	**F/S-20c90**	**F/S-32c40**	**F/S-32-c90**
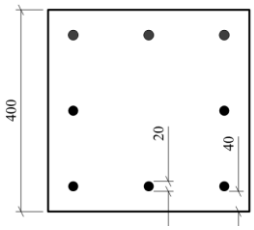	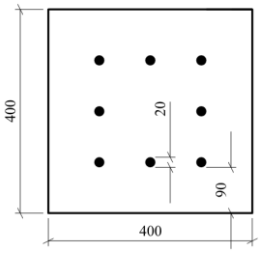	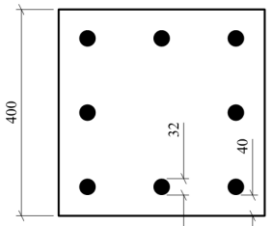	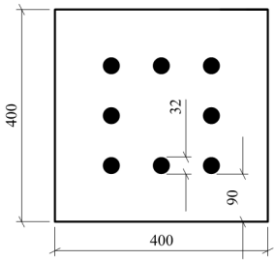

Table 6 Material properties for the investigated RC-ties

Author	Specimen	f_{ctm} $[MPa$	E_c $[MPa]$	E_s $[MPa]$	A_s $[mm^2]$
Chavin et al.	R.40.1	2,2	30000	200000	201
	R.40.2				
	R.60.1				
	R.60.2				
	R.80.1				
Tan et al.	F-20-c40	4,14	27400	200000	2512
	S-20-c40				
	F-32-c40				6431
	S-32-c40				
	F-20-c90				2512
	S-20-c90				
	F-32-c90				6431
	S-32-c90				

5.2 Measuring technique using image analysis

For the investigated cracks from Tan et al. [20], three sides of the RC-ties were closed with a putty compound before a slow-hardening sealant epoxy resin was poured at the top and placed in a bath, as shown in Figure 11. After 12 hours, the specimens were unloaded.

Figure 11 Injection of epoxy-resin for RC-tie S-20-c40, 320MPa (Beam ID no. 5)

In both experimental series [20, 21], both an average crack width representing the whole crack at one side of the specimens and the crack width variation along cracks using steps of one millimetre were recorded. In both cases, the performance of the measurements consisted of three main parts:

1. Crack image acquisition using a digital camera [20, 21].
2. Image processing with the image analysis open-source software Fiji (ImageJ) to describe the crack [20, 21].
3. Crack width determination using image analysis of the crack [20].

In the RC-tie tests by Tan et al. [20], a Digital Single Lens Reflex camera model, Canon 60D with a 50 mm f2.5 macro lens, was applied. The camera shooting mode was set to manual. Two external flashes were used for cracks located on the large specimens, and an ultraviolet (UV) light source was used for the epoxy-impregnated cracks. The lens focus was turned to the closest possible distance in manual mode (approximately 10 cm

from crack to lens surface); therefore, the focusing was done by moving the camera closer or further away from the focusing plane. The specimens were painted white before the test to contrast the crack images better. The printed scale was glued on the specimen beside the crack, as shown in Figure 12 (a), to determine the ratio of the image size in millimetres to the image size in pixels. The image processing by the open-source software Fiji (ImageJ) applied for both Tan et al. [20] and Chavin et al. [21] consisted of two main steps: setting the scale of the image and creating a binary image of the crack. The image scale was determined by selecting the distance between two horizontal lines of the scale bar shown in Figure 12(a) and specifying the known distance in millimetres. The program then automatically calculated the pixel-to-millimetre ratio. After setting the scale, the crack's binary image (in black and white) was produced, as shown in Figure 12 (b). Determining the crack width and the variation along the whole crack length visible in the image (i.e., part of the crack that fits in the camera's field of view) was done by measuring the area and perimeter of the crack.

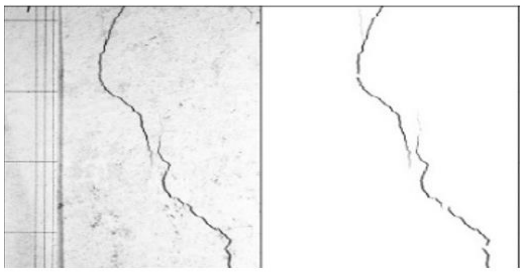

(a) (b)

Figure 12 (a) Crack width image with a scale bar, (b) Binary image of the crack

5.3 Mapped crack width locations

The measured crack width variation over the cover thickness at three locations, as shown in Figure 13, and the specific cracks investigated are presented in Table 7. Further description of the cracks and their location along the surface of the RC members can be found in [27].

Table 7 RC-ties injected with epoxy-resin

Beam ID number	Specimen	Sealed crack numbers	Loading at crack sealing [kN]	Steel stress [MPa]
1	F-20-c90	IV and V	580	231
2	S-20-c90	II & V	1000	400
3	S-32c90	I & V	1360	212
4	F-32-c90	III & V	800	125
5	S-20-c40	IX & V	750	298
6	F-20-c40	Not mapped		
7	F-32-c40			
8	S-32-c40			

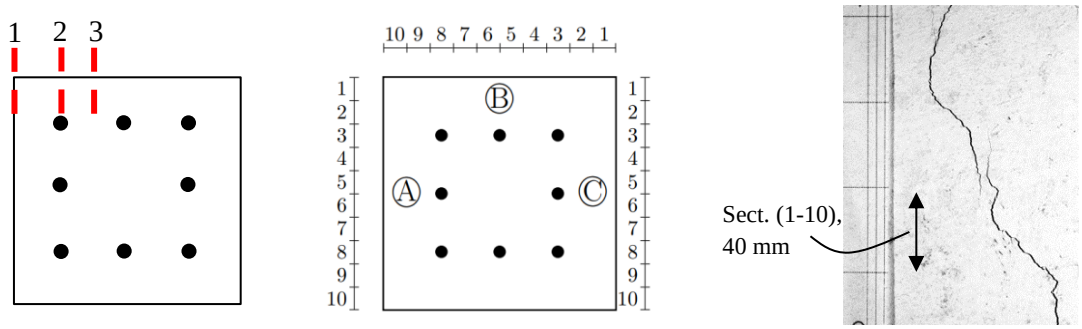

(a) (b) (c)

1. Concrete surface
2. Sawn section with reinforcement bar
3. Sawn section between bars

Figure 13 (a) Location of crack width profiles (b-c) Crack width readings for the formed cracks were averaged over 40 mm due to the inhomogeneous propagation of cracks.

Chavin et al. measured the crack width variation over the cover thickness at locations representing the situation at point 2 in Figure 13 (a), and in detail, the crack width readings were taken over the sawn sections, as shown in Figure 14.

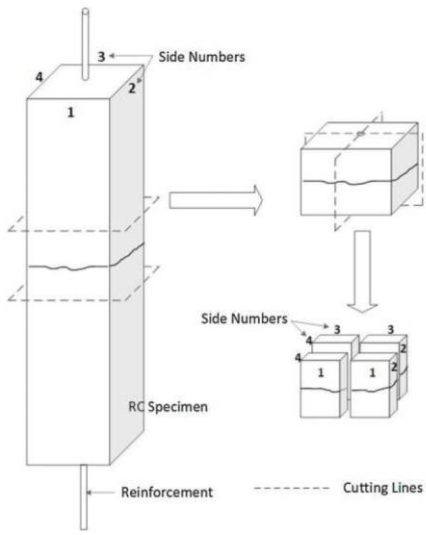

Figure 14 RC ties by Chavin et al. [21] cut to observe the crack width distribution over the concrete cover thickness.

5.4 Calculated surface crack widths versus experimental

The experimentally determined surface crack widths from the RC-ties were compared to crack widths predicted by EC2, FprEC2 [5, 6], MC2010 [7], MTCM, and finally, SMTCM proposed in this paper. For MTCM and SMTCM, the effective concrete area in tension was calculated as:

$$A_{\mathrm{c,ef}} = \min\left\{2h_{\mathrm{c,ef}}b_{\mathrm{c,ef}}\,;A_{\mathrm{c}}\right\} \tag{44}$$

where $h_{\mathrm{c,ef}}$ and $b_{\mathrm{c,ef}}$ were determined according to Figure 6 and Equations 31-32.

The experimental crack widths of the investigated RC-ties are shown in Table 8. The experimental crack widths from Chavin et al. [12] were reported at the sawn surfaces, as shown in Figure 14, and the maximum crack width in Table 8 is the average of these four measuring points at the concrete surface. From the results by Tan et al. [20], the reported maximum crack width is calculated by statistical methods using a log-normal distribution according to a detailed description given in [27]. The table also shows the crack widths predicted by the models. The results are depicted in Figure 15, where it can be seen that, generally, for large cover sizes, EC2, FprEC2, DIN, and MC2010 overestimate the crack width at the surface quite extensively. Still, it is interesting that the new edition of FprEC2 is an improvement compared to the current version of EC2. In contrast, both MTCM and SMTCM yield more consistent crack width predictions.

Table 8 Experimental and predicted crack width of the specimens

Specimens	ρ_{ef} [%]	Load (σ_s) [MPa]	Experimental	Maximum crack width [mm]					
				MTCM	SMTCM	DIN	EC2	FprEC2	MC2010
R.40.1	2,18	397	0,40	0,41	0,41	0,46	0,82	0,55	0,61
R.40.2			0,45						
R.60.1	1,09		0,69	0,45	0,52	0,84	1,29	0,85	0,97
R.60.2			0,68						
R.80.1	0,65		0,78	0,51	0,50	1,22	1,66	1,09	1,20
F-20-c40	2,51	200	0,13	0,24	0,24	0,16	0,24	0,18	0,15
S-20-c40		207	0,13	0,25	0,25	0,17	0,25	0,22	0,16
		265	0,16	0,29	0,27	0,25	0,32	0,28	0,21
		321	0,22	0,37	0,39	0,33	0,41	0,34	0,32
F-32-c40	5,74	117	0,08	0,13	0,13	0,07	0,11	0,10	0,07
S-32-c40		115	0,07	0,13	0,13	0,07	0,11	0,09	0,06
		157	0,10	0,16	0,16	0,11	0,16	0,13	0,12
F-20-c90	1,57	233	0,21	0,30	0,30	0,22	0,52	0,35	0,25
S-20-c90		228	0,21	0,29	0,29	0,21	0,51	0,34	0,24
		293	0,31	0,43	0,43	0,31	0,65	0,44	0,31
		399	0,4	0,56	0,59	0,50	0,88	0,60	0,59
F-32-c90	4,02	125	0,16	0,16	0,16	0,08	0,22	0,15	0,10
S-32-c90		125	0,17	0,16	0,16	0,08	0,22	0,15	0,10
		156	0,21	0,20	0,20	0,11	0,27	0,19	0,15
		187	0,24	0,23	0,21	0,15	0,32	0,22	0,21
		212	0,27	0,27	0,27	0,18	0,38	0,26	0,26

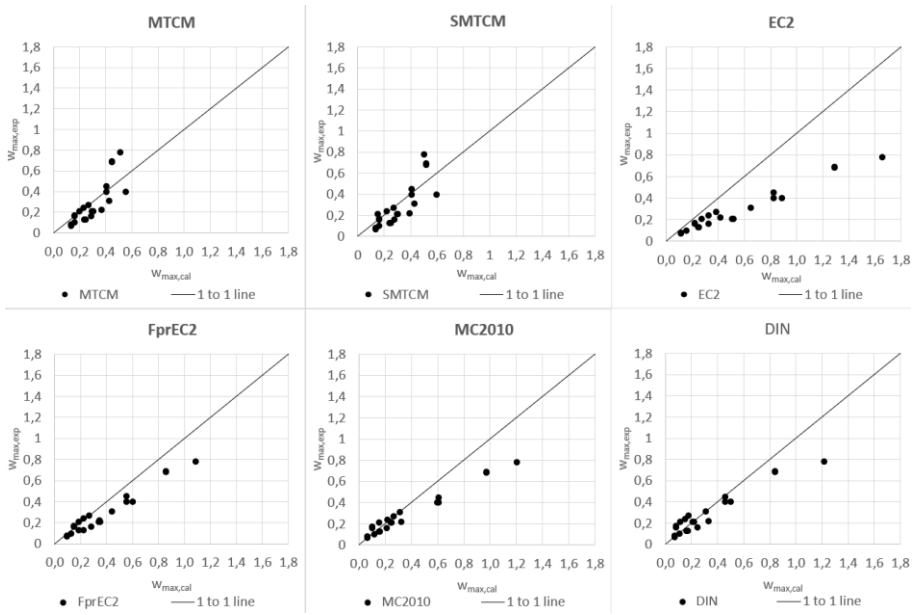

Figure 15 Experimental crack width vs predicted crack widths from Table 8

5.5 Crack width profiles

The crack width variation over the concrete cover thickness was recorded by Tan et al. [28] in an investigation of five RC ties and ten crack width locations along each RC member, as presented in Table 7 and identified by the system depicted in Figure 16. As

an example, the results for two crack locations from RC-tie F-20c90 can be seen in Figure 17. The crack profiles show that the crack widths recorded at the concrete surface represent the crack width profile between the reinforcing bars reasonably well; therefore, the surface crack widths are suitable for tightness requirements. On the other hand, it is interesting to see that the crack width profile towards the reinforcement significantly differs from the crack widths at the surface. This is further considered in the following.

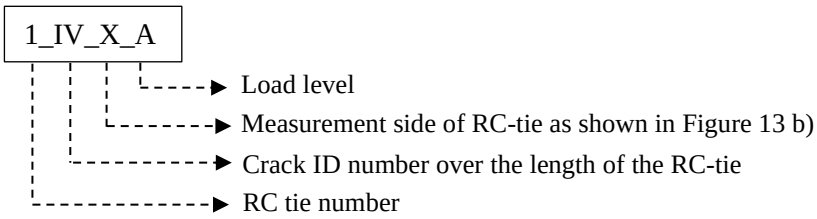

Figure 16 Identification of the cut surfaces from RC-ties by Tan et al. [20].

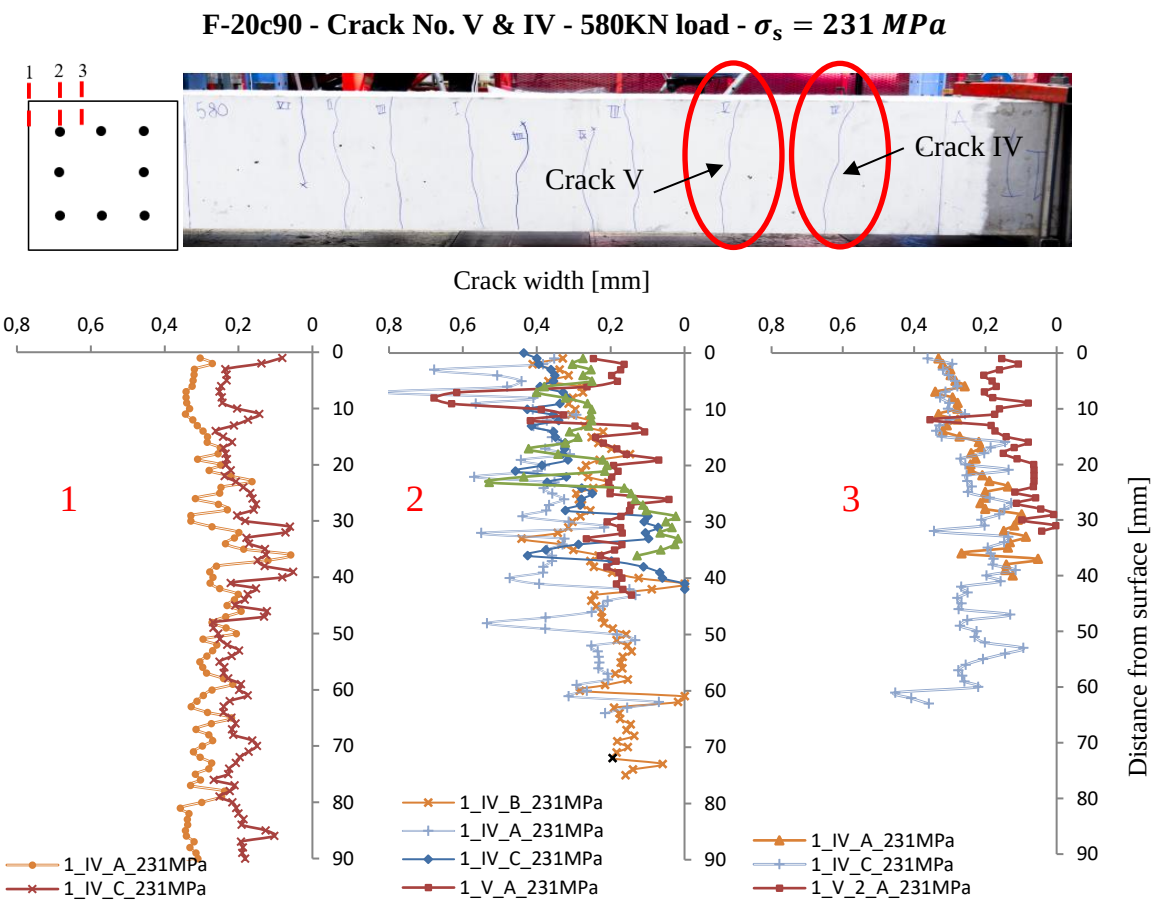

Figure 17 Measured crack width profiles of RC-tie F-20c90 at 233 MPa for crack no. V & IV.

5.5.1 Effect of rebar diameter

The results in Figure 18 show the average recorded crack widths from a total of 13 cuts and eight crack numbers over the cover depth towards the reinforcement, as depicted by cut plane 3 in Figure 13a. The Figure includes reinforcing bars ø20 and ø32 with 90mm cover at different stress levels. The steel stress required for the detectable crack profile to reach the reinforcement with a 20mm rebar is between 233 and 400MPa. In contrast, for a 32mm rebar, the steel stress needed for the crack to reach the reinforcement is between 125 and 212 MPa. This indicates that small bars might be less vulnerable to the ingress of harmful substances and cracking than large bars. This statement might deviate from the common understanding and might be important for corrosion protection.

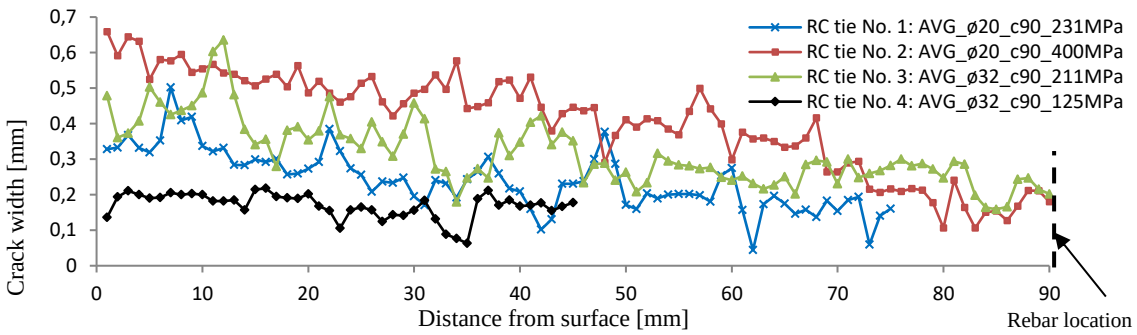

Figure 18 Averaged crack width variation over the cover depth of 90 mm for identical RC-ties with different stress levels, rebar sizes, and reinforcement ratios.

5.5.2 Effect of cover size

The effect of cover size on the crack width profile over the cover thickness can be seen in Figure 19 for reinforcing bars ø20. It is seen from the figure that both the crack width profile and the crack width near the reinforcement strongly depend on cover size. The average crack width at the surface for cover size 40 mm with steel stress 298 MPa is 0,23 mm with a detectable crack profile that reaches the reinforcement. For a cover size of 90 mm and steel stress of 231 MPa, the average crack width at the surface is 0.34 mm, but the detectable crack profile does not reach the reinforcement. In contrast, if the steel stress is increased to 400 MPa, the crack width does reach the reinforcement.

Figure 19 shows that it is difficult to directly relate the crack width at the surface of the concrete to the crack width profile close to the reinforcement, which is essential concerning the effect of cracks on the ingress of harmful substances and, therefore, the structural RC member's durability. The results indicate that large concrete covers give

good protection against the ingress of harmful substances, even for large crack widths at the surface.

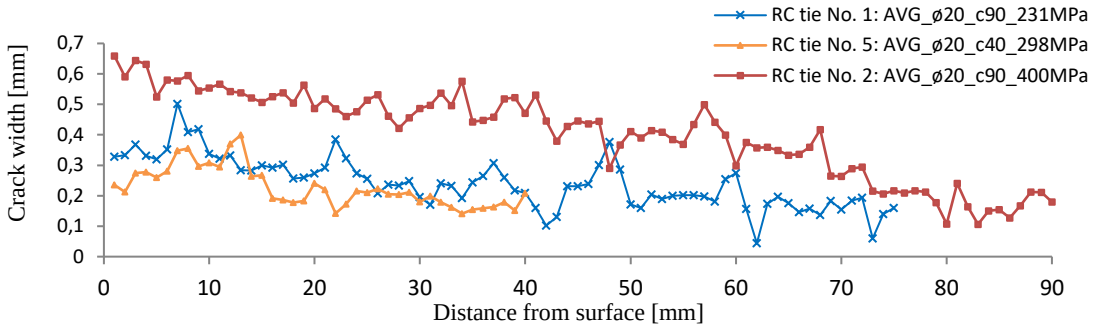

Figure 19 Averaged crack width variation over the cover depth for identical RC ties with rebar size of 20mm and covers of 40 and 90mm.

6 Discussion

6.1 Location of the predicted crack width

According to the design codes, the calculated crack width usually refers to the outermost concrete surface or at the reinforcement level but still at the concrete surface. All the crack models use an assumed effective concrete area in tension for special structures like bridge decks, shell structures, and regular and retaining walls. These effective cross-sections are treated like RC ties in bending or pure tension for the predicted crack widths, as shown in Terjesen et al. [1]. However, for these types of structures, the effective area might be asymmetrical and relating a crack width to a particular direction is, in a design code format, a calibration of the models to typical cross-sections tested in typical laboratory conditions. To highlight this effect, two effective cross-sections in tension ($A_{\mathrm{c,ef}}$) are shown in Figure 20. The RC-tie shown in Figure 20a will, according to EC2, FprEC2 and MC2010, give a crack width without influence on which surface the crack width refers to ($w_{\mathrm{k1}} = w_{\mathrm{k2}}$). On the other hand, Figure 20b, will give a different crack width at the two surfaces $w_{\mathrm{k1}}$and w_{k2} due to the cover term in the crack spacing formulas. In contrast, MTCM, SMTCM and DIN determine a crack width ($w_{\mathrm{k,eq}}$) at the surface of the equivalent effective concrete area in tension; however, it is also often measured on a physical surface. Tension Chord Models generally yield a representative crack width over the surface of the effective tensile area, which cannot always be directly related to a measured crack width at the surface, as shown in Terjesen et al. [1].

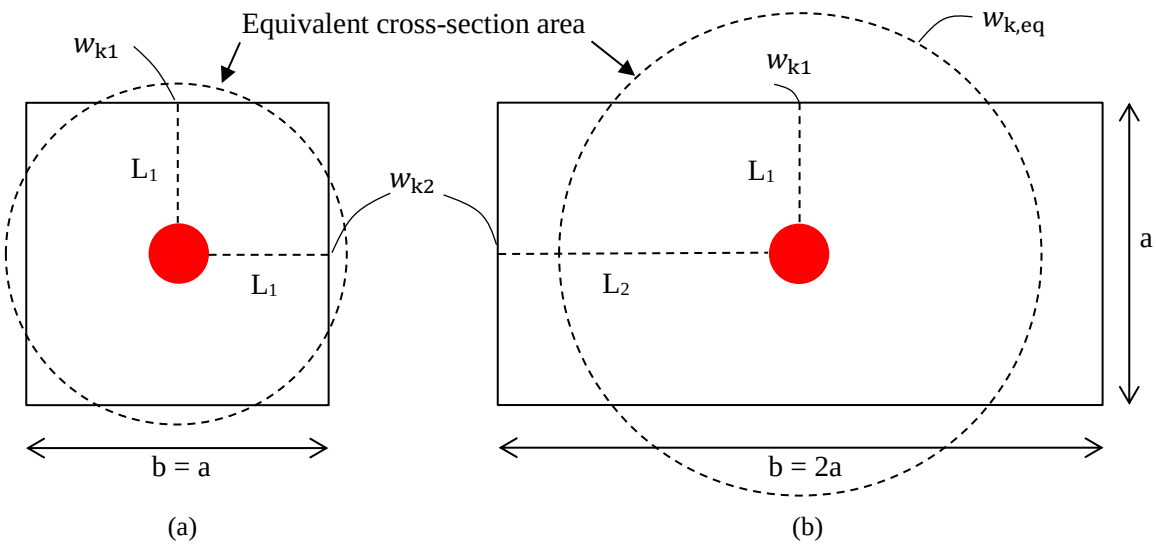

$E_{cm} = 30GPa$, $E_s = 200GPa$ $\phi_s = 20mm$, a=100mm, $L_1 = 40mm$, $L_2 = 90mm$, $f_{ctm} = 3{,}5\ MPa$

Figure 20 Geometry and material properties for two parametric effective concrete areas in tension

The crack width w_{k2} for Figure 20b is larger than w_{k1} due to the cover addition in the crack spacing formulas applied by EC2, FprEC2 and MC2010. In contrast, the mechanical models MTCM, SMTCM and DIN do not have any empirical adjustment of the crack width by the concrete cover and the increase in crack width is only due to the increased effective concrete area in tension.

Considering the geometry of the effective area in tension, there might be a significant difference between the measured values of w_{k1} and w_{k2} however, as the results in Figure 18-19 show, the crack width profile would also differ from the surface to the reinforcement location. For this reason, the authors believe that using empirical modifications to predict the largest surface crack in a certain direction is only a calibration of the models to represent specific cross-sections often applied in typical laboratory experiments and are therefore not always representative of large cross-sections in real structures like bridge decks, large columns or walls.

6.2 Physical interpretation of the SMTCM

The experimentally recorded crack pattern for RC-tie S-32c90 [27] is depicted in Figure 21, while some of the crack parameters applied by SMTCM are given in Table 9. The cracking load, according to [29], can be described as:

$$F_{cr,0} = 0{,}7 f_{ctm} A_c (1 + \alpha_E \rho_s) \tag{45}$$

In the experiment, the first crack occurred relatively close to when the concrete stresses reached the assumed lower limit of the tensile strength of the concrete ($f_{\mathrm{ctk,0.05}} = 0.7 f_{\mathrm{ctm}}$). Furthermore, the cracks occurred in the sequence of their numbering in Figure 21a, thus illustrating the crack formation stage.

Table 9 The parameters needed to describe the CLLM behaviour of the SMTCM

RC-member	$\boldsymbol{\varepsilon_{\mathrm{s,cr}}}$ **(Eq. 5)**	$\boldsymbol{\sigma_{\mathrm{s,cr}} = \varepsilon_{\mathrm{s,cr}} E_{\mathrm{s}}}$	$\boldsymbol{F_{\mathrm{cr,1}} = \sigma_{\mathrm{s,cr}} A_{\mathrm{s}}}$	$\boldsymbol{F_{\mathrm{cr,0}}}$
S-32c90	7,236*10^{-4}	145 MPa	932 kN	594 kN

$\boldsymbol{\varepsilon_{\mathrm{sr,cr}}}$ = Calculated steel strain needed to reach a stabilized cracking stage
$\boldsymbol{F_{\mathrm{cr,1}}}$ = Calculated steel force needed to reach a stabilized cracking stage
$\boldsymbol{F_{\mathrm{cr,0}}}$ = Calculated steel force needed to create the first crack

The force level above which the stabilized crack stage prevails ($F_{\mathrm{cr,1}}$) illustrated in Figure 21 (b-d) is determined based on the condition that the concrete tensile stresses along the member can nowhere be greater than the concrete tensile strength. Beyond this load level, the member stiffness is dominated by the opening of existing cracks, and the SCHLM behaviour is governing. The physical interpretations of these interactions were previously shown in Figure 1.

The crack spacings shown in Figure 21 are values determined from photos from the testing [27]. The numbering of the cracks shown in Figure 21a indicates the crack formation sequence, and for this load level (F = 805 kN), the two cracks (No. II and IV) can be considered to be in the CLLM stage according to the MTCM and SMTCM. This means that the concrete strains over the transfer length have not exceeded the concrete's tensile strength. In contrast, the crack numbers V, I, VI, and III can be considered to be in the CHLM stage.

$F = 805\ kN\ (\sigma_s = 125\ MPa) < F_{\mathrm{cr},1} = 932kN$

$w_{\mathrm{k,exp}} = 0{,}17\ mm,\ w_{\mathrm{k,SMTCM}} = 0{,}16\ mm\ ,\ S_{\mathrm{r0}} = 335\ mm,\ \ S_{\mathrm{cr0}} = 360mm$

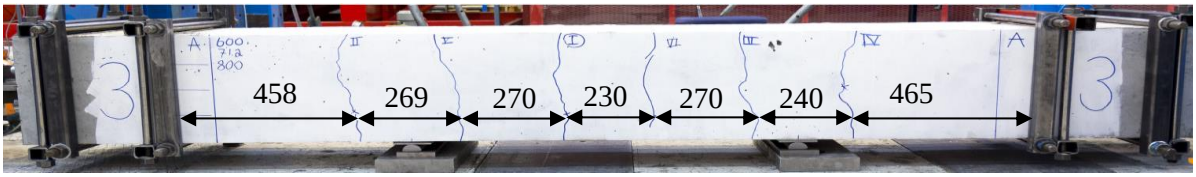

(a) Crack formation stage

$F = 1004\ kN\ (\sigma_s = 156\ MPa) > F_{\mathrm{cr},1} = 932\ kN$

$w_{\mathrm{k,exp}} = 0{,}21\ mm,\ w_{\mathrm{k,MTCM}} = 0{,}20\ mm,\ w_{\mathrm{k,SMTCM}} = 0{,}20\ mm,\ S_{\mathrm{cr0}} = 360\ mm$

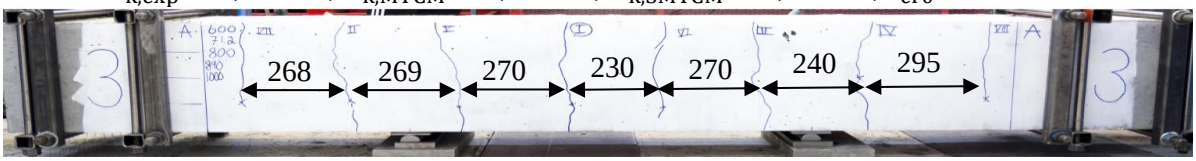

(b) Stabilized crack stage

$F = 1363\ kN\ (\sigma_s = 212\ MPa) > F_{\mathrm{cr},1} = 932kN$

$w_{\mathrm{k,exp}} = 0{,}27\ mm,\ w_{\mathrm{k,MTCM}} = 0{,}27\ mm,\ w_{\mathrm{k,SMTCM}} = 0{,}27\ mm,\ S_{\mathrm{cr0}} = 360\ mm$

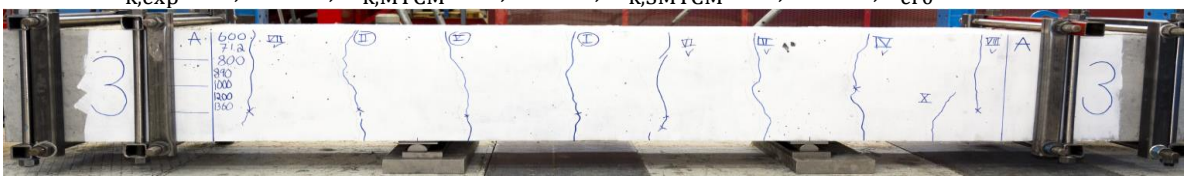

(c) Stabilized crack stage

Figure 21 Crack widths and patterns for RC-tie S-32c90 with values calculated by MTCM and SMTCM.

As shown in Figure 21b, the applied reinforcement force (F = 1004 kN) is now larger than $F_{cr,1}$ and the member stiffness is now dominated by the opening of existing cracks, i.e., the SCHLM behaviour is governing. However, in a design setting for this loading, the CHLM- and SCHLM stages predicted crack widths smaller than predicted by the CLLM behaviour, which becomes governing. This is due to the recent opening of Crack No. VII and VIII, and therefore, the design crack width is still found by CLLM behaviour at the formation of a nearby crack, as shown in Figure 10. For the last load levels in Figure 21 (c), the entire member is now in a fully stabilized crack stage, where only the opening of the existing cracks influences the maximum crack width, which is decided based on the new member length (S_{cr0}).

6.3 Main differences in mechanical formulation

The main differences in mechanical formulation between the semi-empirical formulations in EC2, MC2010, DIN, prEC2 and MTCM/SMTCM are now discussed and elucidated. These are:

1. The semi-empirical formulations assume a constant mean bond-stress distribution over the transfer length. For the MTCM/SMTCM, however, the bond-stress distribution and the corresponding mean bond stress over the transfer lengths vary as a function of the steel stress level, geometry and material parameters of the RC tie both in the CLLM and CHLM stage. The bond stress distribution in determining the transfer length in both formulations and assuming constant bond stress distribution independent of the load level is inconsistent, as Tan et al. proved [16, 18]. This mechanical inconsistency looks to be one of the main reasons for the need to calibrate the semi-empirical formulas continuously to cover a broader range of applications.
2. The MTCM/SMTCM provides a transient formulation of the transfer length in the CLLM stage. This means that the transfer length becomes explicitly dependent on the steel stress level, which was proven by the experimental observations in the previous subchapters. This is not the case for the semi-empirical formulas, which only distinguish the crack formation stage and the stabilized cracking stage using a lower bound for the difference in mean strains for steel and concrete. In particular, this is important when designing for crack widths due to restraint deformations in combination with static loads. Assuming a constant transfer length when considering the deformation compatibility is mechanically inconsistent and will not capture the behaviour correctly when the cracked member is expected to remain in the crack formation stage, which could potentially cause a considerable underestimation of the crack widths for such cases.

Given i) these differences in mechanical behaviour and ii) the fact that the SMTCM provides accurate crack width predictions without any empirical calibration towards any experimental database, it suggests that it provides a broader range of applicability than the semi-empirical formulations.

7 Conclusion

The Simplified Modified Tension Chord Model (SMTCM) is proposed and evaluated as an analytical code-type format model for crack width calculation. The SMTCM is based on the previously published MTCM and founded on a mechanical basis, and, in contrast to the design codes investigated in the previous paper, it contains no empirical modifications. The proposed model is compared to the crack widths recorded at the surface of the experimental specimens. In addition, several experimental crack width profiles over the cover thickness are shown, and the effects of large covers and bar diameters are discussed. Based on this, the following conclusions may be drawn:

1. The comprehensive MTCM has been simplified to SMTCM in a design code format for practical application for design purposes. The SMTCM offers closed-form analytical solutions and is structured so that hand calculations can be applied, in contrast to the MTCM. In addition, there are no openings for ambiguous interpretations of the calculations, which can increase the risk of obtaining two different crack widths from two different designers, e.g., so-called good or poor bond conditions (k_{b}) in FprEC2, which might be inconvenient during the design stage. In most practical cases, the crack width calculations are performed in a postprocessing software tool where the developers must interpret the formulas. This ambiguity often causes different predictions of crack widths for different software tools, which should not be the case.
2. It has been shown that, in general, SMTCM predicts crack widths quite accurately as the MTCM, which has previously been proven by Terjesen et al. [1] to yield more accurate crack width predictions than the investigated design codes.
3. Generally, for RC-ties, EC2, FprEC2, DIN, and MC2010 overestimate the crack width at the surface quite extensively for large cover sizes. The new edition of FprEC2 is an improvement compared to the current version of EC2.
4. This paper's experimental crack width profiles show that the crack width at the outermost concrete surface and the reinforcement differ significantly depending on the rebar diameter and the size of the concrete cover.
5. Concerning the durability of RC structures, the crack width calculated by the SMTCM or any other tension chord model should not be stated as a design crack width that can be measured on the concrete surface but rather as a representative design crack width over the effective concrete tension area.

6. The mechanical differences between the SMTCM and the design codes and the fact that it provides accurate crack width predictions without any empirical calibrations whatsoever suggest that it covers a broader range of applicability. Hence, it should be considered a serious alternative to replacing the crack width calculation methods proposed by the design codes.

8 Future Research

The findings in this paper show that the MTCM and SMTCM yield a consistent mechanical formulation when an RC member is in the crack formation stage described by the CLLM behaviour, where the strains become compatible between two consecutive cracks. Therefore, the formulation might be beneficial for design when reinforcement stresses and strains are caused by imposed deformations and should be investigated further.

9 References

[1] O. Terjesen, G. Pinto, T. Kanstad, and R. Tan, "Performance study of crack width calculation methods according to Eurocodes, fib model codes and the modified tension chord model," *Structural Concrete*, vol. n/a, no. n/a, doi: https://doi.org/10.1002/suco.202300367.

[2] M. Basteskår, M. Engen, T. Kanstad, and K. T. Fosså, "A review of literature and code requirements for the crack width limitations for design of concrete structures in serviceability limit states," *Structural Concrete*, vol. 20, no. 2, pp. 678-688, 2019, doi: https://doi.org/10.1002/suco.201800183.

[3] M. Basteskår, M. Engen, T. Kanstad, H. Johansen, and K. T. Fosså, "Serviceability limit state design of large concrete structures: Impact on reinforcement amounts and consequences of design code ambiguity," *Engineering Structures*, vol. 201, p. 109816, 2019/12/15/ 2019, doi: https://doi.org/10.1016/j.engstruct.2019.109816.

[4] R. Tan, M. A. N. Hendriks, M. Geiker, and T. Kanstad, "Analytical Calculation Model for Predicting Cracking Behavior of Reinforced Concrete Ties," *Journal of Structural Engineering*, vol. 146, no. 2, p. 04019206, 2020. [Online]. Available: https://ascelibrary.org/doi/abs/10.1061/%28ASCE%29ST.1943-541X.0002510.

[5] "CEN. EN 1992-1-1, Eurocode 2: Design of Concrete Structures—Part 1-1: General Rules and Rules for buildings. Brussels: European Committee for Standardization; 2004.."

[6] "CEN-TC250-SC2-WG1_N1296_FprEN_1992-1-1_e_stf_2022-07-24 FIN clean," 2022.

[7] *fib Model Code for Concrete Structures 2010*, Berlin: International Federation for structural concrete, 2013.

[8] "2nd Draft of ModelCode 2020 - December," 2022.

[9] K. Tammo and S. Thelandersson, "Crack Behavior near Reinforcing Bars in Concrete Structures," *ACI Structural Journal*, vol. 106, pp. 259-267, 05/01 2009.

[10] A. W. Beeby *et al.*, "The influence of the parameter φ/ρeff on crack widths," *Structural Concrete*, vol. 6, pp. 155-165, 01/01 2005, doi: 10.1680/stco.2005.6.4.155.

[11] B. B. Broms, "Crack width and crack spacing in reinforced concrete members," *ACI Journal*, vol. 62, pp. 1237-1255, 01/01 1965.

[12] A. Caldentey, R. Garcia, V. Gribniak, and A. Rimkus, "Tension versus flexure: Reasons to modify the formulation of MC 2010 for cracking," vol. 21, pp. 2101-2123, 09/30 2020, doi: 10.1002/suco.202000279.

[13] A. Rasmussen, "Modelling of reinforced concrete in the serviceability limit state: A study of cracking, stiffness and deflection in flexural members," 2019.

[14] R. Tan, "Consistent crack width calculation methods for reinforced concrete elements subjected to 1D and 2D stress states A mixed experimental, numerical and analytical approach," Philosophiae Doctor, Department of Structural Engineering, Norwegian University of Science and Technology, 2019. [Online]. Available: http://hdl.handle.net/11250/2607051

[15] "Edwards AD, Picard A. Theory of cracking in concrete members. Proc ASCE – J
Struct Div 1972;98(12):2687–700.."
[16] R. Tan, M. A. N. Hendriks, and T. Kanstad, "An investigation of the strain profile over the cover in reinforced concrete elements subjected to tension," in *fib 2018 - Proceedings for the 2018 fib Congress*, 2018, pp. 1784-1791.
[17] "Eligehausen, R., E. P. Popov, and V. V. Bertero. 1983. Local bond stressslip relationships of deformed bars under generalized excitations: Experimental results and analytical model. Rep. No. UCB/EERC 83/23. Berkeley, CA: Univ. of California.."
[18] R. Tan, M. A. N. Hendriks, M. Geiker, and T. Kanstad, "A numerical investigation of the cracking behaviour of reinforced-concrete tie elements," *Magazine of Concrete Research*, vol. 72, no. 3, pp. 109-121, 2018, doi: 10.1680/jmacr.18.00156.
[19] P. G. Debernardi and M. Taliano, "Deduction of the bond low from test on short RC tie in service conditions," *Structural Concrete*, vol. n/a, no. n/a, 2023, doi: https://doi.org/10.1002/suco.202201146.
[20] R. Tan *et al.*, "Experimental and theoretical investigation of crack width calculation methods for RC ties," *Structural Concrete*, vol. 19, no. 5, pp. 1436-1447, 2018, doi: https://doi.org/10.1002/suco.201700237.
[21] C. N. Naotunna, S. M. S. M. K. Samarakoon, and K. T. Fosså, "Experimental investigation of crack width variation along the concrete cover depth in reinforced concrete specimens with ribbed bars and smooth bars," *Case Studies in Construction Materials*, vol. 15, p. e00593, 2021/12/01/ 2021, doi: https://doi.org/10.1016/j.cscm.2021.e00593.
[22] D. Borosnyoi-Crawley and I. Snóbli, "Crack width variation within the concrete cover of reinforced concrete members," *Építőanyag-Journal of Silicate Based and Composite Materials*, vol. 62, pp. 70-74, 01/01 2010, doi: 10.14382/epitoanyag-jsbcm.2010.14.
[23] W. Lindquist, D. Darwin, J. Browning, and G. Miller, "Effect of cracking on chloride content in concrete bridge decks," *ACI Materials Journal*, vol. 103, pp. 467-473, 11/01 2006.
[24] B. AW., *Corrosion of reinforcing steel in concrete and its relation to cracking*. 1978, pp. 77-81.
[25] K. Tammo, K. Lundgren, and S. Thelandersson, "Crack Widths Close to the Reinforcement," *IABSE Symposium Report*, vol. 93, 01/01 2007, doi: 10.2749/222137807796119915.
[26] J. Hegger, M. Empelmann, J. Schnell, J. Schoening, V. Oettel, and M. Schäfer, *Weiterentwicklung von Bemessungs- und Konstruktionsregeln bei großen Stabdurchmessern (>Ø 32mm, BSt500)*. 2015.
[27] O. O. K. B. Eileraas, "Design of large concrete structures in SLS: Experimental tests for determination of crack widths," Master thesis, Norwegian University of Science and Technology, 2017.
[28] "R. Tan et al., "Experimental and theoretical investigation of crack width calculation methods for RC ties," Struct. Concr., vol. 19, no. 5, pp. 1436–1447, 2018, doi: 10.1002/suco.201700237."

[29] D. Schlicke, E. M. Dorfmann, E. Fehling, and N. V. Tue, "Calculation of maximum crack width for practical design of reinforced concrete," *Civil Engineering Design*, vol. 3, no. 3, pp. 45-61, 2021, doi: https://doi.org/10.1002/cend.202100004.